SJCE

SCIENTIFIC
JOURNAL
OF CIVIL
ENGINEERING

EDITORIAL - Preface to Volume 8 Issue 1 of the Scientific Journal of Civil Engineering (SJCE)

Todorka Samardzioska EDITOR – IN - CHIEF

Dear Readers,

Scientific Journal of Civil Engineering (SJCE) was established in December 2012. It is published bi-annually and is available online at the web site of the Faculty of Civil Engineering in Skopje (www.gf.ukim.edu.mk).

This Journal welcomes original works within the field of civil engineering, which includes: all the types of engineering structures and materials, water engineering, geo-technics, highway and railroad engineering, survey and geo-spatial engineering, buildings and environmental protection, construction management and many others. The Journal focuses on analysis, experimental work, theory, practice and computational studies in the fields.

The international editorial board encourages all researchers, practitioners and members of the academic community to submit papers and contribute for the development and maintenance of the quality of the SJCE journal.

As an editor of the Scientific Journal of Civil Engineering (SJCE), it is my pleasure to introduce the First Issue of Volume 8. This Issue includes eight papers in different topics, which illustrates the comprehensive nature of the Journal. 2019 marks the 70th anniversary of our University and the Faculty of Civil Engineering. This Issue is dedicated to the celebration of this significant jubilee – 70 years of tradition, recognized values and quality in the education, research, and innovations.

The first two papers were originally presented at the XVI Danube-European Conference on Geotechnical Engineering. They have been updated herein. The first paper focuses on experimental and numerical studies for control of under-seepage pressures in aquifers and for hydraulic failure prevention stabilizing measures at the landside dyke or levee toe zones. The second paper describes a practical application of the First Order Reliability Method (FORM) in a geotechnical design. The basic characteristics and formulas of Tissot compensation projecttion and its implementation at the territory of Republic of Macedonia are presented in the third paper, while the fourth one is dedicated to the processing of the data from precise levelling measurements in the seismic active area of the Skopje valley. The fifth paper describes a hydraulic analysis of the water hammer in branch water supply network depending on the branch distance. The sixth paper refers to the uncertainties and risks in tunnelling, and implementation of appropriate measures and management. An initial representation of the theoretical approach in the analysis of the transport of people or urban mobility through description of a specific case is shown in the seventh paper. The last paper presents methods for spatial data acquisition and data processing, exploring the possibilities of obtaining 3D Building Models by processing point cloud data generated from photos produced by Unmanned Aerial Vehicle. I hope you will enjoy this variety of topics.

The approaching summer vacation is a chance to relax, recharge and to think of new research and papers, why not? We encourage you to publish them in the next Issue of SJCE!

Sincerely Yours,
Prof. Dr. Sc. Todorka Samardzioska
July, 2019

CONTENTS

Become a student of the Faculty of Civil Engineering and a part of the impetus that creates and build the world! Step in the world of the successful people, because even the longest roads start with the first step. You will spend a part of your youth with us, and the youth is expensive to be misspent in vain. Your choice is an exceptional profession, for people who do believe in themselves, profession that requires prompt and courageous decisions. This profession will provide you with great privileges: your actions will remain an eternal record in the space and in the time being.

- STRUCTURAL ENGINEERING
- HYDRO-TECHNICAL ENGINEERING
- ROADS AND RAILWAYS ENGINEERING
- GEODESY
- GEOTECHNICAL ENGINEERING

SS CYRIL AND METHODIUS UNIVERSITY
FACULTY OF CIVIL ENGINEERING
gf.ukim.edu.mk

HYDRAULIC FAILURE BY UNDERSEEPAGE OF DYKES AND LEVEES

AUTHORS

Heinz BRANDL

Em.O.Univ.Prof. Dipl.-Ing. Dr.techn. Dr.h.c.mult.

Vienna University of Technology, Karlsplatz 13/220, 1040 Vienna, Austria;

email: heinz.brandl@tuwien.ac.at

Marek SZABO

Dipl.-Ing. Dr.techn.; 3P Geotechnik ZT GmbH, Eichenstraße 20, 1120 Vienna, Austria;

email: m.szabo@3pgeo.com

The increase in frequency, magnitude and duration of floods during the past decades has become an outstanding challenge to geotechnical engineering. When dykes or levees do not have a cut-off wall fully penetrating the aquifer, underseepage may occur during high river levels. In such cases, appropriate measures against hydraulic fracture require comprehensive knowledge of failure modes of dams, dykes and levees. The installation of water pressure relief elements at the landside toe zone of dykes and dams has proven successful. The paper focuses on different relief systems based on mathematical approaches, laboratory and field tests, and on site observations. Finally, the hydraulic behaviour of relief drainage columns based on numerous experimental tests and numerical parametric studies is described.

Key words: Flood protection; Dykes; Hydraulic failure; Inner erosion; Piping; Underseepage; Relief drainage.

1. INTRODUCTION

Floods have affected millions of people worldwide in recent decades. In several regions the magnitude and frequency of flood waves have increased dramatically since long-term measurements and historical reports have existed. In Austria, for instance a 2 000 to 10 000-year flood event was back-calculated from the flood disaster in the year 2002 (Fig. 1). Such hitherto singular values cannot be taken as design values for flood protection dykes, but they underline the need for local overflow crests or spillway sections. Moreover, they clearly demonstrate that a residual risk is inevitable – despite most costly protective measures.

The risk of dykes or levees failure increases not only with the magnitude of a flood but also with its duration. For instance, the peak period of flood waves along the Austrian section of the river Danube usually lasts one to three days, whereas its tributary, the river March/Morava (Austria/Slovak border) frequently undergoes flood waves up to three or six weeks (Fig. 2). Figure 2 also illustrates

the increase of magnitude and frequency of the floods since the 1990s.

Especially long-lasting flood waves exhibit in combination with a required groundwater communication below dykes a high risk potential regarding hydraulic failure. But also periodic short hydraulic loadings of flood protection dams and their subgrade can produce a failure caused by an inner erosion processes in a long-term.

Leeve underseepage analyses are commonly performed to assess the risk of excessively high pore pressure in the aquifer. These results are used for the assessment of possible failure mechanisms. After today´s practice the hydraulic failure due to

underseepage may be prevented mainly by two permanent measures at landside dyke or dam toe by installing pressure relief elements or by placing of berms. Especially, relief drainages have proved very successful in Austria during the last excessive floods along the rivers Danube and Morava.

However, until now the existing design criteria for relief drainages were insufficient. Most of these approaches determine the pressure relief and the discharges only based on assumptions and experience from former projects. Therefore, various small-scale as well as large-scale model tests were performed to study the pressure relief behaviour including the quantification of discharge.
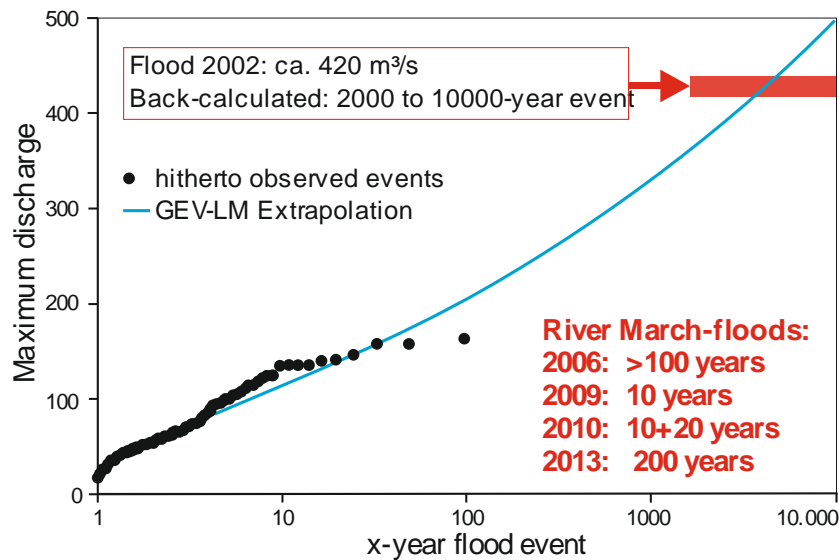

Figure 1. Statistics for the annual maximum discharge values of the river Kamp in Austria (modified / extended after Gutknecht et al. 2002). Comparison with the subsequent river March floods
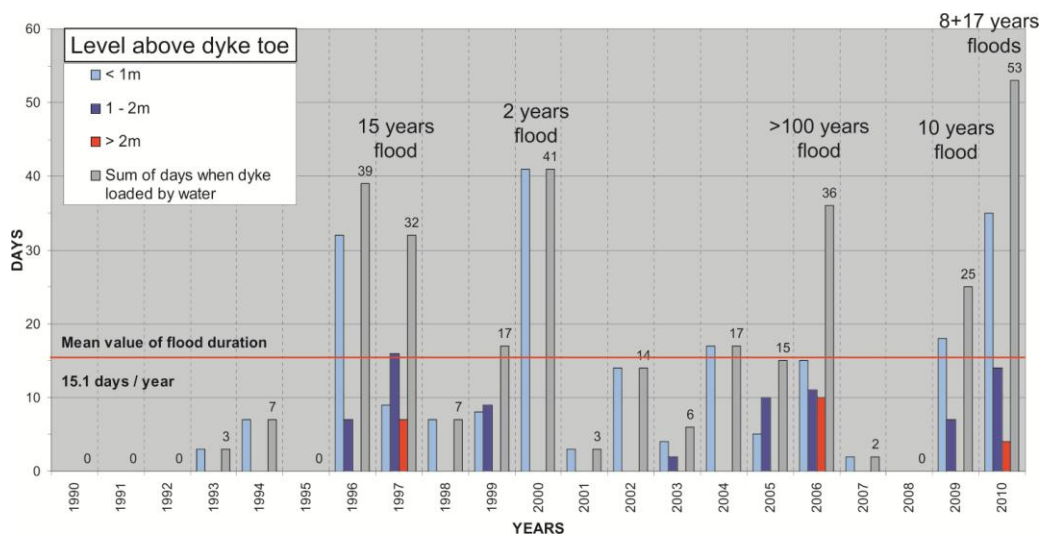

Figure 2. Duration of floods along the River March dykes (Water level at Dürnkrut – Austria/Slovakia; adapted after via Donau). Two floods within three weeks in 2010

2. FAILURE MODES OF DYKES AND LEVEES

Knowledge of possible failure modes is an essential prerequisite, both for a reliable quality assessment of existing dykes and dams and for an optimised design of new ones, frequently in connection with the application of geosynthetics. Therefore, large scale 1:1 failure tests were performed by the Institute for Ground Engineering and Soil Mechanics of the Vienna University of Technology already in the 1960s at the river Danube in Vienna. A section of the dam was flooded by creating a sheet piled area, where the water level could be raised and lowered (Fig. 3). Thus, a flood with a discharge of $Q = 14.000 \ m^3/s$ was simulated.
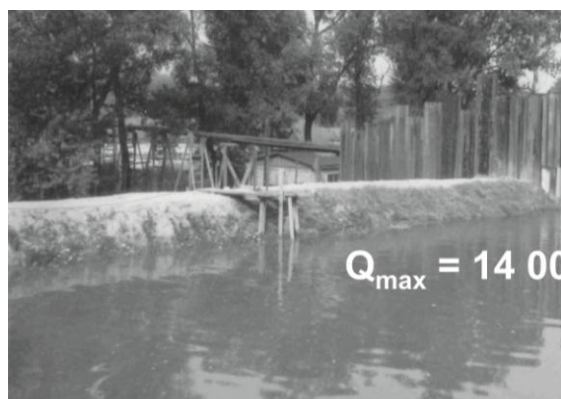
Figure 3. Large scale tests on river Danube dyke in Vienna (1967)
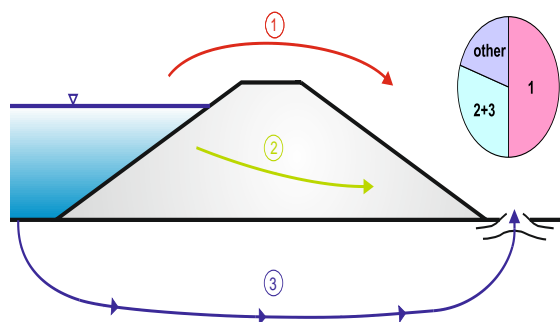
Figure 4. Main failure modes of dykes; schematic.

1 = Overflowing, overtopping → Erosion failure.
2 = Seepage through dyke → Internal erosion, Slope failure. 3 = Underseepage → Internal erosion, Upheave, Ground failure.

The simplified scheme of figure 4 illustrates the main failure modes as observed in most cases. The percentages differ regionally more or less. The dominating failure modes for typical ground conditions along rivers (near-surface low-permeability sandy to clayey silts underlain by high permeability sand or gravel) can by summarized as follows:

- slope failure due to excessive pore-water pressures, seepage or internal erosion
- overtopping or overflowing of the dyke/dam crest
- slope failure due to a rapid drop of the flood water level
- hydraulic fracture
- surface erosion and failure of the water-side slope due to wave action
- piping due to animal activities, especially from beavers and rats
- unsuitable planting of dykes (especially trees with flat roots).

Actually, it is often difficult to precisely determine the causes of a dyke failure. Several types of processes might be involved in a breach and multiple modes in a dyke failure. Statistical analyses show that overtopping and internal erosion are the most common modes of failure. While many of these failure mechanisms occur relatively fast, the erosion by underseepage develops more inconspicuously. If a groundwater communication below the dyke is possible, the aquifer or the overlaying low permeable layer can be progressively eroded during hydraulic loading. Hydraulic failure is critical because there may not be any external evidence, mostly only soil boiling can be found.

Due to this unpredictable behaviour hydraulic failure is frequently underestimated in practice and may occur in different forms (e.g. Eurocode 7; CEN 2004):
- by uplift (buoyancy),
- by heave,
- by internal erosion (Fig. 5),
- by piping (Fig. 6).

In the case of groundwater communication under a dam construction, the landside surface layer is exposed to hydrostatic stress due to underseepage. If confined conditions can develop in the aquifer, the safety against a failure of the subsoil reduces significantly. The loss of stability is usually initiated by uncontrolled hydraulic rupture (uplift) of the blanket or by concentrated transport of fine particles (erosion, suffusion, piping) from the subgrade.

Hydraulic failure may reach several tens of meters away from dykes or dams, as experience has shown (Fig. 7). This could be observed even for low flood protection embankments with a relatively small hydraulic gradient. Soil boiling may create large volcanoes (e.g. Fig. 8) that require urgent flood defence and stabilizing measures.

Figure 5. Breach of a Sava River dyke with an extensive scour on the landside (120 x 300 x 12m) due to internal erosion of the ground below the dyke. (Croatian Ministry of Agriculture, 2014)

Figure 6. Piping through a railway embankment during an already sinking flood. Train traffic was stopped

Eurocode 7 (CEN 2004) states that in situations where the pore-water pressure is hydrostatic (negligible hydraulic gradient) it is not necessary to check other than for failure by uplift. In the case of danger of material transport by internal erosion, filter criteria should be used. If the filter criteria are not satisfied, it should be verified that the critical hydraulic gradient is well below the design value of the gradient at which soil particles begin to move.

Figure 7. Piping (soil boiling) far away from the dyke and stabilizing measures to reduce the hydraulic gradient (photo: L. Nagy)

Figure 8. Boiling "volcanoes" after the flood. Retrogressive internal erosion towards the dyke causes stability loss in the long-term (photo: L. Nagy)

Hydraulic failure may occur despite cut-off walls. If they are "imperfect" (i.e. with underseepage), groundwater communication below the dykes or levees (for environmental reasons) occurs and overpressure can develop beneath the landside blanket. Fine-grained blanket with local "windows" and low residual shear strength favours such failure modes (Fig. 9).
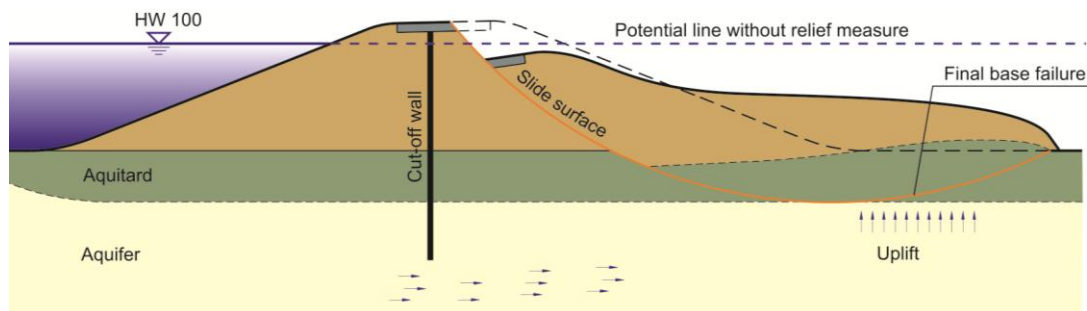

Figure 9. Hydraulic base failure despite cut-off wall, favoured by low shear strength of low permeable fine grained blanket (aquitard with "windows")

Therefore, ground investigation should also comprise the determination of residual shear strength φr. This value is not a „constant" soil parameter, but depends on normal stress and degree of water saturation (Fig. 10).
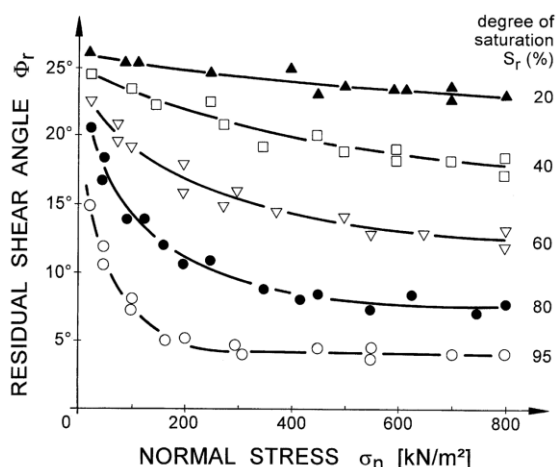
Figure 10. Residual shear angle φr of a slide prone clayey silt depending on normal stress and degree of water saturation. Results of comprehensive test series with same material (reconstituted). Direct shear tests on consolidated drained samples.

2.1 UPLIFT

The hydraulic failure by **uplift** is characteristic for a two-layer subgrade system with low permeable blanket above the highly permeable aquifer (Fig. 11). When the hydrostatic overpressure reaches the unit weight of the blanket, the soil becomes practically weightless and the uplift safety drops significantly. After exceeding the critical water pressure, the blanket ruptures mostly in the area of the landside dam toe or in adjacent hinterland. This failure process leads progressively to stability loss of the dyke due to progressive internal erosion or piping. "Volcanoes" are often formed in hinterland (Fig. 8). The uplift failure mechanism is very complex and that makes the definition of the state of failure difficult.

As uncontrolled rupture is usually preceded by a lifting of the cohesive blanket, which allows temporarily the formation of narrow cavities at the boundary layer to the aquifer. This may lead to a transport of soil particles, as it could be confirmed in experiments. However, such mechanism requires sufficient thickness as well as homogeneity of the blanket, which is not always the case. Especially, blankets with low thickness have natural or artificial cracks, which reduce the hydraulic stability of this low permeable soil layer. Due to the confined conditions in the aquifer, the water flows mostly along these cracks and inhomogeneities to the surface, thus eroding the subgrade. Therefore, the failure does not occur only as a result of uplift, but rather as combination with internal erosion and subsequent piping.

Figure 11. Uplift failure caused by an excessive pore water pressure in the foundation due to underseepage of the dyke (schematic drawing).

2.2 HEAVE

The hydraulic failure by **heave** occurs in cohesionless soils when vertical seepage forces act on the soil grains. The seepage forces are increasing until the effective stress becomes zero. At this point, the hydraulic gradient is equal to the critical hydraulic gradient i_{crit} ($i_{crit} = γ'/ γ_w$) and there is an erosion of fine particles in the soil leading to a formation of erosion channels, accompanied by a significant increase in permeability. This failure behavior is typical primarily in semipervious blankets, where vertical seepage can occur (Fig. 12). Also the fine-grained soils are also affected. Although due to the internal stresses, the cohesive soil has a much higher resistance against the internal erosion processes then cohesionless soils.

Experience has shown that the magnitude of the critical hydraulic gradient where internal erosion begins is frequently overestimated, thus underestimating the actual long-term risk. Figure 13 summarizes the critical values on the basis of field observations, geotechnical measurements, literature and long-term

experience for different soils. For comparison, the conventional criterion ($i_{crit} = γ'/γ_w$), Lane's criterion, and the critical zones after Eurocode 7 (CEN 2004) or Chugaev (1965) respectively are also plotted in the diagram.
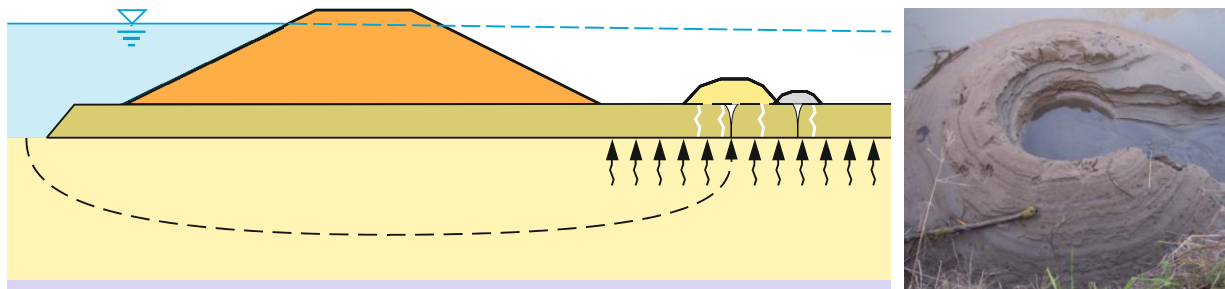
Figure 12. Hydraulic failure by heave accompanied by inner erosion of soil particles from the semipervious blanket and permeable subgrade caused by an excessive pore water pressure in the foundation due to underseepage of the dyke (schematic drawing) and a detail of a "volcano" at the dyke toe zone.
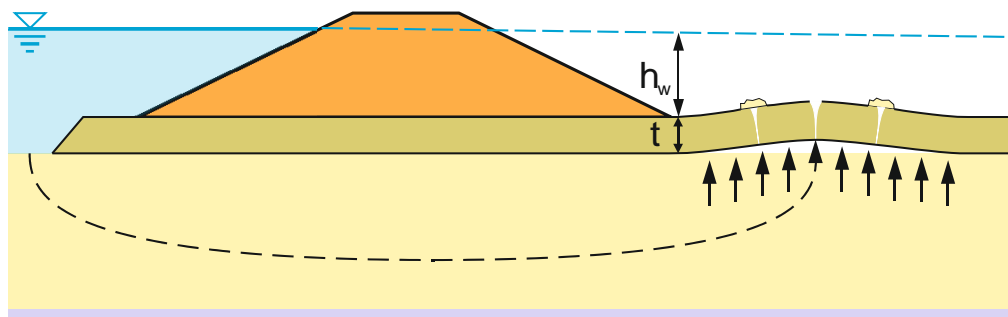
2.3 INTERNAL EROSION, SUFFUSION AND PIPING

Hydrodynamic processes by **internal erosion**, **suffusion** and **piping** always have to be considered in the close connection with the before mentioned failure mechanisms, which often represent the initial stage of a hydraulic ground failure (Fig. 15). From a long-term perspective, there is a high risk of progressive erosion, especially due to temporary hydraulic loading. After an initial local rupture of the blanket, an erosion channel forms retrogressively from the landside to the waterside during one or more floods. If this reaches the river, breaching occurs as a result of hydraulic ground failure.
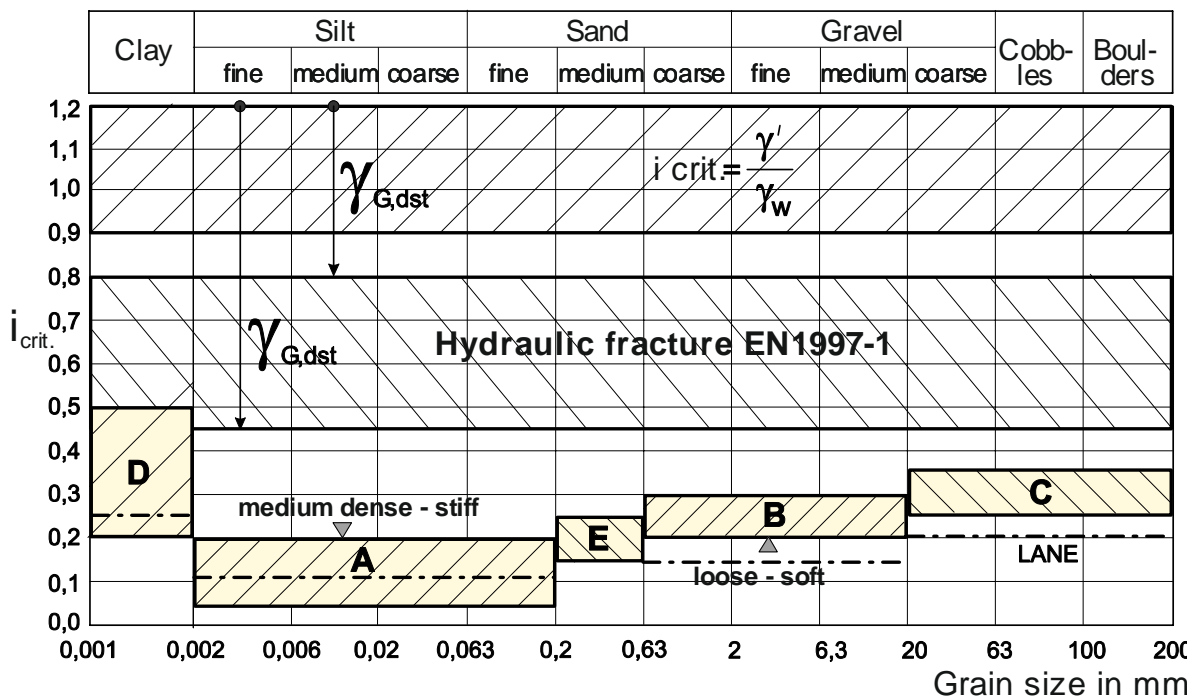
Figure 13. Critical hydraulic gradients for hydraulic fracture (internal erosion) (Brandl and Hofmann, 2006); icrit. depends not only on grain size distribution and density/stiffness but also on flow pressure; $γG,dst$ = partial safety factor for permanently unfavourable effects.

For the assessment of internal erosion or piping, different approaches (e.g. by Chugaev, Bligh, Lane, Müller-Kirchenbauer, Weijers and Sellmeijer, Witt et al., etc.) are used to determine the critical hydraulic gradient in practice. However, due to the interaction of several hydrodynamic mechanisms, these criteria typically apply to very limited types of soils and mostly to homogenous soil conditions.

3. MAESURES AGAINST HYDRAULIC FAILURE

Hydraulic failure as an effect of underseepage may be prevented mainly by two permanent measures landside of a dyke or flood protection dam by:

- Filling of berms, thus displacing the possible starting point of internal erosion or piping farther away from the structure, and decreasing the hydraulic gradient at this point. Such berms should be designed and constructed such that they work simultaneously as access ways/roads for quick and easy dam defence in the case of severe floods.
- Installing pressure relief drainage systems in form of trenches, relief stone columns or relief wells.

Another emergency method, how to increase the stability against inner erosion is to reduce the hydraulic gradient by raising the water level at the landside in local reservoirs (Fig. 7). This method represents an emergency measure by placing sandbags around the erosion crack and is often used after recognizing local hydraulic fracture in the initial stage.

A filter stable berm compensates through its counterweight the hydrostatic pressure beneath the blanket (Fig. 14a) and prevents hydraulic failure by seepage or uplift, or by internal erosion and piping. When seepage through or beneath the dyke occurs, a free water outflow must be allowed; clogging would be counterproductive. Otherwise an excessive pore-water pressure could cause a sudden failure. Filter stable berms (filter geotextiles covered with sand, gravel, or other granular material) are often used as an emergency measure, when seepage occurs.
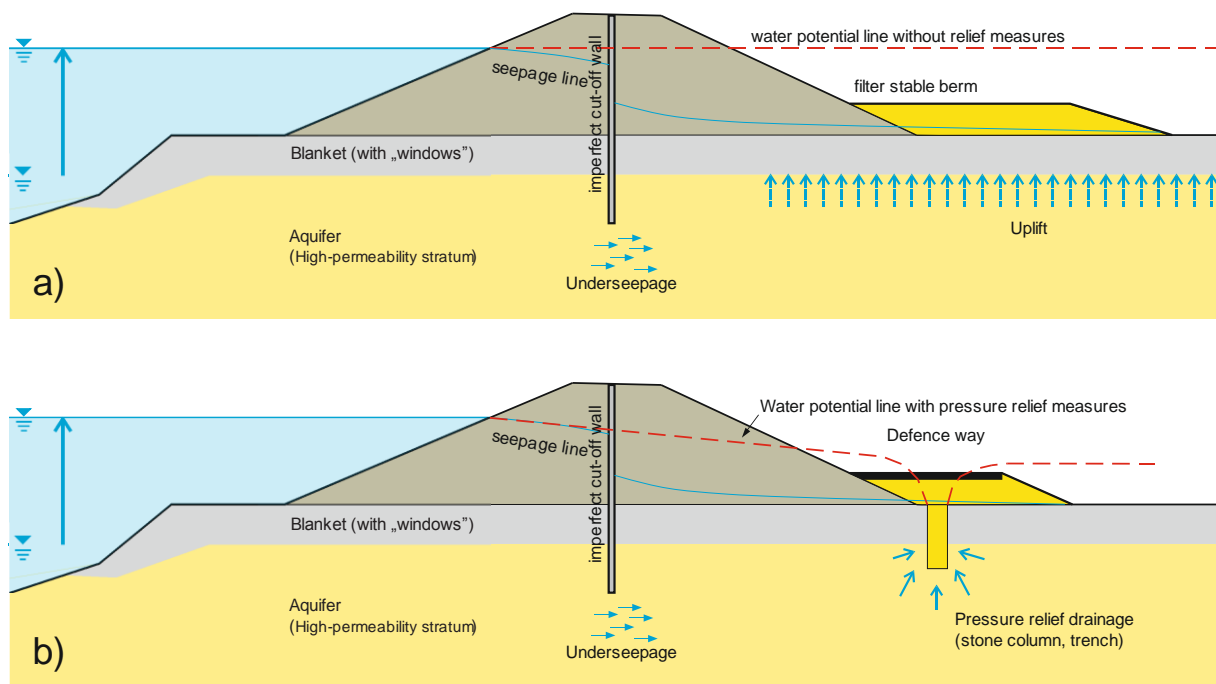
Figure 14. Permanent measures against hydraulic failure caused by underseepage of flood protection dykes:
a) Filter stable berm as a counterweight; b) Relief drainage columns or trenches.

In many cases berms merely move the hydraulic problem farther away from the dyke or dam, and retrogressive internal erosion may finally reach it in the long term (after several floods). Boiling and internal erosion have been observed up to 20 to 50 m away from dykes and dams (Fig. 7), even though they were only 3 to 6 m high. Moreover, wide berms are frequently not possible under confined space conditions; therefore relief drainages are preferred under these circumstances.

Pressure relief systems are linear or punctual drainage elements with high permeability and variable embedment length into the aquifer (Fig. 14b). They are an integral part of the dyke at the landside embankment toe and connect the terrain surface with the permeable soil layer. This hydraulic connection allows a controlled pressure relief during floods, while water can freely discharge the drainage at the landside dam toe. To prevent the drainage element from clogging due to fine particles transport caused by suffusion of the aquifer,

they must be wrapped into a filter stable geotextile.

Filter protection of berms is generally provided by the use of non-cohesive granular material (natural soil) that fulfils adequate design criteria for filter materials. Filter geotextiles have been used increasingly since the early 1970s. Common filter criteria for soils are from Terzaghi and Sherard, and for geotextiles from Holtz et al. (1997), Giroud (2003, 2010), and Heibaum et al. (2006). All criteria have particular limitations, whereby non-cohesive and cohesive soils have to be distinguished. While two criteria are sufficient for granular filters (the permeability criterion and the retention criterion), four criteria are required for geotextile filters (Giroud 2010): the porosity criterion and the roughness criterion also have to be considered.

The roughness criterion is important especially for the installation (temporary state), whereas the hydraulic criteria influence the long-term behaviour of relief drainages. However, an increase of the strength parameters leads to a reduction of the nonwoven geotextile permeability. Therefore, a compromise between both criteria has to be found when selecting suitable geotextiles.

3.1 RELIEF TRENCHES

A pressure relief trench is a longitudinal drainage of coarse gravel fill material wrapped in a filter stable geotextile at the landside dyke toe. Wider trenches may consist of granular fill material with horizontally differing grain curves as separating two- or three-stage filters (also in the base). They usually do not penetrate into the permeable aquifer, but rest mostly on top of it. However, a hydraulic connection must always be ensured so that the pressure relief is possible. At the same time, the groundwater must always freely discharge the relief drainage and is mostly conducted within the trench or flows into the adjacent hinterland.

The trench geometry is based on the dimensions of excavating tools. According to experience, the minimum drainage width is about 60 cm. The embedment depth is influenced by the soil characteristics of the subgrade as well as by the groundwater level. Mostly, a hydraulic excavator with a backhoe carries out the excavation. However, trenches excavated in very soft soil collapse immediately before geotextiles and the fill material can be placed. The installation of trussed retaining panels would be too expensive. These problems could be

overcome by installing of relief granular columns coated with a filter geotextile.

3.2 RELIEF STONE COLUMNS ("GRAVEL PILES")

Jacketed (coated) stone or gravel columns have been installed in Austria since 1992. At first they were used mainly for drainage purposes, for instance as drainage walls to improve the stability of old flood protection earth dams, dykes and levees, resp. This method has significant construction advantages over conventional drainage trenches in loose or soft soil.

Pressure relief stone columns are cylindrical pressure relief elements at the landside dyke or dam toe, which penetrate through the low permeable blanket and embed into the high permeable ground layer (aquifer). They are made of high permeable fill material (usually rounded grains, clean: 16/32 mm; permeability factor: $k \geq 1 \times 10^{-2}$ m/s) that is wrapped with a nonwoven geotextile. This geotextile filter has to fulfill the separation and the filter function.

The common diameter of these "gravel piles" is about 60 cm to 70 cm, but it can be easily adapted to the required relief effect. The installation is carried out with a designed center-to-center distance by means of vibroflotation or auger drilling method (Fig. 15).

The conventional top-feed process of the vibro technique is not suitable for jacketed granular columns. In this case, the sophisticated vibroflotation technique with bottom-feed vibrators is required. The main advantage of this method is that the vibrator remains in the ground during installation, making the technique ideal for unstable ground and high groundwater levels. The granular material is discharged from skips into the chamber at the top of the vibrator and placed at depth. To avoid geotextile damage, the vibrator is sometimes first lowered without the geotextile sleeve into the ground to displace soil.

The classical auger technique was modified for the purpose of geotextile coated columns installation. In this case, the bore hole is cased during the whole excavation to the final depth. This allows the installation of a geotextile sleeve into the casing and filling it with gravel fill material. Finally, the casing is withdrawn. The advantage of this method is the possibility of visual assessment of soil parameters as well as of the aquifer horizon that has a significant influence on the column's drainage length.

Figure 15. Installation methods of relief drainage columns wrapped in nonwoven geotextile. (left: vibroflotation method; middle: rotary drilling method with casing; right: "infinite" relief column system at the dyke toe)

Both techniques allow a rather flexible adaptation of the element length to the local soil profile. Thus, each stone column forms a part of the relief system along the dam/dyke section and is mostly connected to a longitudinal drainage on top of the column heads. This trench collects the water from relief columns and brings it to pump stations.

Figure 16. shows a cross-section through a new flood protection dam after removal of the old one, which had been destroyed by a severe flood. The coated gravel columns usually exhibit a spacing between 2.0 and 8.0 m, depending on local factors (geotechnical and ecological parameters, infrastructure, risk potential, etc.).
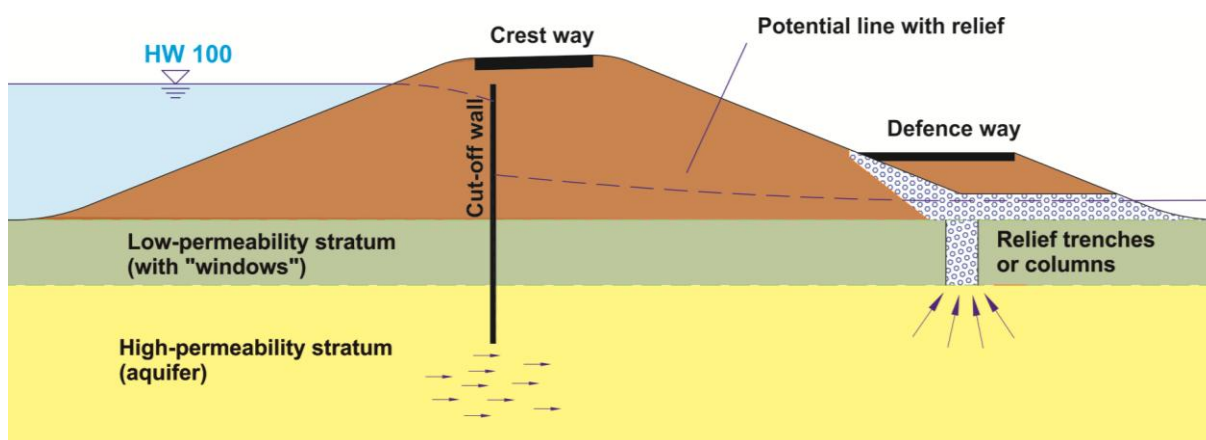
Figure 16. Standard cross-section of a new 75 km long flood protection dam in Austria. Widely reuse of old fill material from removed dykes. Cut-off wall works also as a barrier against beavers.

4. ANALYTICAL APPROACH FOR THE ASSESSMENT OF PRESSURE DISTRIBUTION DUE TO DYKE UNDERSEEPAGE

An uncontrolled underseepage due to seasonal floods represents a high risk for dykes and levees in terms of excessively pore pressure beneath the blanket. This overpressure can lead to hydraulic failure of the subgrade at the dyke toe or in adjacent hinterland. In order to assess the pressure distribution beneath the impervious/semipervious blanket and to determine appropriate measures, a levee underseepage analysis is required. This can be performed by numerical simulations. However, the accuracy of numerical results depends strongly on idealizations and the assumptions made. A simple method of assessing the pressure distribution can be done by analytical approaches. They provide exact solution for simplified flow systems with defined boundary conditions. Based on these results first estimations of the hydraulic

behavior of the subsoil due to groundwater flow are possible.

The first analytical approaches for the determination of the pressure potential due to a steady-state flow in a homogeneous aquifer were published by Bennett (1946) and later adapted by U.S. Army Corps of Engineers (1956, 2000). Today, the blanket theory is commonly used in the practice. In the following, analytical approaches for a steady-state flow model with a dam on semipervious blanket and homogenous aquifer will be exemplified based on Benett (1946), Mehaan (2012), Szabo (2017).

4.1 DAM MODEL ON IMPERVIOUS BLANKET WITH A HOMOGENOUS AQUIFER

Underseepage of dams on impervious blankets (e.g. low permeable, silty-clayey soil top layer) can be mathematically described by one-dimensional flow in a porous media with an impervious horizontal boundary at the top and the bottom of the flow field. The inflow and outflow boundary conditions are also important for the estimation of the pressure distribution.
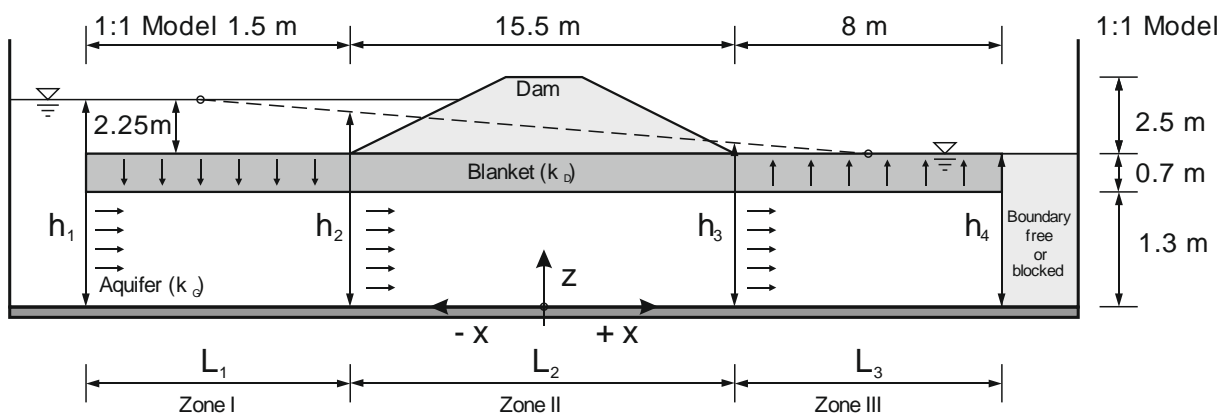
Figure 17. Idealized cross-section of dam on a semipervious/impervious blanket above a homogenous aquifer (flow field) with free inflow boundary and free or blocked outflow boundary (Szabo, 2017)

The steady-state flow in a confined aquifer is defined by following differential equation:

$$\frac{\partial}{\partial x}\left(k \ m \frac{\partial h}{\partial x} \right) = 0 \qquad (1)$$

The general solution of the Eq. 1 results for an aquifer with a constant thickness m and permeability k into:

$$h(x) = C_1 \ x + C_2 \qquad (2)$$

The mathematical solution results into a linear pressure distribution between the two water potentials (h_1 and h_4; see Fig. 17) at the inflow and outflow boundary of the flow field with a length L_i, where a free groundwater flow is defined.

$$h(x) = h_1 + \frac{h_4 - h_1}{L_1 + L_2 + L_3}\left(x + L_1 + \frac{L_2}{2} \right) \qquad (3)$$

In the case of blocked water flow at the outflow boundary the groundwater flow will stagnate. Considering such conditions, the water potential in the whole flow field corresponds with the water pressure at the inflow boundary (pressure potential h_1). This flow behavior can be described by following equation:

$$h(x) = h_1 \qquad (4)$$

4.2 DAM MODEL ON SEMIPERVIOUS BLANKET WITH A HOMOGENOUS AQUIFER AND FREE INFLOW AND BLOCKED OUTFLOW BOUNDARY CONDITION

Semipervious blankets above a pervious foundation (aquifer) can be found relatively often in the nature. They are characterized as soil layers with low permeability. If the water pressure acting on the soil layer is high enough, seepage in vertical direction may occur.

In order to describe the water pressure distribution for a dam model with homogenous aquifer on a semipervious blanket, the flow

field must be divided into different zones according the fragment theory. If the dam is assumed to be impermeable, the aquifer zone beneath the dam corresponds to a confined aquifer between two impervious boundaries (see chapter 0). In contrast, leaky-aquifer conditions prevail in foreland as well as in hinterland of the dam. In such case, the water flows in horizontal direction through the aquifer and in vertical direction through the blanket. The mathematical solution for the whole model is derived from the combination of the elementary solutions for each fragment (zone) considering the element boundary conditions.

Based on the fragment method, the pressure distribution is determined for the foreland zone considering the seepage through the blanket. The general equation of the steady-state flow is:

$$\frac{\partial^2 h}{\partial x^2} - \frac{h - h_1}{\lambda^2} = 0 \tag{5}$$

The parameter λ is the leakage factor, which defined the water flow in vertical direction through the blanket.

$$\lambda = \sqrt{\frac{k_G\, m\, t}{k_D}} \tag{6}$$

The general elementary equation for the leaky-aquifer in the zone I is:

$$h(x) = h_i + C_1\, e^{\frac{x + L_1 + \frac{L_2}{2}}{\lambda}} + C_2\, e^{-\frac{x + L_1 + \frac{L_2}{2}}{\lambda}} \tag{7}$$

Thus, the equation for the determination of the pressure distribution in the zone I can be determined under consideration of the boundary condition (water potential h_1 and h_2; see Fig. 17) and the flow through the semipervious blanket to:

$$h_I(x) = h_1 + (h_2 - h_1)\, \frac{\sinh\left(\frac{2x + 2L_1 + L_2}{2\lambda}\right)}{\sinh\left(\frac{L_1}{\lambda}\right)} \tag{8}$$

In the zone II (see Fig. 17), confined aquifer conditions prevails in the flow field beneath the dam. The pressure distribution can be calculated according to the general Eq. 2 considering the water potential h_2 und h_3 at the fragment boundaries.

$$h_{II}(x) = \frac{h_2 + h_3}{2} + \frac{(h_3 - h_2)}{L_2}\, x \tag{9}$$

In case of a blocked outflow in hinterland, no-flow condition has to be considered at the landslide model boundary of the fragment III. This results into a stagnation of the flow. Therefore, the flow behaviour as well as the pressure distribution depends only on the leakage through the semipermeable blanket in the vertical direction. The pressure distribution in the zone III (hinterland) can by calculate with following equation:

$$h_{III}(x) = h_4 + (h_3 - h_4)\, \frac{\cosh\left(\frac{-2x + 2L_3 + L_2}{2\lambda}\right)}{\cosh\left(\frac{L_3}{\lambda}\right)} \tag{10}$$

The groundwater flow rate over the model width B can be calculated as a first derivation of the Eq. 10 with following solution:

$$Q_{III} = T\, \frac{(h_3 - h_4)}{\lambda}\, \tanh\left(\frac{L_3}{\lambda}\right) = k\, m\, \frac{(h_3 - h_4)}{\lambda}\, \tanh\left(\frac{L_3}{\lambda}\right) \tag{11}$$

Assuming that the flow rate Q must be constant at the fragment boundaries for continuity reasons, the unknown piezometer heads h_2 and h_3 can be solved by equating the flow rates for the adjoining zones $Q_I = Q_{II}$ or $Q_{II} = Q_{III}$.

$$h_2 = \frac{\lambda\, h_1 + h_1\, L_2\, \tanh\left(\frac{L_3}{\lambda}\right) + \lambda\, h_4\, \tanh\left(\frac{L_1}{\lambda}\right)\tanh\left(\frac{L_3}{\lambda}\right)}{\lambda + L_2\, \tanh\left(\frac{L_3}{\lambda}\right) + \lambda\, \tanh\left(\frac{L_1}{\lambda}\right)\tanh\left(\frac{L_3}{\lambda}\right)} \tag{12}$$

$$h_3 = \frac{\lambda\, h_1 + h_4\, L_2\, \tanh\left(\frac{L_3}{\lambda}\right) + \lambda\, h_4\, \tanh\left(\frac{L_1}{\lambda}\right)\tanh\left(\frac{L_3}{\lambda}\right)}{\lambda + L_2\, \tanh\left(\frac{L_3}{\lambda}\right) + \lambda\, \tanh\left(\frac{L_1}{\lambda}\right)\tanh\left(\frac{L_3}{\lambda}\right)} \tag{13}$$

This exemplified analytical solution of underseepage beneath a dam on a semipervious blanket describes simplified method for the determination of the pressure distribution in a homogeneous leaky-aquifer with steady-state groundwater flow with blocked outflow at the hinterland boundary. Such flow conditions are characteristic for the performed physical model tests, which are described in the following chapter.

Figure 18 shows the pressure curves for different permeability factor from $k = 1 \times 10^{-4}$ m/s to $k = 1 \times 10^{-9}$ m/s of the semipermeable blanket in the 1:1 model (chapter 5.1.2). In case of high leakage factor, the hydrostatic pressure in the aquifer is relieved due to the vertical flow through the blanket. If the permeability of the blanket is low, confined aquifer condition can be found (see chapter 4.1).
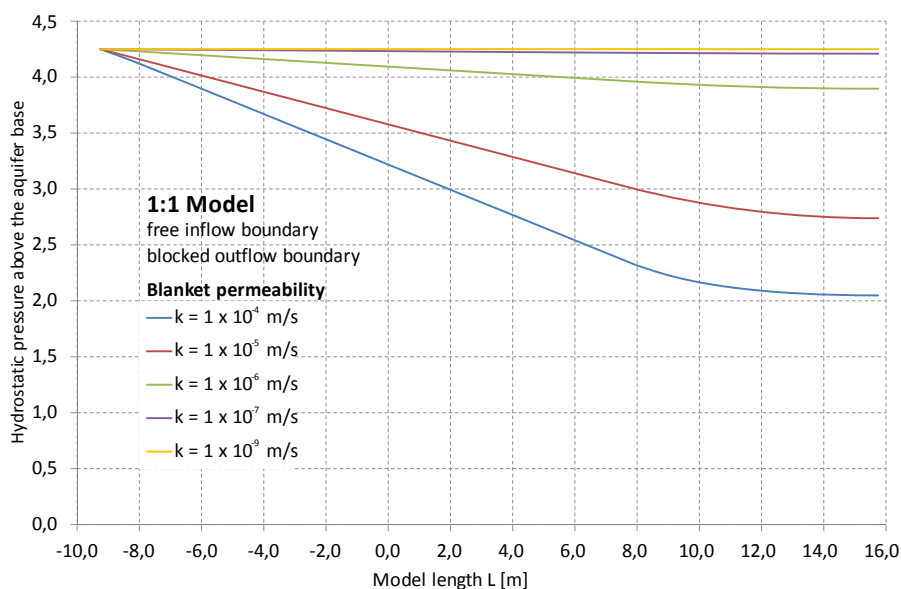
Figure 18. Pressure curves depending on leakage factor of the semipervious blanket in a flow field with blocked outflow boundary

5. MODELLING OF RELIEF DRAINAGE BEHAVIOUR

Until now the design of relief measures (drainage columns or trenches) was based on rather insufficient basic principles, strong simplifications and idealizations. For the quantification of the water outflow from relief columns as well as for a pressure assessment beneath the blanket only assumptions based on numerical models are in use. These approaches allow indeed comparative calculations of the quantity of seepage through and under the dyke.

Consequently, model tests on dykes including the subgrade (blanket and aquifer) are the best solution to assess the relief behaviour and to quantify the water outflow from relief elements during hydraulic loading. Experimental tests performed under laboratory conditions allow a higher degree of reliability than mere numerical simulations. But based on the results from physical modelling an exact calibration of numerical models can be performed.

5.1 EXPERIMENTAL MODEL TESTS

In the first phase of experimental underseepage studies small-scale (1:10) model tests were carried out at the Vienna University of Technology, Institute of Geotechnics (Fig. 19). The tests results were used for the design of an experimental facility, which served for 1:1 underseepage model tests (Fig. 22).

5.1.1 Small-scale modelling

The small-scale dam model represents within a glass channel a vertical cross-section of a dyke including the subgrade in a scale 1:10. Thus, the channel walls form an impermeable boundary condition for the investigation of relief elements behaviour due to underseepage.

The 25 cm high dam model is founded on a two-layer strata. Beneath the silty-clayey blanket ($k = 10^{-9}$ m/s) with a thickness of about 10 cm follows a homogenous aquifer layer of coarse sand with a thickness of about 18 cm. In addition, the dam has an imperfect cut-off wall (i.e. with underseepage), which slightly embeds into the aquifer.

The pressure distribution beneath the blanket due to underseepage and pressure relief was measured by means of piezometers pipes in the longitudinal and transversal model axis. During the tests different types (trench, stone columns and wells) and geometries of relief elements (width, diameter, embedment length, etc.) were studied. In addition to pressure measurements also discharge from relief elements was quantified.
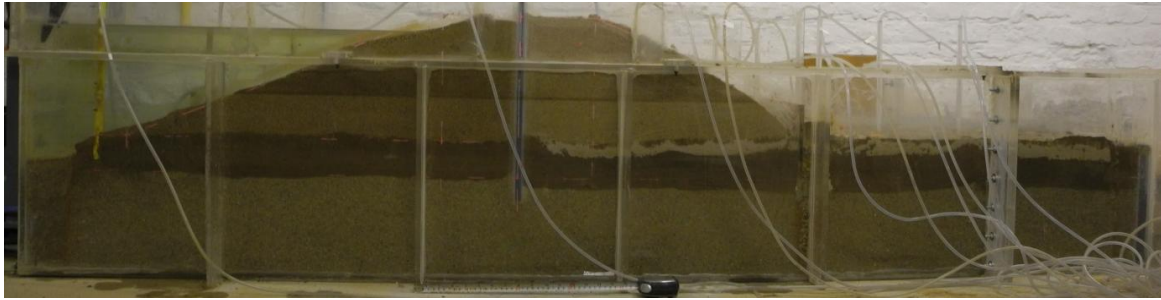
Figure 19. 1:10 small-scale dam model on two-layer subgrade for pressure relief behaviour study

Figures 20 and 21 show the pressure distribution lines beneath the blanket for test series with single and multiple relief elements depending on its permeability and embedment length into the aquifer. Both – the relief gravel column as well as the relief well – lead to a significant reduction of the hydrostatic pressure on the waterside. If no relief measures would be installed, due to the blocked outflow boundary the hydrostatic conditions on the landside would became equal to the hydrostatic head on the waterside. It can be also seen that the element permeability significantly influences the pressure reduction. A similar behaviour can also be observed in terms of embedment length. However, the effect of embedment depth on the pressure relief, as supplementary investigations with the calibrated numerical model show, is also strongly influenced by parameters of the aquifer.
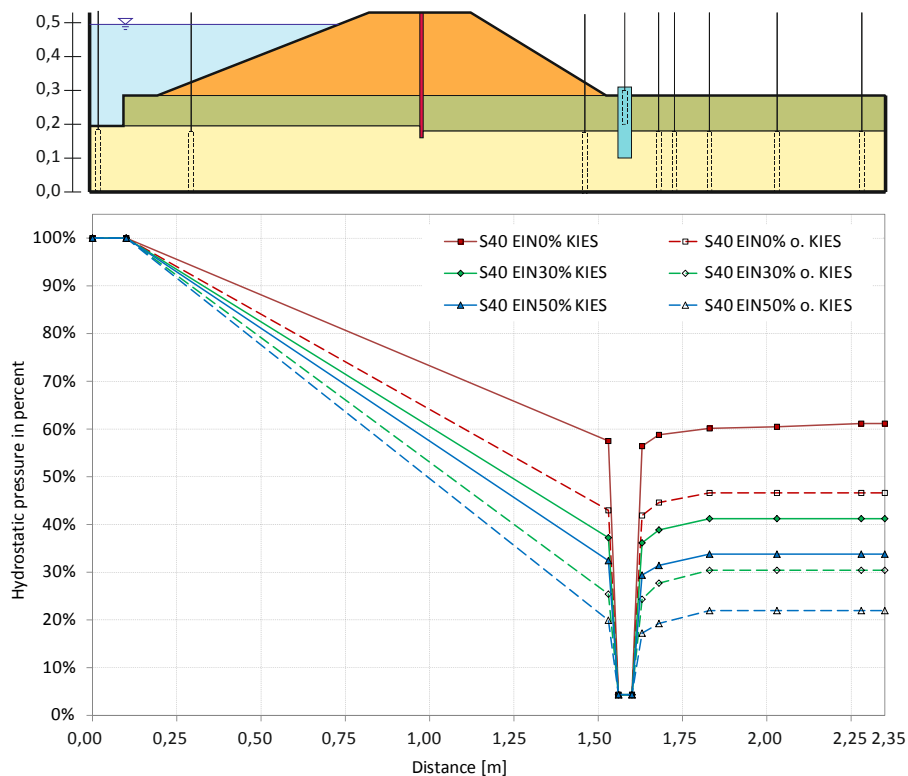
Figure 20. Pressure lines along the longitudinal axis of the 1:10 model with a single relief column depending on column length and permeability. (S40 = single column system with Ø 40 mm; EIN = column embedment in percent; KIES /o. KIES = with / without gravel; HW = water level)
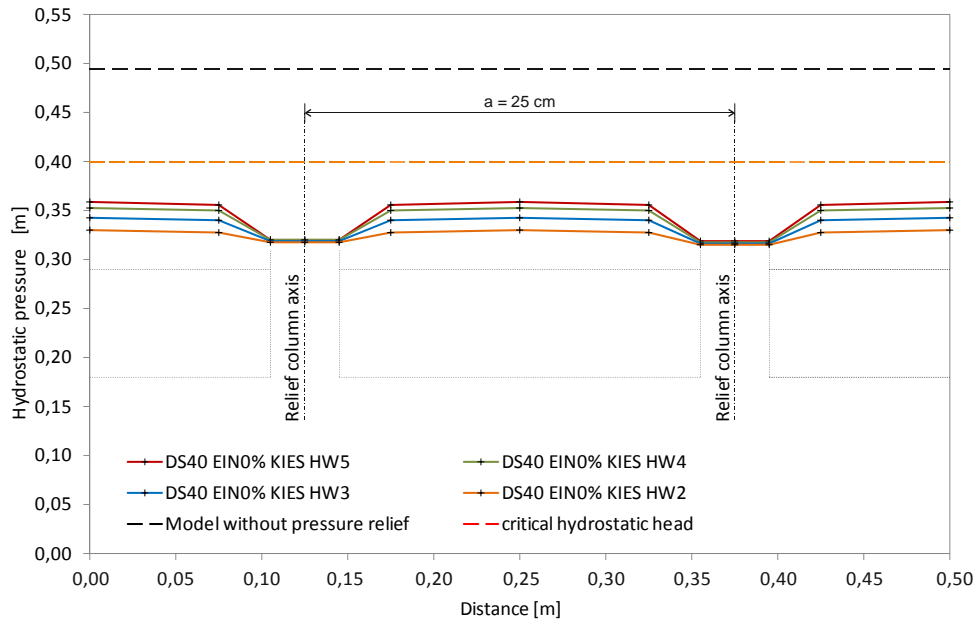
Figure 21. Pressure lines along the transversal axis of the small-scale model with a multiple relief column system. (DS40 = multiple column system with Ø 40 mm; EIN = column embedment in percent; KIES = with gravel; HW = water level)

5.1.2 Large-scale modelling

Based on the small-scale modelling, a large scale test facility (1:1) was built to study pressure relief drainages. The ground plan area of the reinforced concrete box was 25 x 4 m with a constant wall height of 5 m (Fig. 22).

The 1:1 dam model represents a 4 m wide and 25 m long cross-sectional model of rehabilitated dyke at the river March together with a two-layer subgrade (Fig. 23). The homogenous dam had a height of 2.5 m and the slope ratio of 1:2.5. For the dam sealing a silty-clayey core was installed, which penetrated the clayey blanket (thickness of about 0.7 m) and embedded only few centimetres into the 1.3 m thick aquifer layer of sandy gravel.

For the pressure relief observation due to the controlled underseepage, a measuring system was used, which allowed a continuous recording of the pressure potentials beneath the blanket as well as a time-synchronous recording of the water discharge from the relief gravel column.

Figure 22. The large scale test facility (length 25 m, height 5 m und width 4 m) for investigating the underseepage of dykes and levees in a 1:1 scale
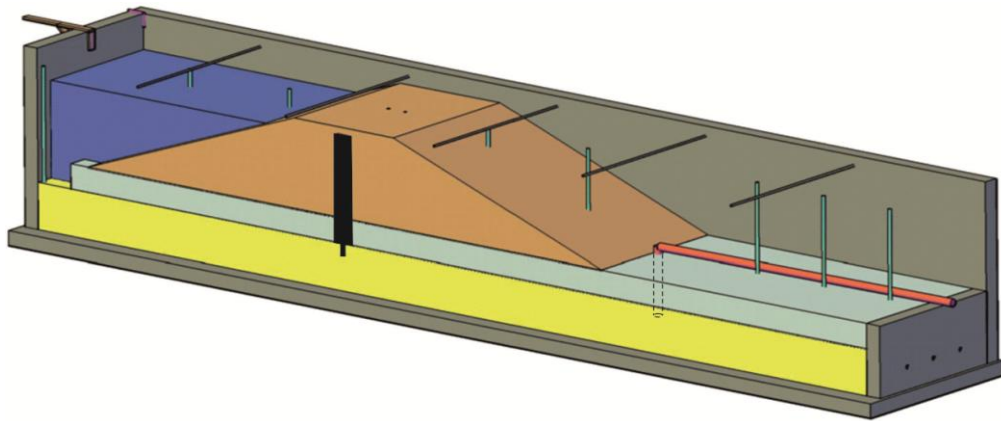
Figure 23. Schematic drawing of the 1:1 dam model on a two-layer foundation.

In numerous series of measurements with varied column parameters, the relief behavior of drainage columns could be confirmed despite certain anomalies. An example of the pressure relief behaviour due to a single relief gravel column (Ø 600 mm) without embedment into the aquifer shows figure 24. The pressure reduction at the beginning of the measuring profile was partly caused by possible local clogging of the aquifer in combination with the relieving effect through the relief column. This resulted in a reduction of 50% in the hinterland. The maximum discharge for the highest water level was about 0.95 l/s per relief column with 4 m spacing.
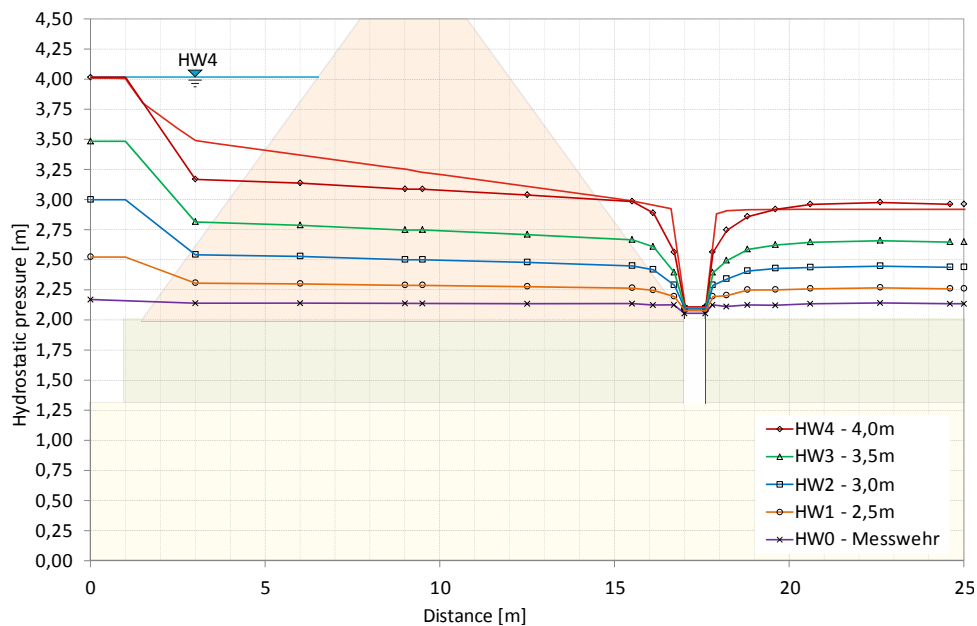
Figure 24. Pressure distribution lines due to a single relief drainage column of 600 mm diameter and without embedment into the aquifer in a 1:1 model. (HW = water level)

5.2 NUMERICAL MODELLING

The numerical modelling of underseepage is an important contribution to the description of the pressure relief behaviour and is often used for the design of such relief systems. In order to examine the general application of numerical results, a model calibration with the GGU Software was carried out based on the model tests. For this purpose, the small-scale model test results were used, because the 1:10 model had a higher degree of homogeneity as the 1:1 dam model. The calibration was first carried out for a fully penetrating relief trench by variation of the aquifer permeability and subsequently extended to a three-dimensional model with a single relief column (Fig. 25). After the calibration, numerous comparative simulations were performed for the small-scale model as well as the large-scale model. They verified the application of the calibrated three-dimensional numerical model for further studies of different parameters beyond the limits of the physical modelling.
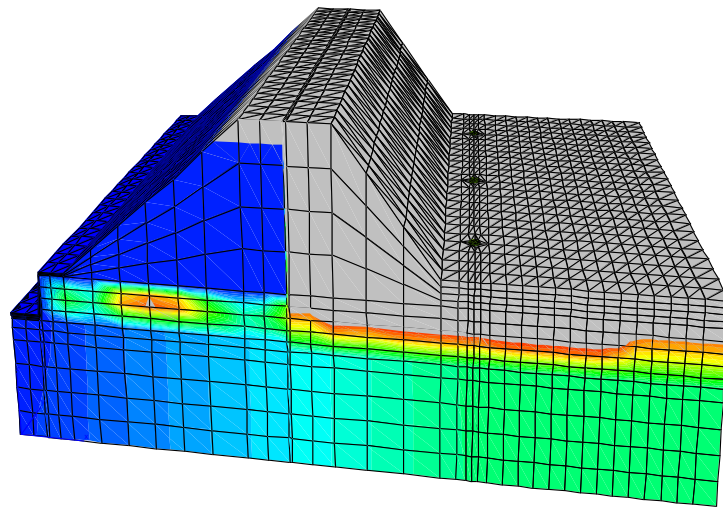
Figure 25. Three-dimensional calibrated dam model with "infinite" relief drainage column system

Figure 26 shows the pressure distribution beneath the blanket over the whole flow field of the calibrated numerical model due to a single relief drainage column. The hydrostatic pressure at the relief element spot falls to the minimum and then increases to a constant value in hinterland that is primarily influenced by the outflow boundary condition. This was defined as a blocked boundary and correspondents with the physical model, where the outflow was prevented by the impermeable channel walls.
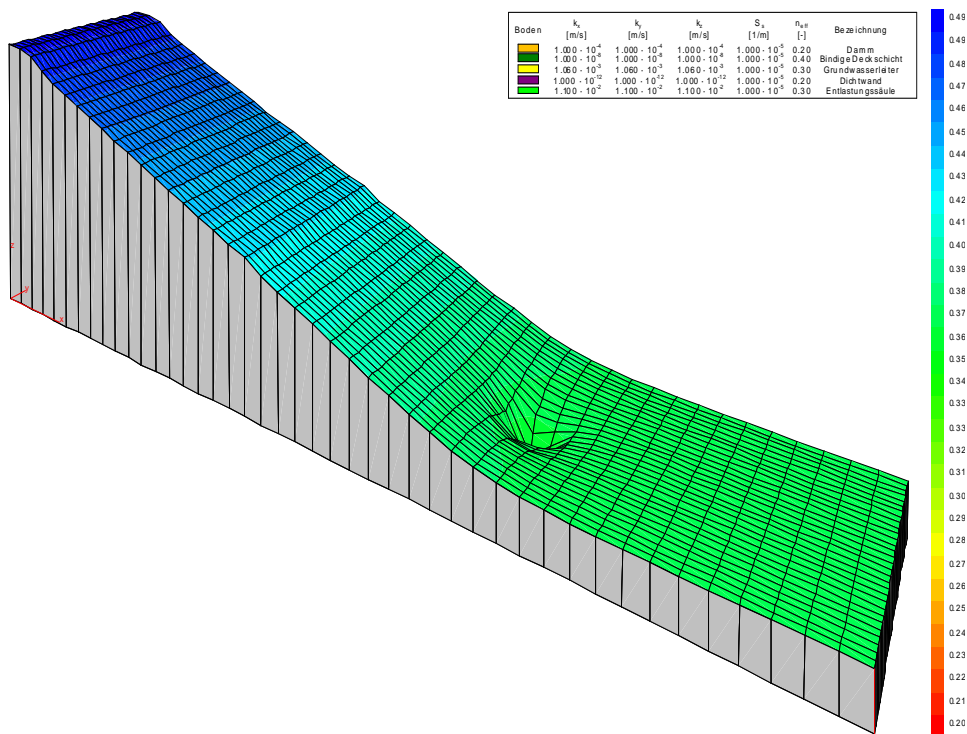
Figure 26. Pressure distribution in the aquifer due to a single relief drainage column

In addition, the parameters of the relief column (diameter, permeability, embedment length, spacing of a multiple column system), the influence of the model geometry (distance between the river and the dyke, thickness of the subgrade, etc.) as well as different permeability factors of the aquifer were studied (Fig. 27). Based on these calculation results, recommendations were derived for the practical use of relief columns. It was found that the permeability of the relief drainage fill material significantly affects the relief

H. Brandl, M. Szabo

behaviour. The effect of the embedment length is also strongly influenced by the column permeability in combination with the thickness of the aquifer. For the standard relief drainage column (Ø 600 mm and k ≥ 1 x 10^{-2} m/s) and an aquifer thickness of about 10 m only little differences in the pressure reduction depending on the embedment length could be found.

Figure 28/left shows the midway pressure for an infinite relief drainage column system in a homogenous flow field with defined geometry and blocked outflow boundary as a function of column spacing and aquifer permeability. In the diagram, also the discharge (Fig. 28/right) associated with the achieved pressure reduction can be achieved.
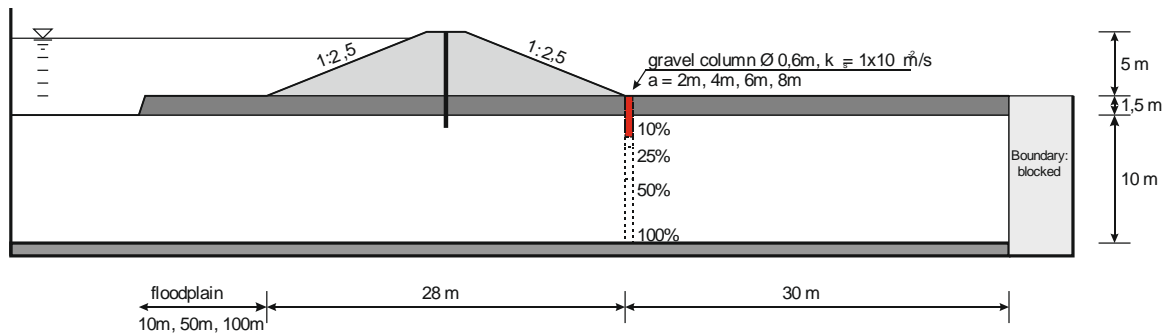
Figure 27. Cross-section of a dyke on two-layer subgrade - calculation profile for parametric studies of the relief behaviour due to an infinite relief column system (a = spacing of relief columns)
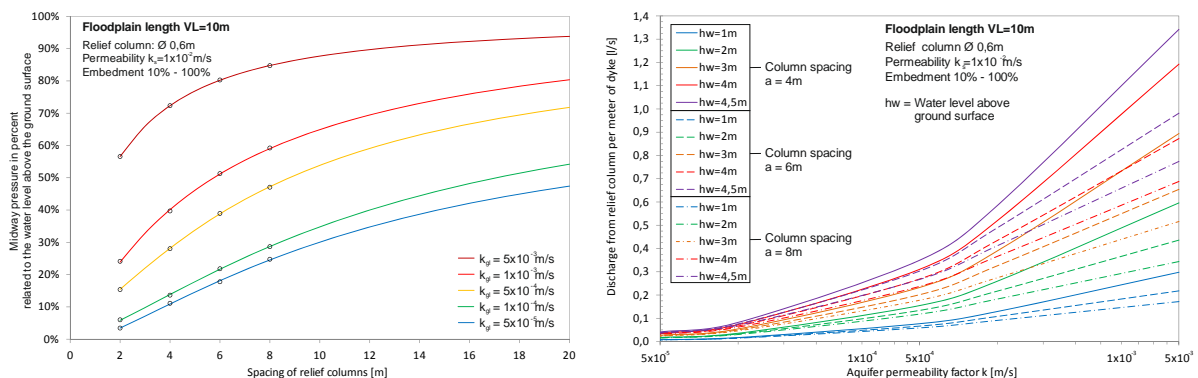
Figure 28. Results of parametric studies depending on column spacing and aquifer permeability (definition of model parameters see figure 27): Diagram on the left: midway pressure for a relief gravel column system. Diagram on the right: calculated discharge from relief drainage columns.

6. CONCLUSIONS

Underseepage of dams, dykes or levees may lead – especially in long-term – to erosion of the ground due to (subsequent) floods. The pressures that develop landside of the dyke during floods may cause heaving or uncontrolled rupture of the near-surface blanket resulting in a concentration of seepage flow, often accompanied by piping, and potential dyke failure. Such a hydraulic failure develops mostly rather inconspicuously; therefore it is often underestimated in practice. Erosion criteria can be used to describe the critical state for different soil types found during ground investigation. For the control of underseepage pressures in the aquifer and for hydraulic failure prevention stabilizing measures at the landside dyke or levee toe zone are essential. Filter stable berms, relief

drainage columns or trenches, sometimes also relief wells have proven very successful.

If pressure relief measures are required, the selection of a suitable relief system has to consider the geotechnical, hydraulic and local conditions. For the design of the selected relief system (drainage columns, trenches, wells) numerical methods are commonly used in practice. A technically and economically optimized design is only possible, if hydraulic boundaries of the flow field (e.g. long-term data from groundwater observation) and the permeability of the aquifer (field and laboratory tests) can be determined as precisely as possible, as could be experienced in the performed experimental and numerical studies. Finally, monitoring of existing projects contributes significantly to continuous calibration and sophistication of numerical modelling and practical design.

REFERENCES

[1] Beennett, P. T. (1946). The effect of blankets on seepage through pervious foundations. Transactions of the American Society of Civil Engineers, Vol. 111, pp. 215 – 228.

[2] Brandl H. (2012). Failures and defense of flood protection dykes and levees. Sicherung von Dämmen, Deichen und Stauanlagen – Handbuch für Theorie und Praxis, Vol. IV (Herausg. R. A. Herrmann, J. Jensen), Universität Siegen, pp. 3-20.

[3] Brandl H., Hofmann R. (2006). Erosionsstabilität und Standsicherheit von Schutzdämmen gegen Wildbäche und Murengänge mit besonderer Berücksichtigung von Einbauten. Sicherung von Dämmen, Deichen und Stauanlagen – Handbuch für Theorie und Praxis, Vol. I (Herausg. R. A. Herrmann, J. Jensen), Universität Siegen, S. 139-171.

[4] Brandl H., Szabo M. (2013). Hydraulic failure of flood protection dykes. Proceedings of the 18th International Conference on Soil Mechanics and Geotechnical Engineering, Paris.

[5] CEN (2004). EN 1997-1. Eurocode 7: Geotechnical Design – Part 1: General Rules. Comiteé Europeén de Normalisation, Brussels.

[6] Chugaev, R. R. (1965). Calculation of the filter stability of the ground below dams. Gidrotechniceskoe Stroitel'stvo, No. 2 (in Russian).

[7] Giroud, J. P. (2010). Development of criteria for geotextiles and granular filters. Prestigious Lecture 1. Proceedings of the 9th International Conf. on Geosynthetics, Guaruja´, Brazil, pp. 45 – 66.

[8] Heibaum, M., Fourie, A., Girard, H., Karunararne, G. G., Lafleur, J. & McGrath, J. (2006). Hydraulic application of geosynthetics. Special Lecture. Proceedings of the International Conference on Geosynthetics (IGS), Yokohama, Japan, Millpress, Rotterdam, the Nether- lands, pp. 79 – 120.

[9] Holz R.D., Christopher B.R., Berg R.R. (1997). Geosynthetic Engineering. Richmond, BiTech Publishers Ltd. – ISBN: 0-921095-20-1.

[10] Meehan Ch. L., Benjasupattananan S. (2012). An analytical approach for levee underseepage analysis. Journal of Hydrology 470–471, pp. 201 – 211.

[11] Nagy, L. (2011). Investigation of soils outwashed from piping. Österreichische Ingenieur- und Architekten-Zeitschrift, Jhg. 156, No. 1-12/2011, pp. 211-215.

[12] Nagy L. (2014). Buzgárok az árvizvédelemben. (ISBN 978-963-12-0319-6) und persönliche Mitteilungen (TU Budapest).

[13] Szabo M. (2017). Experimentelle und numerische Untersuchungen der Wirkungsweise von Druckentlastungsdrainagen bei der Unterströmung von Dämmen. Technische Universität Wien, Dissertation.

[14] US ARMY CORPS OF ENGINEERS (1956). Investigation of Underseepage and Its Control, Lower Mississippi River Levees. Technical Memorandum 3-424, Waterway experiment station, Vicksburg, Mississippi.

[15] US ARMY CORPS OF ENGINEERS (2000). Design and Construction of Levees. Engineer Manual EM 1110-2-1913, U.S. Army Corps of Engineers Washington.

[16] Ziems, J. (1967). Neue Erkenntnisse hinsichtlich der Verformungsbeständigkeit der Lockergesteine gegenüber Wirkungen des Sickerwassers. Wasserwirtschaft – Wassertechnik 17, No. 7, 50 – 55 (in German).

H. Brandl, M. Szabo

PRACTICAL APPLICATION OF RELIABILITY-BASED DESIGN WITH EXAMPLES INCLUDING RELIABILITY ASSESSMENT OF DESIGN APPROACH DA2*

AUTHORS

Peter DAY

DEng. PrEng., Adjunct Professor; University of Stellenbosch, Stellenbosch, South Africa

email: day@jaws.co.za

Nico DE KOKER

PhD, Researcher; University of Stellenbosch, Stellenbosch, South Africa

email: ndekoker@gmail.com

In this paper we look at the application of reliability-based design to various types of problems in a geotechnical design office. For the selected design examples, comparisons are presented between the results from reliability analyses and those from traditional design methods such as working stress design and limit states design using design approach DA1-2. In addition, we compare the reliability of eccentrically loaded footings designed according to DA2 and DA2*. Our conclusion is that reliability-based design can readily be applied to problems with closed form solutions provided sufficient data is available to adequately characterise the input parameters. Eccentrically loaded footings designed according to DA2* are less reliable than those designed using design approach DA2 from EN1997-1. Limit states design using design approach DA1-2 from EN1997-1 achieves fairly uniform levels of reliability for different types of structures and is suitable for routine design.

Key words: Reliability-based design; Geotechnical design; Limit states design; Design approaches.

1. INTRODUCTION

A number of factors have combined to facilitate the application of reliability-based design methods in geotechnical engineering practice. These include faster computers, more efficient solution algorithms and increased understanding of the likely variation of input parameters to geotechnical design problems. In this paper, we compare the reliability of common geotechnical structures designed in accordance with Design Approach 1 Combination 2 (DA1-2) from EN1997-1. In the case of eccentrically loaded spread footings, this comparison is extended to include design approach DA2 from EN1997-1 and the proposed DA2* design approach for spread footings.

2. METHODS OF RELIABILITY ANALYSIS

The First Order Reliability Method (FORM) and Monte Carlo simulations can readily be applied to problems with closed-form solutions, i.e. problems where the solution can be found by substitution of the design parameters into equations which have explicit solutions. Examples of such problems are the bearing capacity of a footing or the stability of a retaining wall. In the context of a design office, FORM analyses may be undertaken using spread-sheets such as that developed by Low & Tang (2007). This spreadsheet requires a performance function g to be defined such that failure occurs when $g < 0$. Using the terminology of the Eurocodes, the performance function can be expressed as the difference between the effect of actions (E) and resistance (R), i.e. $g = R - E$. The FORM algorithm determines the value of the reliability index β as the distance in units of standard deviation from the mean point (point in multi-dimensional parameter space where all parameters assume their mean value) to the closest point on the failure surface boundary ($g = 0$), known as the design point. The probability of failure is computed by approximating the failure domain as a linear plane tangential to the failure surface at the design point.

3. EXAMPLES

The examples chosen were based on Orr et al (2005) and are shown in the first column of Figure 1. All these problems have closed form solutions. In each example, the design determines one controlling dimension of the structure, such as the width of a footing or the length of a pile. A single soil type was assumed throughout, a cohesionless sand with a friction angle $\phi' = 32^o$ and a density $\gamma = 20$ kN/m^3. The statistical distributions, coefficients of variation and ratios of characteristic to mean loading were based on Retief and Dunaiski (2010) and Phoon and Kulhawy (1999). The characteristic values for imposed loads were taken as the upper 5% fractile. The characteristic value of the shear strength of the soil was selected as 28,8^o, one standard deviation below the mean (Schneider, 1977) except in the case of piles where the selected value was 30,4^o, half a standard deviation below the mean. Partial factors were based on the National Annex to BS EN 1990:2002 and National Annex to BS

EN 1997:2004. The first step in the process was to find the "Eurocode-compliant" solution using characteristic values of loads and material properties. The solution obtained (minimum required value of B or L) is shown in the fourth column of Figure 1. Thereafter, the factor of safety was determined using unfactored values of the mean and characteristic values of the input parameters. The values obtained are given in Column 5 of Figure 1. Finally, the reliability index was determined using both FORM and Monte Carlo simulations (10^6 trials). Variable vertical actions and shear strength were assumed to be log-normally distributed, variable horizontal actions Gumbel distributed and soil density normally distributed. The reliability indices and the FORM design points are given in the final two columns of Figure 1. Further details of the analysis and an assessment of the variation in reliability indices and factor of safety with changes in parameters are given in De Koker and Day (2017).The reliability indices in Figure 1 show good agreement between the FORM and Monte Carlo methods indicating that FORM is suitable for use in many geotechnical problems. There is a remarkable consistency in the reliability indices (3,2 to 3,7) despite the different failure modes for the various examples. The factors of safety, however, varied widely between examples confirming that the factor of safety is a poor measure of reliability of a structure. Limit states design according to EN1997-1 is considered suitable for routine design in preference to working stress design methods.

4. RELIABILITY ASSESSMENT OF DA2*

Design approach DA2* is a variation of design approach 2 in which the actions on a footing are combined before they are factored (Frank et al, 2004), i.e. all components of the load vector attract the same partial action factor. This approach is favoured by the German design specification as it yields economical designs with similar levels of safety to previous design methods based on the global safety concept (Vogt & Schuppener, 2006). Simpson (2007) queried the acceptability of design approach DA2* as it requires significantly narrower strip footings compared to other design approaches when footings are subjected to vertical and horizontal loads. To assess the reliability of DA2* in comparison to design approach DA2 from EN1997-1, a similar procedure was followed to that described above, i.e. the width of a footing

required to resist various combinations of vertical and horizontal loads was determined for both design approaches followed by a reliability analysis of the footing.
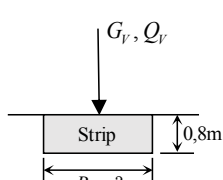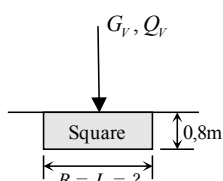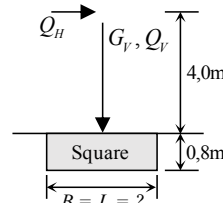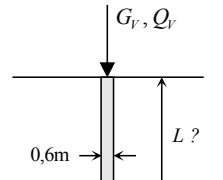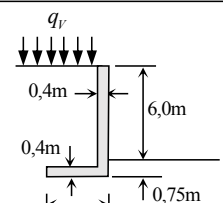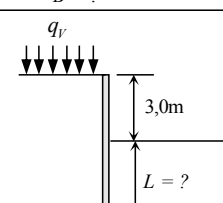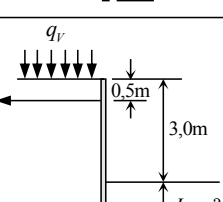
Example	Actions	Partial factors	Solution	Factor of safety	Reliability index	Design point
A (Strip, 0,8m, B = ?) G_V, Q_V	$\overline{G_V} = 900$ kN/m $G_{Vk} = 900$ kN/m $\overline{Q_V} = 412.5$ kN/m $Q_{Vk} = 412.5$ kN/m	$\gamma_G = 1,0$ $\gamma_Q = 1,3$ $\gamma_{\phi'} = 1,25$ $\gamma_\gamma = 1,0$	$B = 3,10$m	$FoS_{char} = 2,50$ $FoS_{mean} = 5,18$	$\beta_{MC} = 3,409$ $\beta_{FORM} = 3,486$	$\phi' = 25,28^o$ $\gamma = 19,85$ kN/m^3 $Q_V = 482,6$ kN/m
B (Square, 0,8m, B = L = ?) G_V, Q_V	$\overline{G_V} = 3000$ kN $G_{Vk} = 3000$ kN $\overline{Q_V} = 1375$ kN $Q_{Vk} = 2000$ kN	$\gamma_G = 1,0$ $\gamma_Q = 1,3$ $\gamma_{\phi'} = 1,25$ $\gamma_\gamma = 1,0$	$B = L = 3,24$m	$FoS_{char} = 2,45$ $FoS_{mean} = 5,04$	$\beta_{MC} = 3,472$ $\beta_{FORM} = 3,497$	$\phi' = 25,27^o$ $\gamma = 19,83$ kN/m^3 $Q_V = 1617$ kN
C (Q_H, G_V, Q_V, 4,0m, Square 0,8m, B = L = ?)	$\overline{G_V} = 3000$ kN $G_{Vk} = 3000$ kN $\overline{Q_V} = 1375$ kN $Q_{Vk} = 2000$ kN $\overline{Q_H} = 207$ kN $Q_{Hk} = 400$ kN	$\gamma_G = 1,0$ $\gamma_Q = 1,3$ $\psi_0 = 0,7$ $\gamma_{\phi'} = 1,25$ $\gamma_\gamma = 1,0$	$B = L = 3,89$m	$FoS_{char} = 2,55$ $FoS_{mean} = 6,54$	$\beta_{MC} = 3,617$ $\beta_{FORM} = 3,720$	$\phi' = 25,57^o$ $\gamma = 20,18$ kN/m^3 $Q_V = 1333$ kN $Q_H = 626$ kN
D (G_V, Q_V, 0,6m, L ?)	$\overline{G_V} = 1200$ kN $G_{Vk} = 1200$ kN $\overline{Q_V} = 412.5$ kN $Q_{Vk} = 600$ kN	$\gamma_G = 1,0$ $\gamma_Q = 1,3$ $\gamma_{\phi'} = 1,0$ $\gamma_\gamma = 1,0$ $\gamma_{Rs} = 1,4$ $\gamma_{Rb} = 1,7$	$L = 16,1$m	$FoS_{char} = 1,56$ $FoS_{mean} = 2,20$	$\beta_{MC} = 3,208$ $\beta_{FORM} = 3,218$	$\phi' = 26,34^o$ $\gamma = 19,76$ kN/m^3 $Q_V = 143,6$ kN
E (q_V, 0,4m, 6,0m, 0,4m, 0,75m, B = ?)	$\overline{q_V} = 6,875$ kPa $q_{Vk} = 10$ kPa	$\gamma_Q = 1,3$ $\gamma_{\phi'} = 1,25$ $\gamma_\gamma = 1,0$	$B = 3,52$m	$FoS_{char} = 3,12$ $FoS_{mean} = 6,88$	$\beta_{MC} = 3,301$ $\beta_{FORM} = 3,326$	$\phi' = 25,48^o$ $\gamma = 20,19$ kN/m^3 $q_V = 14,95$ kPa
F (q_V, 3,0m, L = ?)	$\overline{q_V} = 6,875$ kPa $q_{Vk} = 10$ kPa	$\gamma_Q = 1,3$ $\gamma_{\phi'} = 1,25$ $\gamma_\gamma = 1,0$	$L = 4,00$m	$FoS_{char} = 1,63$ $FoS_{mean} = 2,34$	$\beta_{MC} = 3,351$ $\beta_{FORM} = 3,398$	$\phi' = 25,34^o$ $\gamma = 20,22$ kN/m^3 $q_V = 7,17$ kPa
G (q_V, 0,5m, 3,0m, L = ?)	$\overline{q_V} = 6,875$ kPa $q_{Vk} = 10$ kPa	$\gamma_Q = 1,3$ $\gamma_{\phi'} = 1,25$ $\gamma_\gamma = 1,0$	$L = 2,57$m	$FoS_{char} = 1,25$ $FoS_{mean} = 1,43$	$\beta_{MC} = 3,237$ $\beta_{FORM} = 3,242$	$\phi' = 25,65^o$ $\gamma = 20,30$ kN/m^3 $q_V = 7,29$ kPa

Figure 1. Results of analysis for example problems

The strip footing chosen for this analysis is the same example used by Simpson (2007) and is shown in Figure 2. The required width of footing for both design approaches is shown in Figure 3a and the corresponding reliability indices in Figure 3b. From Figure 3b, it is clear that the reliability the footing designed using DA2* is considerably lower than for design approach DA2 for high Hk/Vk.
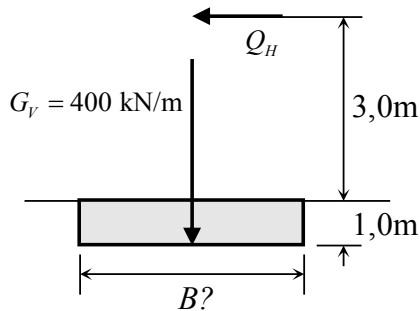
Q_H variable,
$CoV = 0.5$ (Gumbel)

$\overline{\phi}' = 36.1^o$, $CoV = 0,1$ (Log-normal)
$\overline{\gamma} = 19$ kN/m^3, $CoV = 0,05$ (Normal)
$\phi'_k = 32,5^o$
$\gamma_k = 19$ kN/m^3

Figure 2. Strip footing example, DA2*
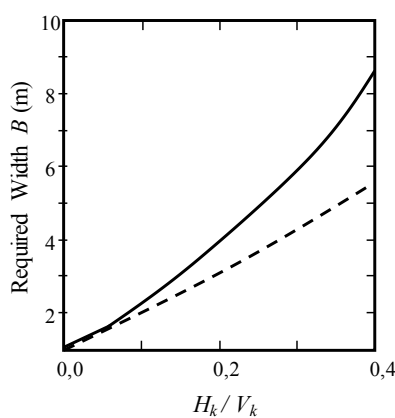
Figure 3a. Required footing width
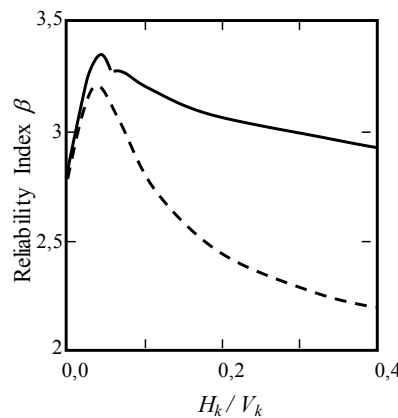
Figure 3b. Reliability index

5. CONCLUSIONS

The First Order Reliability Method (FORM) is sufficiently accurate and easy to apply to justify its use in a geotechnical design office. The major problem remains obtaining sufficient data to justify the choice of input parameters. Limit states design is acceptable for routine design purposes.

DA2* gives significantly lower levels of reliability for highly eccentric loads than DA2.

REFERENCES

[1] DeKoker, N. and Day, P.W. (2017). Assessment of reliability based design for a spectrum of geotechnical design problems. ICE Geot. Engineering, 171(3); 147-159.

[2] Frank, R., Bauduin, C., Driscoll, R., Kavvadas, M., Krebs Oversen, N., Orr, T., and Schuppener, B. Designers' guide to EN1997-1. Thomas Telford: p77.

[3] Low, B.K. and Tang W.H. (2007). Efficient spreadsheet algorithm for First-Order reliability method. ASCE J. Eng. Mechanics, 133(12): 1378-1387.

[4] Orr T.L.L. (2005). Design examples for the Eurocode Workshop. Evaluation of Eurocode 7. Trinity College, Dublin: 67-74.

[5] Phoon, K.K. and Khulawy, F.H. (1999). Characterisation of geotechnical variability. Canadian Geotech Journal, 36: 612-624.

[6] Retief, J.V. and Dunaiski, P.E. (2010). The limit states basis for structural design for SANS 10160-1. Background report to SANS 10160, African SunMedia, Stellenbosch: Ch. 1-2.

[7] Schneider, H. (1997). Panel discussion: definition and determination of characteristic values of soil properties. Proc. 14th Int. Conf. Soil Mechanics and Foundation Eng., Hamburg, Vol 4: 2271-2274.

[8] Simpson, B. (2007). Approaches to ULS design – the merits of Design Approach 1 in Eurocode 7. 1st Int. Symp. on Geotech. Safety and Risk, Shanghai, China: 527-538.

[9] Vogt, N. and Schuppener, B. (2006). Implementation of Eurocode 7-1 in Germany. Int. Symp. New Generation Design Codes for Geotechnical Engineering Practice. Taipei, Taiwan: 1-12.

Authors

Zlatko Srbinoski

PhD, Full Professor

Ss. Cyril and Methodius University

Faculty of Civil Engineering – Skopje

email: srbinoski@gf.ukim.edu.mk

Zlatko Bogdanovski

PhD, Assistant Professor

Ss. Cyril and Methodius University

Faculty of Civil Engineering – Skopje

email: bogdanovski@gf.ukim.edu.mk

Filip Kasapovski

MSc, assistant

Ss. Cyril and Methodius University

Faculty of Civil Engineering – Skopje

email: kasapovski@gf.ukim.edu.mk

Tome Gegovski

MSc,

Ss. Cyril and Methodius University

Faculty of Civil Engineering – Skopje

email: gegovski@gf.ukim.edu.mk

TISSOT COMPENSATION PROJECTION FOR THE TERRITORY OF MACEDONIA

Presenting of Earth area in the plane is always followed with deformation of angles, lengths and areas. Attempting to find cartographic projection for successful minimizing deformation of basic elements was occupation of many cartographs in the past. In this group, the most important is French cartographer M. A. Tissot.

In this work are presented basic characteristic and formulas of Tissot compensation projection. This projection have characteristic for minimizing deformation of angles and lengths, and also have wide usage in cartography especially in the field of states cartographic projection. In common with basic characteristic of projection, in this paper are presented the aspects of use of Tissot compensation projection in the mapping of territory of Republic of Macedonia.

Key words: states cartographic projection, Tissot compensation projection, minimal deformations.

1. INTRODUCTION

Presentation of the curved surface of the Earth on plane is always accompanied by certain deformations of angles, lengths and surfaces. The efforts to find a cartographic projection that can successfully minimize the deformations of the basic elements were the preoccupation of several cartographers. In this respect, the most prominent place belongs to the French cartographer Tissot, who suggested several ways of depicting a part of the Earth's surface on plane from which particular significance has the projection presented in the paper "Memoire sur la représentation des surfaces et les projections des cartes géographiques", which in the literature is known as the Tissue Compensative Projection.

The "compensation" of the projection is due to special concessions referring to the deformations of the angles and the distances, in order to obtain projection of a given territory with an absolutely minimal deformation of angles and distances. Due to this feature, the Tissot projection has a very large application in the

cartography, especially in the field of defining of state cartographic projections. In doing so, this projection serves as a benchmark for comparing other projections of the spectrum of possible (conformal) cartographic projections. The Tissot compensatory projection is also significant because of the fact that it answers the question of the size of the territory that can be projected into one coordinate system, that is, in one projection plane, according to a predetermined deformation of lengths.

2. BASIC CHARACTERISTICS OF THE TISSOT PROJECTION

Tissot proposed his projection for mapping territories with relatively small dimensions, i.e. for territories where the differences in the latitudes and longitudes of the extreme points (expressed in absolute measure) are smaller than the unit, taking into account the unit value of the circle arc: $\rho^o = 57^o.29578$, which actually represents the circle arc value of the angle of a radian ($\rho = 1^{rad}$).

The basic task as in all projections is reduces to the definition of the functions f_1 and f_2 which define the analytical relationship between the geographical coordinates of a point on the Earth's ellipsoid and the Cartesian coordinates of the same point in the projection plane.

Instead of geographical coordinates (φ and λ), Tissot introduces s and t, which relate to the auxiliary coordinate system, whose coordinate start is at the central point of the mapped territory. In addition, s represents the length of the arc of the meridian of the middle parallel of the mapped territory by the latitude φ_o, to the parallel across the point T with latitude φ_T, while the coordinate t represents the length of the arc of the middle parallel with the latitude φ_o of the mean meridian with longitude λ_o to the meridian through the point T with latitude λ_T. The coordinates s and t are defined according to known expressions for determining the arc length of a meridian and parallel. By introducing a new coordinate system, the Cartesian coordinates x and y are defined as functions of the coordinates s and t:

$$x = a_1 + a_2 s + a_3 t + a_4 s^2 + a_5 st +$$

$$a_6 t^2 + \frac{A}{3}s^3 - B\ s^2 t + C\ st^2 + \frac{D}{3}t^3 + ...$$

$$y = b_1 + b_2 s + b_3 t + b_4 s^2 + b_5 st + b_6 t^2$$

$$+ \frac{A'}{3}s^3 + B's^2 t - C'st^2 + \frac{D'}{3}t^3 + ... \tag{1}$$

Unknown coefficients (a_1-a_6, b_1-b_6, A, B, C, D, A', B', C' and D') Tissot determined it by introducing additional conditions for the projection, and after satisfying the conditions, the polynomials for x and y continue to retain the character of convergent progression. The mentioned conditions of the projection are as follows:

1. The coordinate start of the ellipsoid has the coordinates φ_o and λ_o, and coincides with the central point of the territory being mapped. It is also the coordinate start of the Cartesian coordinates in the plane. Axes x and y are defined as tangents of the corresponding meridian, or parallel at the coordinate start.

2. The deformations of the lengths at the coordinate start, that is, at the central point of the territory being mapped, should be equal to zero. The coordinate start in all directions (and therefore in the direction of meridian and parallel) is not changed and is equal to the unit.

3. The sizes (1-m) and (1-n), which represent the deformations of the lengths in the direction of the meridian and the parallel, must not contain the members of the first potencies of s and t, and they can differ from each other for the members of the third potencies of s and t.

4. The angle between meridians and parallels in projection can differ from 90° only for members of the third potencies of s and t.

5. Differences (m-n) and (90-Θ), respectively Θ may not depend on members that contain the second potencies of s and t. Θ represents the deformation of the angle (Θ) that forms the meridians and the parallel in the projection and is defined as:

$$\varepsilon = 90 - \Theta \tag{2}$$

Applying the stated conditions, we arrive at the definitive expressions for determining the Cartesian coordinates (x and y) in the Tissot compensation projection, which according to (*Borčić, 1955*) and (*Stojanovski, 1960*) read:

$$x = s + \frac{\sin \varphi_o}{2r_o}t^2 + \frac{A}{3}s^3 - B\ s^2 t + C\ st^2 + \frac{B}{3}t^3$$

$$y = \frac{r}{r_o}t + \frac{B}{3}s^3 + As^2 t - Bst^2 + \frac{C}{3}t^3 \tag{3}$$

Z.Srbinoski, Z. Bogdanovski, F. Kasapovski, T.Gegovski

The terms (3) define the projection in which the deformations of the lengths depend on the second-row members, while the deformations of the angles depend only on the members of the third row. Given the minimal deformations of the angles, the Tissot projection is distinguished by *practical* conformity, and the expression which determines the scales in the direction of the meridian and the parallel is:

$$m = n = 1 + As^2 - 2Bst + \left(\frac{1}{2} - A\right) t^2 \quad (4)$$

The determination of the constants A, B, and C, as well as the coordinates φ_o and λ_o of the coordinate start, are carried out under the condition that the linear deformations (m - 1) are minimal. To this end, the expression (4) gets a new shape:

$$As^2 - 2Bst + \left(\frac{1}{2} - A\right) t^2 - (m - 1) = 0 \quad (5)$$

To determine the coefficients A and B, two new variables are introduced -F and ε.

$$\tan\varepsilon = \frac{B}{A - \frac{1}{4}} \qquad F - \frac{1}{4} = \left(A - \frac{1}{4}\right) \sec\varepsilon \quad (6)$$

Angle ε is function of rotation (α) between the coordinate system with axes s and t and the local coordinate system of the ellipse of equal deformations:

$$\varepsilon = 2 \ (90^o - \alpha) \quad (7)$$

Figure 1 shows two coordinate systems with a common coordinate start. The coordinate axes of the system (u, v) overlap with the ellipse axes.
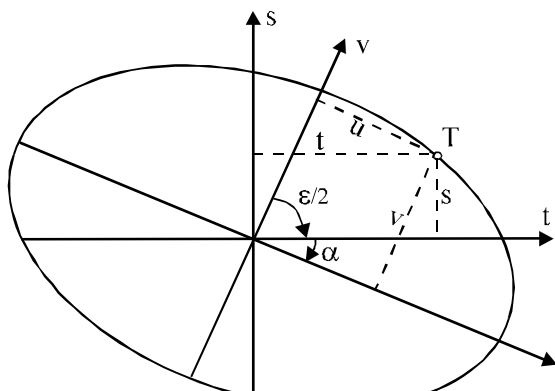
Figure 1. Coordinate system of the ellipse of deformations

To switch from one system to another, it is necessary for the axes s and t to rotate in the direction of the clockwise movement by α.

Examining the characteristics of the projection, Tissot proved two very important properties of the ellipse of deformations.

1. The square of the fourth of the diameter which with the axes of the ellipse (u, v) closes an angle of 45°, is equal to the deformation of the lengths of this projection, that is:

$$\left(\frac{\rho_{45^o}}{4}\right)^2 = m - 1 \quad (8)$$

ρ_{45^o} - the diameter of the ellipse which with the axes (u, v) closes the angle from 45°

2. The square of the axes of the so-called ellipse are inversely proportional to the sizes F and (1/2-F).

Based on the second attribute, the value of the coefficient F is determined according to the expression:

$$F = \frac{b^2}{2 \ (a^2 + b^2)} \quad (9)$$

a, b -semi-axes of the ellipse of deformations

The procedure for defining the basic parameters of the Tissot projection (coordinate start and coefficients) is graphic-analytic *(Stojanovski, 1960)*. To that end, it is necessary to construct a map in a small scale on the mapped area, on which the distinguished points from the border line are clearly defined.

The map can be made in some projection or constructed on the basis of calculated coordinates (s and t) for the boundary points in relation to the center of the territory with φ_o and λ_o, in which is placed the coordinate system defined by the axes s and t. After the creation of an auxiliary map, a certain number of ellipses with different ratio of their axes a/b are constructed and they are applied to the transparent paper. Thus the constructed ellipses are placed in a row on the map and their rotation and displacement are done until a position is determined which will cover the entire draft of the auxiliary map. For ellipses that cover the entire map (and they touch it in several border points), calculation is performed of their diameter ρ_{45} according to the expression (10) or it can be read graphically.

$$\rho_{45^o} = \frac{2ab\sqrt{2}}{\sqrt{(a^2 + b^2)}} \quad (10)$$

After comparing the obtained results, the ellipse that has a minimum diameter it represents the boundary ellipse. After the *boundary ellipse* is established, the elements are read and calculated for the Tissot projection, which will serve to define the expressions for the Cartesian coordinates x and y, as follows:

- First, geographic coordinates are read (φ_o and λ_o) at the center point of the boundary ellipse relative to the auxiliary map.
- Angle $\varepsilon/2$, which close the semi axis of the boundary ellipse with the coordinate axes s and t, are read directly from the map.
- After determining the rotation angle, according to the expression (9), calculation of the coefficient F is performed.
- Coefficients A and B, as a function F and ε, are calculated according to the expressions:

$$A = \left(F - \frac{1}{4}\right)\cos \varepsilon + \frac{1}{4} \qquad B = \left(F - \frac{1}{4}\right)\sin \varepsilon \quad (11)$$

- Coefficient C is calculated based on the read value of the main parallel φ_o and the calculated coefficient A, according to the expression:

$$C = \frac{\cos 2\varphi_o}{2\cos^2 \varphi_o} - A = \frac{1}{2} - A - \frac{1}{2}\tan^2 \varphi_o \quad (12)$$

This procedure defines the basic parameters of the Tissot projection, which can be used to determine the Cartesian coordinates at any point in the mapped territory.

3. ELEMENTS FOR DEFINING THE TISSOT PROJECTION FOR THE TERRITORY OF MACEDONIA

3.1 CONSTRUCTION OF AN AUXILIARY MAP AND DEFINING THE BOUNDARY ELLIPSE OF DEFORMATIONS

The classic approach to the auxiliary map construction, which is used to determine the boundary ellipse in the Tissot projection, requires the choice of a central point in the mapped territory. This point is defined by the coordinates φ_o and λ_o. Then the coordinate differences (φ - φ_o) and (λ - λ_o) are determined between the characteristic boundary points and the center point, and they are shown in a given scale to a paper, giving an approximate image of the mapped area, with precisely defined border points.

The elaboration of this paper avoided the classical approach, and the auxiliary map was obtained by scanning and digitizing cartographic maps in scales 1:200000 (TK 200). Thus, the Macedonia's border line is defined in digital form, with relatively high accuracy and as such it is suitable for further processing and determination of the parameters of the Tissot projection. The auxiliary map is additionally oriented in the existing state coordinate system and georeferenced, thus obtaining a map in the scale of 1:1000000 on which the geographic coordinate network is applied.

On the map are marked 17 characteristic points for which Gauss-Kruger and geographical coordinates are determined (Figure 2). The above points also include the extreme points on the territory of Macedonia - the most northern, the most eastern, the southernmost and the westernmost.
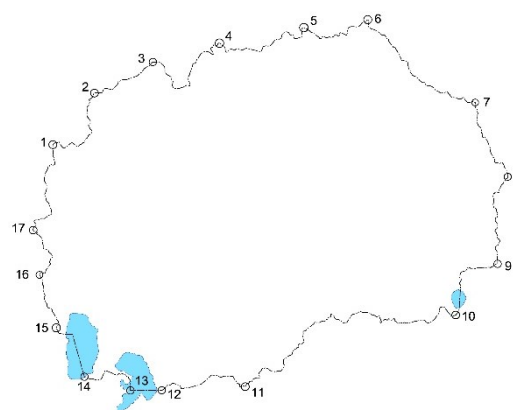
Figure 2. Characteristic borderline points of state territory

On the basis of the so-defined basis, several ellipses have been constructed, which, with the help of translational displacement and angular rotation, are brought into a position to cover the entire state territory and, in addition, to tangent it in several border points. The purpose of the above procedure is to detect the ellipse that best adapts to the shape of the mapped territory, with the diameter of the ellipse, which with its axes occupies an angle of 45°, has a minimal value. This creates a *boundary ellipse* that defines the length deformations in the Tissot projection. To the border ellipse for the territory of the Macedonia, more than 40 trials have been done, some of which whit more characteristic results are presented in tab. 1. The values of the parameters of the test ellipses are expressed in millimeters which because of the scale of the auxiliary map define kilometers in nature.

Z.Srbinoski, Z. Bogdanovski, F. Kasapovski, T.Gegovski

Table 1. Trial ellipses for determining
the boundary ellipse

Point num.	Tangent boundary points	a (mm)	b (mm)	ρ_{45} (mm)
1	6, 8, 14	100.0	98.0	198.0
2	2, 6, 10, 14	125.0	83.5	196.4
3	**2, 6, 10, 13, 14**	**130.0**	**81.5**	**195.3**
4	2, 3, 6, 10, 13	135.0	80.5	195.6
5	3, 6, 10, 11, 13	150.0	78.5	196.7

From the table it can be concluded that the boundary ellipse for the Tissot projection of Macedonia is the ellipse under number 3, which has a minimum diameter:

$$\rho_{45} = 195.3 \text{ mm (km)}$$

and semi-axes:

a = 130.0 mm (km) and **b = 81.5 mm (km).**

After the establishment of the position of the main border ellipse on the auxiliary map, the location of the center from the ellipse was deter-mined, which also represents the coordinate start for Tissot compensation projection of Macedonia. The geographical location at the coordinate start is presented in Figure 3, from which it can be seen that it is located near the village of Izvor, southwest of Veles.

The Gauss-Kruger coordinates of the center are directly read on the screen and they are:

Y_o = 7 562 050 m X_o = 4 606 550 m

Applying the formulas for the second geodetic task of the Gauss-Kruger projection, the geographical coordinates of the center of the projection can be calculated and they have the following values:

φ_o = 41° 36' 00" λ_o = 21° 44' 40"
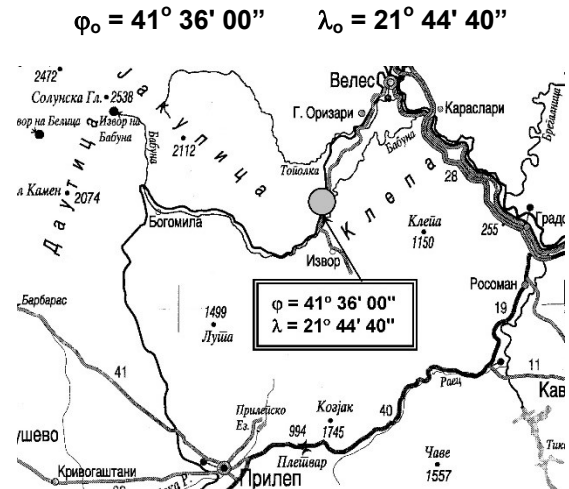
Figure 3. Geographic position of the centre of the projection

Angle of rotation (α) between the axes of the ellipse and the coordinate system (s, t) is graphically read from the auxiliary map and its value is:

α = -15° 00' 45"

The position of the boundary ellipse of the Tissot projection and its orientation with respect to the border line from the territory of Macedonia is presented in Figure 4.
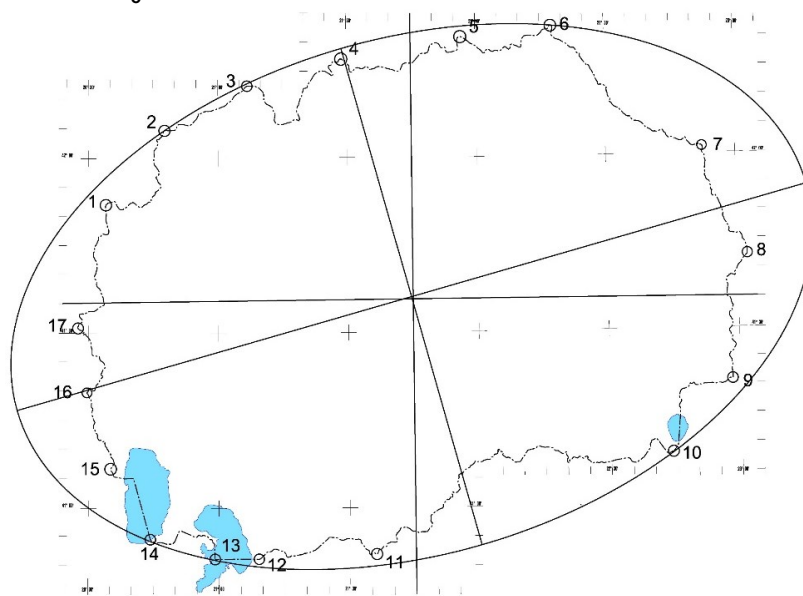
Figure 4. Border ellipse of deformations

3.2 CALCULATING COEFFICIENTS FROM TISSOT COMPENSATION PROJECTION

The values of the angle ε and the coefficient F are determined according to the expressions (7 and 9) are:

$$\varepsilon = 210^o \, 01' \, 30" \qquad F = 0.1410708407$$

The coefficients A and B, as functions of ε and F, are defined by the expressions (11), while the value of the coefficient C is determined by A and the geographic latitude of the projection center (φ_o) according to the expression (12).

$$A = 0.3443116455 \qquad B = 0.05450573606$$

$$C = -0.2384429508$$

3.3 LINEAR DEFORMATIONS AND ISOCOLS IN THE TISSOT PROJECTION

Linear deformations in the Tissot projection can be calculated according to the expression (8) and their value of the boundary ellipse itself is:

$$(m-1) = \left(\frac{\rho_{45^o}}{4}\right)^2 = 2383.9 \ mm^2 (km^2)$$

The linear deformation at any point of the projection is determined by expression (4) and the same expression is also suitable for controlling the calculated coefficients of the projection. In this case, a point that lies on the boundary ellipse is taken, its coordinates s and t are read, and an identical value of the linear deformation with the deformation obtained by expression (8) should be obtained by applying the expression (4).

To obtain the maximum linear deformation, as a relative value with dimensions cm / km, it is necessary to multiply the deformations (m-1) by the expression:

$$\frac{100000}{(MR_o)^2}$$

M - scale of the auxiliary map (1:1000000);

R_o - mean radius of curvature of the center of projection.

The mean radius of curvature in the center of Tissot projection for Macedonia, with latitude $\varphi_o = 41^o \, 36'$ is (*Srbinoski, 2001*):

$$R_o = 6 \, 374 \, 834.043 \ m$$

Thus it comes to the value of maximum linear deformation Tissot compensation projection of Macedonia, which is:

6.0 cm/km

The indicated size is the smallest possible value of the linear deformations that can cover the entire territory of our country *in one coordinate system*.

Lines that merge points with identical linear deformations in the Tissot projection are ellipses, which in the coordinate system (s, t) are defined by the expression (5). The construction of the iscols is facilitated in the coordinate system of the ellipses of deformations with the axes u and v. The axes of this system occupy the angle α with the axes of the system (s, t), and the isocols are defined by the large and small semi-axis, which are obtained according to the following expressions:

$$u = a = \sqrt{\frac{(m-1)}{F}} \qquad v = b = \sqrt{\frac{(m-1)}{\frac{1}{2}-F}} \qquad (13)$$

The isocols in the Tissot projection of Macedonia, determined according to the expressions (13), are given in Table 2, and their graphic representation is given in Figure 5.

Table 2. Isocols of the Tissot projection of Macedonia

Deformations (cm/km)	Isocols (ellipse)	
	a (km)	b (km)
0	0	0
1	53.7	33.6
2	75.9	47.6
3	93.0	58.3
4	107.3	67.3
5	120.0	75.2
6	130.0	81.5

Figure 5. Isocols in the Tissot projection

Z.Srbinoski, Z. Bogdanovski, F. Kasapovski, T.Gegovski
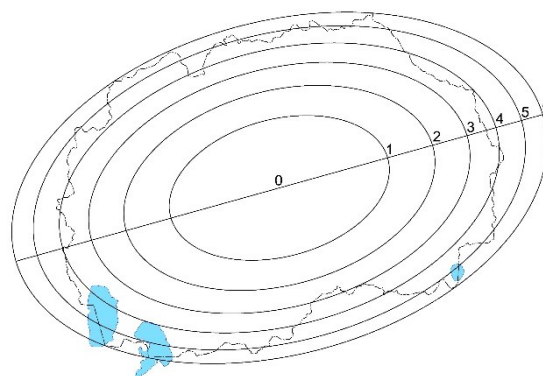
To reduce the absolute size of the deformations it is necessary to reduce the Cartesian coordinates obtained according to the expressions (3) with a module (m) which is determined according to the expression (*Srbinoski, 2001*):

$$m = 1 - \frac{1}{2}\Delta d_{max} = 0.99997 \qquad (14)$$

Δd_{max} - maximum linear deformation of the projection

In this way, the maximum linear deformation (by absolute value) is reduced by half, and deformations in the Tissot projection are distributed in the range from **-3 cm / km** to **+3 cm / km.**

The isocols in the Tissot projection defined by their large and small semi axes, after performing the said reduction, are presented in Table 3, and their graphical representation - in Figure 6.

Table 3. Isocols of Tissot compensation projection after the reduction

Deformation (cm/km)	Isocols (ellipse)	
	a (km)	b (km)
-3	0	0
-2	53.7	33.6
-1	75.9	47.6
0	93.0	58.3
1	107.3	67.3
2	120.0	75.2
3	130.0	81.5
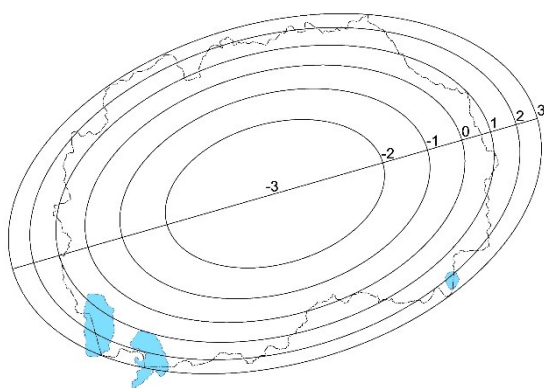
Figure 6. Isocols in Tissot projection after the reduction

The average linear deformation on the whole territory of the Republic of Macedonia is in the Tissot compensation projection:

$$\Theta = 2.34 \text{ cm/km}$$

After the reduction of the Cartesian coordinates and the introduction of a secant-variant of the Tyson projection, the average linear deformation gets a value:

$$\Theta = 1.32 \text{ cm/km}$$

which is an exceptional result that cannot be obtained by applying any other cartographic projection.

5. CONCLUSIONS

On the basis of the above, the basic properties of the Tissot projection for Macedonia can be sublimated:

- Because of its capacity to minimize linear deformations, the Tissot projection is the basis for comparing and evaluating other conformal projections when choosing a state cartographic projection.

- Although the projection in its basis is not conformal, it is characterized by practical conformity (especially when projecting small territories), due to the minimal deformations of angles that depend only on the third movements of the coordinates s and t.

- The boundary ellipse of deformations (for Macedonia) is defined by the parameters:

  a = 130 mm,   b = 81.5 mm   and

  $$\alpha = -15^o \ 00' \ 45"$$

  and the center of the projection, as well as the coordinate start of the Cartesian coordinate system, is located at the point:

  $$\varphi_o = 41^o \ 36' \ 00" \qquad \lambda_o = 21^o \ 44' \ 40"$$

- The maximum linear deformation that arises from the shape and dimensions of the boundary ellipse, in the Tissot projecti-on of Macedonia is **6 cm/km**.

- The average linear deformation of the entire state territory is 2.34 cm/km.

- Increasing the accuracy of the projection is achieved by modulating the Cartesian co-ordinates with a module m = 0.99997, i.e. by introducing a negative linear deformati-on of -3 cm/km, which allows the entire territory of Macedonia to be covered by deformations that are not larger from ±3 cm/km.

- After the reduction, the average linear deformation is 1.32 cm/km.

- The layout of the linear deformations is correct, and the isocols have the form of centric ellipses.

REFERENCES

[1] Borčić B. (1955): Mathematical mapping (cartographic projections), Technical book, Zagreb.

[2] Jovanovic V. (1983): Mathematical Cartography, VGI, Belgrade.

[3] Srbinoski Z. (2001): Enclosure to research on defining a new state cartographic projection, Doctoral dissertation, University "St. Cyril and Methodius ", Skopje.

[4] Srbinoski Z. (2009): Mathematical Cartography, Faculty of Civil Engineering - Skopje.

[5] Srbinoski Z. (2018): Study on the selection of a new state cartographic projection, Agency for Real Estate Cadastre, Skopje.

[6] Stojanoski K. (1960): The thistle compensatory projection for the territory of the FPR Yugoslavia, Habilitation dissertation, University "Ss. Cyril and Methodius", Skopje.

Z.Srbinoski, Z. Bogdanovski, F. Kasapovski, T.Gegovski

DATA PROCESSING FROM PRECISE LEVELLING IN SEISMIC ACTIVE REGIONS

AUTHORS

Filip KASAPOVSKI
MSc, assistant
Ss. Cyril and Methodius University
Faculty of Civil Engineering – Skopje
email: kasapovski@gf.ukim.edu.mk

This paper presents the processing of the data from the precise levelling measurements in the seismic active area of the Skopje valley. Precise levelling results are affected by the Earth's gravity field, to eliminate the effect of the gravity field gradient, corrections need to be applied in processing of precise levelling data. For this purpose the processing of levelling data is performed together with GNSS coordinates and gravity data, which are acquired on a part of the state levelling network from first order, located on the territory of the City of Skopje. They are used for transformation of the height differences in the system of dynamic, orthometric and normal heights. Also other corrections are applied to observed levelling data to minimize the effects of known systematic errors.

Key words: precise levelling, gravity, corrections, data processing, orthometric, height systems.

1. INTRODUCTION

If the height differences between points A, B, and C (Figure 1) would be determined only by applying a geometric levelling, then the results of the levelling, which previously are not considered to be laden by accidental and systematic errors, would indicate the following:

- Between points A and B, which are on the same level surface, there is a height difference,
- The value of leveled height differences depends on the path of levelling,

$$\int_A^C dh \neq \int_B^C dh, \qquad (1)$$

- The sum of height differences in a closed polygon is not zero.

$$\oint dh \neq 0, \text{ i.e. } \sum_i \Delta h_i \neq 0, \qquad (2)$$

In order to eliminate these effects, it is necessary to introduce the influence of the gravity force in the results of the measurements. [1]

As it is well known, the Earth's gravity varies according to the locations of observation points. The gravity field is stronger on the poles and weaker on the equator due to the centrifugal effect of the rotating Earth. The variations in the gravity field are also due to the heterogeneous nature of the Earth's interior and crust.
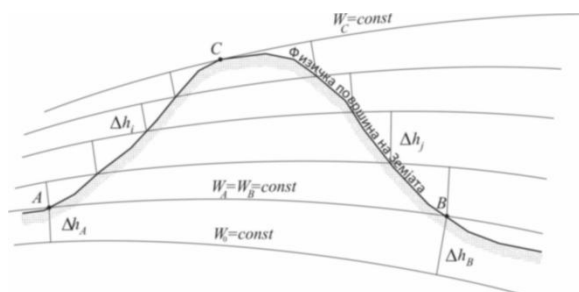
Figure 1. Dependence of the results of the levelling from the levelling path [1]

The processing of the results from the measurements in the levelling network of high accuracy has been carried out in two parts. [1]

The first part of the processing involved:

- Checking the quality of the measured data, in which the conditions defined by the parameters for controlling and monitoring the measurements are independently checked,
- Entering corrections in all height differences for the influence of the mean meter of the relevant pair of rods,
- Transformation of the height differences in the system of geopotenital, dynamic, orthometric and normal heights.

The second part of the processing involved the adjustment of the height differences in all listed height systems, with the fundamental benchmark in Skopje - FRSK adopted for the network's datum.

2. HEIGHT SYSTEMS

The ideal height system must meet the following conditions:

- The height of the points must be unique (they should not depend on the levelling direction),
- In closed polygons, height differences must be determined in such a way that their sum is zero (the closure of the polygon when determining the height systems must be eliminated),

- The heights must be determined only on the basis of the measurements of the physical surface of the Earth without the introduction of hypotheses,
- The reference surface of the heights must be physically clearly defined,
- The heights must have a unit of measure,
- The heights must have a geometric interpretation,
- The heights must be able to connect with the height networks of neighboring countries.

All the aforementioned requirements cannot be provided simultaneously because the first two conditions are fulfilled only when the differences in the Earth's gravity are used to determine the height of the points. In that case, the heights do not have a geometric interpretation nor have a unit of measure.

In this direction, a number of height systems are proposed which can satisfy only one of the quoted conditions, most often used are the following: geopotential, orthometric, normal, dynamic and spheroidal heights.

2.1 GEOPOTENTIAL NUMBERS

For the unambiguous determination of the height of the points, regardless of the path of levelling, the potential difference is used.

Practically the geopotential numbers are using the results of the measurements of the acceleration of the gravity force and the levelling for computing the line integral:

$$C_{P_i} = dW = -\int_{P_i}^{P_0} g \cdot dh = \int_{P_0}^{P_i} g \cdot dh \approx \sum_{k=P_0}^{P_i} g_k \cdot \Delta h_k \qquad (3)$$

Units of the geopotential numbers are the units of potentials, $m^2 s^2$. The same year, when it was proposed by the International Association, it was decided that the geopotenital height will be with unit **1 g.p.u = 1 kgal • m**, where g.p.u. is shortcut for a *geopotential unit*.

The heights determined with the use of geopotential numbers are not suitable for practical application because they do not have a geometric interpretation, and the unit of geopotential numbers is not a unit of length. For these reasons, the physical heights for practical applications are defined in another way. [1]

If the value of the geopotential number is divided by the contracted value of the

acceleration of the gravity force of the earth gravity (G),

$$H = \frac{C}{G}, \qquad (4)$$

a simple transformation of the geopotential number in metric heights will be performed, and the characteristics of the geopotential number will be retained.

Different G values define different *heights systems*.

2.2 DYNAMIC HEIGHTS

The height difference in the system of dynamic heights can be calculated in two ways:

- Directly from the difference of geopotential numbers,
- By calculating dynamic correction.

Dynamic correction and dynamic height difference is obtained as:

$$\Delta H_{DYN} = \Delta H + DC, \qquad (5)$$

$$DC = \frac{g - \gamma_0}{\gamma_0} \cdot \Delta H, \qquad (6)$$

where *DC* is dynamic correction and γ_0 is normal gravity.

For normal gravity γ_0 it is necessary to adopt a value calculated for the 45^0 latitude. Calculating the value of the normal gravity is to be done by using the expression associated with GRS80 geodetic reference system. [8]

2.3 ORTHOMETRIC HEIGHTS

Orthometric height of the point P is called the vertical section from point P to the geoid (Figure 2)
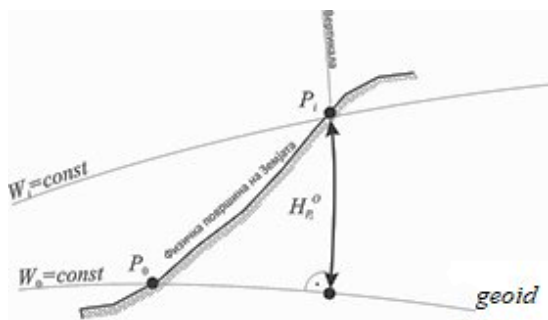
Figure 2. Orthometric heights [1]

Orthometric heights are calculated by the expression:

$$H_P^O = \frac{C_P}{\bar{g}_P} \qquad (7)$$

where the C_P is the geopotential number of the point P, and $\bar{g}_P$ the mean value of the acceleration of the earth's gravity of the vertical between the points P_0 and P. [9]

$$OP_{1,2} = H_{P_1}^O \cdot \frac{\bar{g}_{P_1} - G_0}{G_0} - H_{P_2}^O \cdot \frac{\bar{g}_{P_2} - G_0}{G_0} + \sum_{k=P_1}^{P_2} \frac{g_k - G_0}{G_0} \Delta h_k \qquad (8)$$

Above is the formula for calculating the orthometric correction. Points that have the same orthometric heights are not on the same real level surface, since it follows that the orthometric heights simulate fall.

Poincare Prey reduction

The value of the acceleration of Earth force gravity on the vertical segment from P to P_0 is not known and cannot be accurately determined neither by measurement nor by calculation. For the practical realization of the orthometric heights it is necessary to approximate with the aid of hypotheses about the mass distribution of the part of the earth's crust, between the physical surface of the Earth and the geoid. [1]

One of the ways to calculate the inner value of the acceleration of the force of the earth's gravity is by applying the Poincare Prey reduction.

$$g_Q \approx g_P - 0.84807 \cdot 10^{-6} \cdot (H_Q - H_P) \qquad (9)$$

The Poincare-Prey reduction does not take into account the influence of the topographic masses on the acceleration of the force of the earth's gravity (i.e. it neglects the influence of the masses that are over and the impact of the deficit within the Bouguer's plane).

2.4 NORMAL HEIGHTS

For the calculation of the normal height difference it is necessary to apply the so-called normal correction, indicated below with f on the obtained average height difference.

The normal correction is also called gravimetric correction and reflects the impact of the gravitational field or the non-parallelness of the level surfaces along the line levelling route.

The normal correction to the individual height difference is a sum of two parts: [2]

$$f_{i,i+1} = I_{i,i+1} + II_{i,i+1},$$

(10)

where:

$$I_{i,i+1} = -\frac{1}{\gamma_m}\left(\gamma_0^{i+1} - \gamma_0^i\right)H_m$$

(11)

It's called *first normal correction,*

$$II_{i,i+1} = \frac{1}{\gamma_m}(g - \gamma^N)_m h_{i,i+1}$$

(12)

It's called *second normal correction.*

The formula set for the first normal correction in the Level I and II Level Instruction, GUGKK, 1980 is as follows:

$$I = -\frac{\beta}{\rho'}sin2\varphi\Delta\varphi H_m \; [mm],$$

(13)

According to the Level I and II instructions, the gravimetric data and the method of processing must guarantee an error in determining the normal correction not greater than 0.05 mm and with exception in the high parts 0.10 mm. [2]

3. CORRECTIONS APPLIED TO PRECISE LEVELLING OBSERVATIONS

To achieve the highest degree of accuracy in the measurement of elevation differences corrections must be applied to precise levelling observations. Observational procedures have also been designed to provide the most effective method to acquire data. In addition, those systematic errors which cannot be sufficiently controlled by instrumentation or observational techniques are minimized by applying appropriate corrections to the observed data. [4]

Rod scale correction

Precise levelling rods should be calibrated before and after each project if practical, whenever possible damage has occurred, or at least once during each year of use. The calibrated length of a rod is usually determined by comparing its invar strip to a standard meter. The length excess of an average rod meter is computed from the "actual minus nominal" length differences observed at several points along the rod. The correction for the pair of rods mean meter is entered in the levelling results derived by concrete levelling rods. This correction ensures a uniform scale.

Level collimation correction

The effects of the collimation error of a levelling instrument are best minimized by field procedures. If sight lengths are balanced, i.e., DS = 0 and SDS = 0, where DS is the difference between backward and forward sight lengths at one setup (DS = backsight distance - foresight distance) and SDS is the accumulated DS for a section, the effect of the collimation error approaches zero. A well-adjusted instrument also minimizes this error without balancing sight lengths, although the collimation error of most levelling instruments changes slightly throughout the day as a result of changing temperature. A test for checking the levelling instrument collimation error is the two peg test, which must be carry out before starting the measurements.[4]

Refraction correction

The most suitable formula for the correction of the height differences, arising from the vertical refraction, is a simplified version of the model developed by Professor T. J. Kukkamaki of the Finnish Geodetic Institute (Kukkamaki 1939).[6]

The vertical temperature gradient in the ground aerial layer determines the degree of influence of the refraction on the results of the geometric levelling. Temperature measurement levels are suggested by Kukkamaki, 1938 at heights of 0.3 m, 0.9 m and 2.7 m on the rods or the ratio between two adjacent heights is 1/3. [3]

3.1 ASTRONOMIC CORRECTION

The astronomic correction is applied to account for the effect of tidal accelerations due to the Moon and Sun on the Earth's equipotential surfaces. The astronomic correction is small, amounting, at most, to 0.1 mm/km, but it accumulates in the north-south direction.

The required input for the correction is: time and date of measurements, heights of the benchmarks, and geodetic positions of the "From" and "To" bench marks. [4]

Tidal correction to normal height differences

The determination of normal height differences in the zero-tidal system, according to EUREF, 2008:

$$H_2(\varphi) = -295.41\sin^2\varphi - 0.42\sin^4\varphi + 99.40 \ [\text{mm}]$$
(14)

Add the value computed from the formula above to normal heights in the mean tidal system to get normal heights in the zero tidal system.

Tidal correction to geopotenital numbers

$$W_2(\varphi) = -288.41\sin^2\varphi - 1.95\sin^4\varphi + 97.22 \ [\text{mgpu}]$$
(15)

Add the value computed from the formula above to geopotential numbers in the mean tidal system to get geopotential numbers in the zero tidal system. [7]

4. DATA PROCESSING

In the data processing for the precise levelling measurements the following data is used as input data:

- The results of the measurements of the height differences shown in the levelling field book,
- Gravity data for the levelling benchmarks,
- Terrain forms in which are described benchmarks location and coordinates in ETRS89 system. [2]

4.1 METHODS OF MEASURMENT AND USED INSTRUMENTS

Levelling measurements

For the measurement of height differences the precise digital level **Leica DNA 03** is used, equipped with two three metre barcoded levelling rods with invar tape, with original holders and metal slippers. The instrument has a declared accuracy of **0.3 mm/km.** During the measurement, readings and registration of the temperature values were performed. With the applied measurement methodology and the levelling instrument used, the relative accuracy of determining the height difference is better than **+/- 1 mm • km$^{1/2}$**. [5]

Gravimetric measurements

The value of the acceleration of the force of gravity (g) at the sites where the benchmarks are stabilized is determined by applying relative gravimetric measurements. Gravimetric measurements are performed using the method of profiles using gravimeters of the type Scintrex CG3 and Scintrex CG5, by performing 3 cycles of measurements of 60 seconds. The achieved accuracy of determining the value of the acceleration of the force of the gravity is +/- 60 microgals.

GNSS measurements

The position of the benchmarks was determined by three series of RTK measurements in relation with MAKPOS or with static method with time period of 30'. The coordinates of the benchmarks were determined in the European ETRS 89 coordinate system with an accuracy of +/- 1 to 3 centimeters, and then transformed into the Macedonian state coordinate system with an accuracy of about +/- 10 centimeters.[1]

Based on the values obtained form the forward-backward levelling is calculated "average height differences" column. (Table 1) The values of both forward (I) and backward (II) levelling columns are corrected by a correction for rod scale defined in a certified laboratory also known as "*mean meter of the pair of rod* ". From the corrected height differences average values are calculated. (Table 2)

Table 1. Measured height differences [5]

Nº BM	lm between BM, S, km	Height difference, m		d=II - I mm	Average value of height differences
		I	II		
FRSK V2-R1	2.01	28.53262	-28.53317	-0.55	28.53290
V2-R1 V2-R2p	2.18	20.9649	-20.96575	-0.85	20.96533
V2-R2p V2-R3	1.36	-14.1584	14.15921	0.84	-14.15879
FRSK L17-R1	1.65	-4.51362	4.51348	-0.14	-4.51355
L17-R1 L17-R2	1.95	-2.69487	2.69573	0.86	-2.69530

Table 2. Corrected height differences for mean meter of the pair of rods

L17_R2 - V2_R3

No	Mean rod meter correction			Diff. d [mm]	Allowed D [mm]
	I	II	Average		
	-1.000128	-1.000128			
L17_R1-R2	2.69521	-2.69608	2.69564	-0.86	2.10
FR-L17_R1	4.51420	-4.51406	4.51413	0.14	1.93
FR-V2_R1	-28.53627	28.53682	-28.53655	0.55	2.13
V2_R1-R2p	-20.96758	20.96843	-20.96801	0.85	2.22
V2_R2p-R3	14.16018	-14.16102	14.16060	-0.84	1.75
Суми:	-28.13426	28.13410	-28.13418	-0.16	

4.2 QUALITY CONTROL OF THE MEASUREMENTS

Levelling results are checked before further processing:

- By calculating the values for the height differences measured back and forth;
- By creating differences from the height differences between the front and back levelling;
- By comparing with the criteria defined for the realization of the measurements.[5]

The basic criteria of the accuracy for performing the measurements are defined through:

Allowed deviation of the dual height difference (forward-backward):

$$\Delta_{\Delta H}[mm] \leq 1.5\sqrt{S_{km}}[mm] \qquad (16)$$

s - length of the levelling line in km.

Allowed deviation of the sum of differences d from all levelling distances for the whole levelling line:

$$[d]\,[mm] \leq 2.25\sqrt{L_{km}}[mm] \qquad (17)$$

L - length of whole levelling line in km.

From the analysis of the difference between the height differences in the levelling sides (forward-back) and the allowed deviations, it can be noted that all the height differences fulfill the condition of accuracy.

4.3 ESTIMATION OF THE ACCURACY OF THE LEVELLING LINE

Mean error for 1 km levelling distance

The value **m = 0.26 mm/km** is determined by the differences d between height differences in forward and backward levelling in *mm*, from the levelling distances between benchmarks S in *km* and the number of levelling distances in the line between height differences in forward and backward levelling n_s by the formula [2] :

$$m = \pm\frac{1}{2}\sqrt{\frac{1}{n_s}\left[\frac{d^2}{S}\right]} \leq 0.40\,[mm] \qquad (18)$$

The mean systematic error for 1 km levelling distance

To calculate the systematic part of the total error from the levelling, the differences from the forward and backward levelling and the corresponding lengths of the levelling sides were used.

In formula (19) the length of the line is denoted by L and is in kilometers. L' is the length of a part the line that is roughly with the same constant impact of systematic errors. μ is the difference from the ordinates of the endpoints of the reggresion line, defined as approximation of d for part from the line, characterized by approximately the same influence of systematic errors expressed in mm. [2]

$$\sigma = \frac{1}{2}\sqrt{\frac{1}{L}\left[\frac{\mu\mu}{L'}\right]}\,[mm] \qquad (19)$$

When determining the regression line, its length must met the following requirement: the differences between the ordinates of this line and the graphical values of d should not exceed 4 mm. At the same time: the sum of the areas between the graph of the d and the regression lines on both sides to be equal. The value for is **0.15mm/km**. [2]

The mean random error for 1 km levelling distance

$$\eta = \frac{1}{2}\sqrt{\frac{[dd]}{L} - \frac{[ss]}{L^2}\left[\frac{\mu\mu}{L'}\right]}\,[mm] \qquad (20)$$

The value for η is also **0.15mm/km**.

Linear regression analysis

In addition are shown graphs of regression lines and partial plots of them, characterized by systematic errors with approximately constant impact. [2]
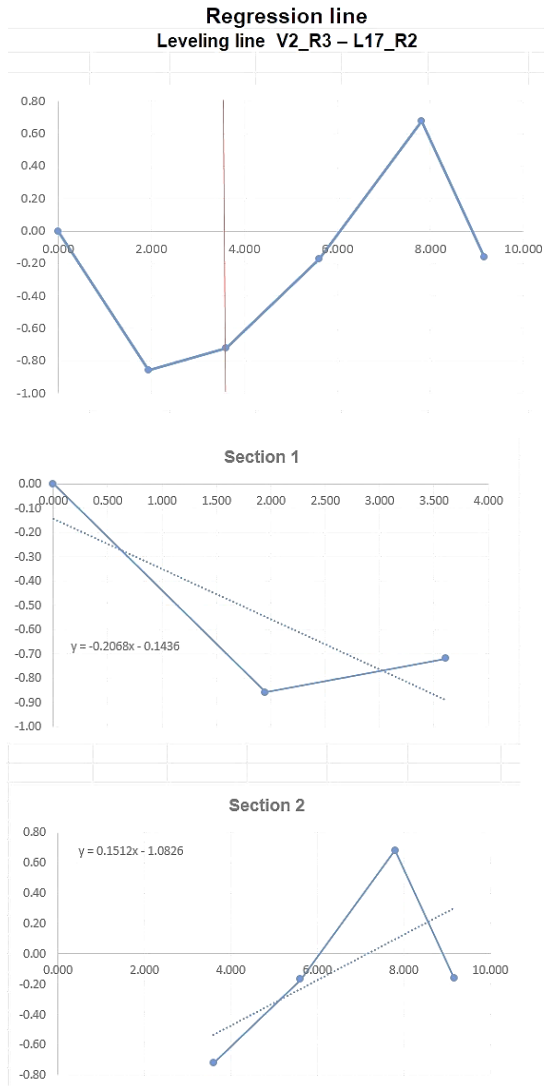
Figure 2. Regression lines and partial plots with similar systematic errors

4.4 TRANSFORMATION OF HEIGHT DIFFERENCES IN PHYSICAL DEFINED HEIGHT SYSTEMS

After the corrections with the mean meter of the pair of rods, the transformation of the height differences in physically defined systems of dynamic, orthometric, and normal heights was performed. For the transformation we use the equations shown in Chapter 2, using the normal value of the Earth's gravity for the coordinates of the central point of the Republic of Macedonia to the ellipsoid. The central point is determined on the basis of the coordinates of the state border of the Republic of Macedonia. For the latitude of the center point, the value B = 41.710193231336 (degrees, decimal) is adopted. [1]

The coordinates of the benchmarks and the values of the acceleration of the force of the earth gravity used in calculating the corrections for the transformation into physical systems are given in Table 3.

The approximate values of the heights of the benchmarks which are necessary for calculating the transformation correction in the physical systems of height are determined on the basis of the results of the levelling and the orthometric height of the FRSK benchmark from the second levelling of high accuracy of the Socialist Federal Republic of Yugoslavia:

$$H^o_{FRSK} = 251.90796 \, \text{m}. \, [1]$$

Table 3. Registry of coordinates in ETRS89 and gravity data

Point	COORDINATES ETRS 89			g	m_g
	B	L	h		
FRSK	41°59'59.89346"	21°25'55.97294"	296.486	980245.4349	5.6
L17-1	41°59'15.81895"	21°26'10.69754"	291.211	980248.2603	10.8
L17-2	41°58'18.50588"	21°26'41.53896"	288.744	980256.9443	15.9
V2-1	42° 00' 45.92706"	21° 25' 37.46418"	324.889	980240.5345	13.5
V2-2	42° 01' 17.94714"	21° 24' 33.93758"	304.3702	980246.1553	17
V2-3	42° 01' 57.62833"	21° 24' 11.31832"	318.2858	980247.7962	20.8

All data in Table 4 are given in meters, except for the Geopotential numbers and the auxiliary values CpVR given in m^2/s^2.

Table 4. Corrections and height differences in various physically defined height systems

From	To	dh-sm	Cp	DC	OC	NC	CpVR	DVR	OVR	OVR
Line:	L17					f = I + II				
FRSK	L17-R1	-4.51413	-39.7224	0.000349	-0.00068	0.00028	-44.235	-4.51378	-4.51481	-3.51481
L17-R1	L17-R2	-2.69564	-23.6862	0.000192	-0.00217	0.000417	-26.377	-2.69545	-2.69781	-1.69781

From	To	dh-sm	Cp	DC	OC	NC	CpVR	DVR	OVR	OVR
Line:	V2					f = I + II				
FRSK	V2-R1	28.53655	251.1433	-0.00233	0.00109	-0.00105	279.6744	28.53888	28.53546	28.53759
V2-R1	V2-R2	-20.96801	-176.339	0.00163	-0.00136	0.00021	-196.372	-20.9696	-20.96664	-20.96822
V2-R2	V2-R3	14.16060	116.4137	-0.00102	-0.00056	-0.00045	129.6388	14.16162	14.16116	14.16105

The tags used in table 4 are as follows:

Dh-sm	Height difference corrected for the mean meter of the pair of rods
Cp	Geopotential number
DC	Dynamic correction
OC	Orthometric correction
NC	Normal correction
CpVR	Auxiliary value
DVR	Height difference in the system of dynamic heights
OVR	Height difference in the system of orthometric heights
NVR	Height difference in the system of normal heights

5. CONCLUSIONS

By applying the dynamic, orthometric and normal correction and the other corrections explained in this paper, we can obtain a "best estimate" of observed, dynamic, orthometric or normal elevation differences. These corrections are applied to observed levelling data to minimize the effects of known systematic errors. And corrections applied for transformation in different physically defined height systems are for eliminating the effect of the nonparallelism of equipotential surfaces.

The data processing itself includes:

- First of all, the quality control of the measurements which was made in this paper and it was concluded that all levelling measurements were performed in accordance with the defined criteria for control and monitoring of the measurements;
- Estimation of the accuracy of the levelling line with mean error for 1 km levelling distance **m=0.26mm/km** and **0.15mm/km** for both systematic and random errors for 1 km levelling distance;
- Also graphs are shown of regression lines and partial plots of them, characterized by systematic errors with approximately constant impact;
- Next, the results of the levelling measurements were corrected with geometric corrections the mean meter of the pair of rods for uniform rod scale;
- Than transformation is performed of measured height differences in different physically defined height systems, with computing and applying dynamic, orthometric and normal correction.

The results of the data processing of the precise levelling measurements uniquely shows the need of applying the above mentioned corrections.

REFERENCES

[1] Agency for Real Estate Cadastre (2016), Report for data processing from the levelling network of high accuracy of Republic of Macedonia, Skopje.

[2] Agency for Real Estate Cadastre (2019), Report for data processing of precise levelling measurements of the three levelling lines (border links) between Bulgaria and Macedonia.

[3] D. Zekov, Gospodinov S. (1989), За отчитане на рефракцията при високоточна геометрична нивелация, *Геодезия, картография и кадастар*.

[4] Emery I. Balazs, Gary M. Young, Corrections applied by the national geodetic survey to precise levelling observations, *National Geodetic Survey.*

[5] F. Kasapovski, et al., (2018): Vertical crustal movements in seismic active regions, *SJCE, Vol. 7 Issue 2*, Skopje.

[6] G.V Marinov, D.G. Ganceva, (2017), A study on the impact of the vertical refraction on the results of precise levelling measrements, *SJCE, Vol. 6 Issue 2*, Skopje.

[7] Jaakko Makinen, (2008) The treatment of the permanent tide in EUREF products, *Finnish Geodetic Institute*.

[8] Odalovic O. (2011), *Levelling Network of Macedonia* , Agency for Real Estate Cadastre, Skopje.

[9] Srbinoski Z. (2008), *Physical Geodesy*, Faculty of Civil Engineering, Skopje.

[10] Srbinoski Z., et al., (2017),Geodetic projects as part of main project for new basic levelling network, *SJCE, Vol. 6 Issue 2*, Skopje.

HYDRAULIC ANALYSIS OF THE WATER HAMMER IN BRANCH WATER SUPPLY NETWORK DEPENDING ON BRANCH DISTANCE

AUTHOR

Goce TASESKI

Assistant Professor

Ss. Cyril and Methodius University

Faculty of Civil Engineering – Skopje

taseski@gf.ukim.edu.mk

It is generally known that water supply systems consist of the following basic components: water source, water treatment plant, reservoirs, supply and main pipelines, and water supply network.

Depending on the terrain configuration and users distribution, the water supply network can usually be of branch type, loop type or combined. The water supply network in the urban areas is mostly a loop type network, whereas in the rural - outskirt areas, there is a branch type network.

Subject of this hydraulic analysis is to comprehend the influence of branch density in the branch water supply network on the size and distribution of water hammer in the network.

Keywords: water supply network, water hammer, method of characteristics

1. INTRODUCTION

The large number of components fitted in one water supply system which should operate continuously, presents a complex system which, due to its complexity, most frequently in practice the hydraulic analysis is made for assumed quasi-stationary regime of flow in systems under pressure. However, in reality the water supply systems are systems in which there are constant changes in pressure and flow, that is, the flow is non-stationary and in case of the need for considering the state in the water supply network when the non-stationary regime of flow occurs, it is advisable for the hydraulic analysis to be made for non-stationary flow in systems under pressure [1].

Size, distribution, form, and duration of the changes in pressure at non-stationary regime in one water supply system cannot be determined with a simple and unique mathematical model for analysis of the water

hammer. That is due to the fact that water supply systems are complex systems and practically each water supply system represents a separate system for hydraulic analysis.

The characteristics of the hydraulic impact in such complex systems depend on a large number of parameters [9] such as:

- Type of the initiator of the immediate change in pressure and flow
- Location of the initiator of the immediate change in pressure and flow
- Current pressure and flow in all lines of the water supply network
- Material from which the water pipes are made
- Density of lines – branches of the water supply network
- Length of lines – branches of the water supply network
- Height configuration of the water supply network.

According to the previously stated, for the hydraulic analysis of water hammer occurrence subject of analysis in this thesis, the mathematical model HTM (Hydraulic Transient Model) aimed at analysis of such systems will be used.

2. BASIC EQUATIONS FOR WATER HAMMER

According Wylie [7] (1993), the water hammer is defined as the hydraulic variable occurrence of flow, which causes an increase of overpressure in a pipeline system. The water hammer can be generated by certain operational measures such as: opening or closing of the valve, turning the pumps on or off, abrupt cracking of the tube etc.

Starting points in the mathematical description of the water hammer [11] are the basic laws in the mechanics of fluids:

- Law of maintaining the amount of movement and
- Law of maintaining weight.

Satisfying these basic principles for conservation/maintenance comes to the dynamic equation and the equation of continuity.

The final form of the dynamic equation for unsteady flow in closed systems under pressure:

$$\frac{\partial V}{\partial t} + V\frac{\partial V}{\partial x} + g\frac{\partial \Pi}{\partial x} + \frac{\lambda}{2D}V|V| = 0 \qquad (1)$$

The convective acceleration $V\partial V/\partial x$ or acceleration along the pipe is significantly lower compared to the acceleration $\partial V/\partial t$ or acceleration over time, so mostly that convective acceleration is overlooked and the dynamic equation is written:

$$\frac{\partial V}{\partial t} + g\frac{\partial \Pi}{\partial x} + \frac{\lambda}{2D}V|V| = 0 \qquad (2)$$

Assuming that the density of the fluid changes very little in terms of piezometric height (ρ= const), the equation of continuity gets the following form:

$$V\frac{\partial \Pi}{\partial x} + \frac{\partial \Pi}{\partial t} - V\sin\alpha + \frac{a^2}{g}\frac{\partial V}{\partial x} = 0 \qquad (3)$$

Where a is the speed of propagation of the pressure wave and it is determined by the ratio of compression of the fluid and the module of elasticity of the tube:

$$a = \sqrt{\frac{K}{\rho\left(1 + \frac{K}{E}\frac{D}{e}c_1\right)}} \qquad (4)$$

The coefficient c1 depends of the pipe anchorage and is equal to:

- $c1=1-\mu/2$ – pipe anchorage only at the upstream
- $c1=1-\mu2$ – pipe anchorage throughout against axial movement
- $c1=1$ – pipe anchorage with expansion joints throughout.

3. METHOD OF CHARACTERISTICS FOR SOLVING BASIC EQUATIONS OF WATER HAMMER

With the method of characteristics [17] the basic partial differential equations which are not integrable in closed form, are transformed into ordinary differential equations which have a solution in a closed form. The basic equations, the equation of continuity and the dynamic equation can be designated with L_1 и L_2:

$$L_1 = g\frac{\partial \Pi}{\partial x} + \frac{\partial V}{\partial t} + V\frac{\partial V}{\partial x} + \frac{\lambda}{2D}V|V| = 0 \qquad (5)$$

$$L_2 = \frac{\partial \Pi}{\partial t} + V\frac{\partial \Pi}{\partial x} + \frac{a^2}{g}\frac{\partial V}{\partial x} - g\sin\alpha = 0 \qquad (6)$$

These linear equations can be combined as follows:

$$L = L_1 + \chi L_2 \qquad (7)$$

The two dependent variables, the speed V and the pressure Π are in a function from the position and time, V=V(x,t) и Π=Π(x,t). The material statements of these dependent variables are total accelerations which are determined by the convective and local acceleration:

$$\frac{d\Pi}{dt} = \frac{\partial \Pi}{\partial x}\frac{dx}{dt} + \frac{\partial \Pi}{\partial t} \qquad (8)$$

$$\frac{dV}{dt} = \frac{\partial V}{\partial x}\frac{dx}{dt} + \frac{\partial V}{\partial t} \qquad (9)$$

Comparing the expression of the convective acceleration of equation (7) to those of equations (8) and (9), follows:

$$\frac{dx}{dt} = V + \frac{g}{\chi} = V + \frac{\chi a^2}{g} \qquad (10)$$

Then equation 7 is written:

$$\chi\frac{d\Pi}{dt} + \frac{dV}{dt} + \frac{\lambda}{2D}V|V| - \chi g \sin\alpha = 0 \qquad (11)$$

The solution of equation 11 is:

$$\chi = \pm\frac{g}{a} \qquad (12)$$

$$\frac{dx}{dt} = V \pm a \qquad (13)$$

From the previous equation it can be concluded that it's about two families of curves that are practically straight lines, where the speed of propagation is constant and many times faster than the basic flow, so the system of two partial differential equations are transformed into system of ordinary four differential equations which are marked with a C+ and C− and determine straight lines:

$$\left.\begin{aligned}\frac{d\Pi}{dt} + \frac{a}{g}\frac{dV}{dt} + \frac{\lambda}{2D}V|V| - V\sin\alpha = 0 \\ \frac{dx}{dt} = V + a\end{aligned}\right\}C^+ \qquad (14)$$

$$\left.\begin{aligned}-\frac{d\Pi}{dt} + \frac{a}{g}\frac{dV}{dt} + \frac{\lambda}{2D}V|V| + V\sin\alpha = 0 \\ \frac{dx}{dt} = V - a\end{aligned}\right\}C^- \qquad (15)$$

4. NUMERICAL MODEL

Figure 1 shows discretization of the physical system in a numerical network with computing steps Δx and Δt where the solutions are obtained at the intersection of the positive and

negative lines of characteristics [8], [9], [10], [11].
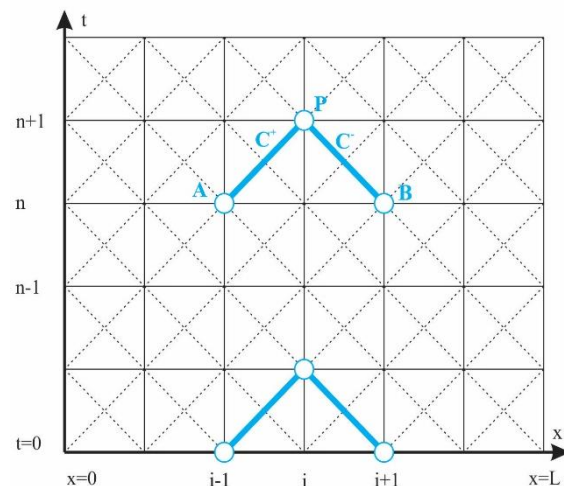
Figure 1. Numerical network for the method of characteristics

According the given numerical network, equations (14) and (15) can be written as follows:

$$\frac{d}{dt}\left(\Pi \pm \frac{a}{g}V\right) + \lambda\frac{a}{D}\frac{V|V|}{2g}\mu V\sin\alpha = 0 \qquad (16)$$

The previous equation can be integrated along the positive and negative characteristics, i.e. along the length of the lines AP and BP, as follows:

$$\int_{tA}^{tP}\frac{d}{dt}\left(\Pi + \frac{a}{g}V\right)dt + \int_{tA}^{tP}\left(\lambda\frac{a}{D}\frac{V|V|}{2g} - V\sin\alpha\right)dt = 0 \qquad (17)$$

$$\int_{tB}^{tP}\frac{d}{dt}\left(\Pi - \frac{a}{g}V\right)dt + \int_{tB}^{tP}\left(\lambda\frac{a}{D}\frac{V|V|}{2g} + V\sin\alpha\right)dt = 0 \qquad (18)$$

After integration, equations of positive and negative characteristic are written:

$$\frac{\Pi_P - \Pi_A}{\Delta t} + \frac{a}{g}\frac{V_P - V_A}{\Delta t} + \frac{\lambda a}{2gD}V_A|V_A| - V_A\sin\alpha = 0$$

$$\frac{\Pi_P - \Pi_B}{\Delta t} - \frac{a}{g}\frac{V_P - V_B}{\Delta t} + \frac{\lambda a}{2gD}V_B|V_B| - V_B\sin\alpha = 0$$

If it is known that the hydraulic analysis is important to determine the change in the flow and height position of the hydrodynamic line in any section along the pipe and at a specified interval, additional approximating is introduced that the cross-section of the pipe throughout its length is constant and if is known that the average speed can be determined by the equation V=Q/A, the previous equations knowing the numerical network can be written in the following form:

$$\Pi_i^{n+1} - \Pi_{i-1}^n + \frac{a}{gA}\left(Q_i^{n+1} - Q_{i-1}^n\right) +$$

$$\frac{\lambda \Delta x}{2gDA^2} Q_{i-1}^n \left|Q_{i-1}^n\right| - \frac{\Delta t}{A} Q_{i-1}^n \sin\alpha = 0 \tag{19}$$

$$\Pi_i^{n+1} - \Pi_{i+1}^n - \frac{a}{gA}\left(Q_i^{n+1} - Q_{i+1}^n\right) -$$

$$\frac{\lambda \Delta x}{2gDA^2} Q_{i+1}^n \left|Q_{i+1}^n\right| - \frac{\Delta t}{A} Q_{i+1}^n \sin\alpha = 0 \tag{20}$$

If:

$$B = \frac{a}{gA} \qquad \text{and} \qquad M = \frac{\lambda \Delta x}{2gDA^2}$$

Using the previous equations, for the pressure, i.e. for the height position of the hydrodynamic line, it can be written:

$$\Pi_i^{n+1} = \Pi_{i-1}^n - B\left(Q_i^{n+1} - Q_{i-1}^n\right) - MQ_{i-1}^n\left|Q_{i-1}^n\right| +$$

$$+ \frac{\Delta t}{A} Q_{i-1}^n \sin\alpha = 0 \tag{21}$$

$$\Pi_i^{n+1} = \Pi_{i+1}^n + B\left(Q_i^{n+1} - Q_{i+1}^n\right) + MQ_{i+1}^n\left|Q_{i+1}^n\right| +$$

$$+ \frac{\Delta t}{A} Q_{i+1}^n \sin\alpha = 0 \tag{22}$$

If the parameters of flow are known in the time interval (n), then we get:

$$\Pi_i^{n+1} = CP - BQ_i^{n+1} \tag{23}$$

$$\Pi_i^{n+1} = CM + BQ_i^{n+1} \tag{24}$$

Where:

$$CP = \Pi_{i-1}^n + BQ_{i-1}^n - MQ_{i-1}^n\left|Q_{i-1}^n\right| + \frac{\Delta t}{A} Q_{i-1}^n \sin\alpha$$

$$CM = \Pi_{i+1}^n - BQ_{i+1}^n + MQ_{i+1}^n\left|Q_{i+1}^n\right| + \frac{\Delta t}{A} Q_{i+1}^n \sin\alpha$$

In the previous equations the article which include the slope of the pipes (sinα) is very small and often overlooked, so the equations (25) and (26) are written:

$$CP = \Pi_{i-1}^n + BQ_{i-1}^n - MQ_{i-1}^n\left|Q_{i-1}^n\right| \tag{25}$$

$$CM = \Pi_{i+1}^n - BQ_{i+1}^n + MQ_{i+1}^n\left|Q_{i+1}^n\right| \tag{26}$$

From equations (25) and (26) is obtained a basic equation of the characteristics for determining the elevation of the hydrodynamic line:

$$\Pi_i^{n+1} = \frac{CP + CM}{2} \tag{27}$$

Knowing the piezometric height (Πi) in the time period (n+1), the flow (Qi) is determined by equations (25) and (26).

5. BOUNDARY CONDITIONS

The conditions of the flow that govern within the boundary of the system under pressure – the water supply system are defined as boundary conditions. Their definition is of crucial importance for getting the solution at the points in the system. Follow-on are the most common cases of boundary conditions encountered in the water supply systems [5].

Serial connection of two pipes in a junction

Pressure: $\Pi_{1,N}^{n+1} = \Pi_{2,1}^{n+1} = \Pi^{n+1}$

Flow: $Q_{1,N}^{n+1} = Q_{2,1}^{n+1} = Q^{n+1} = \dfrac{CP_1 - CM_2}{B_1 + B_2}$

Connection of more pipes in a junction

Pressure: $\Pi^{n+1} = \Pi_{1,N}^{n+1} = \Pi_{2,1}^{n+1} = \Pi_{3,1}^{n+1} = \Pi_{4,1}^{n+1}$

$$\Pi^{n+1} = \frac{CP_1/B_1 + CM_2/B_2 + CM_3/B_3 + CM_4/B_4}{1/B_1 + 1/B_2 + 1/B_3 + 1/B_4}$$

Flow: $-Q_{1,N}^{n+1} = \dfrac{\Pi^{n+1}}{B_1} - \dfrac{CP_1}{B_1}$; $\quad Q_{2,1}^{n+1} = \dfrac{\Pi^{n+1}}{B_2} - \dfrac{CM_2}{B_2}$

$Q_{3,1}^{n+1} = \dfrac{\Pi^{n+1}}{B_3} - \dfrac{CM_3}{B_3}$; $\quad Q_{4,1}^{n+1} = \dfrac{\Pi^{n+1}}{B_4} - \dfrac{CM_4}{B_4}$

Reservoir at the end of pipeline

Pressure: $\Pi_1^{n+1} = \Pi_R$

Flow: $Q_1^{n+1} = \dfrac{\left(\Pi_1^{n+1} - CM\right)}{B}$

Valve at the end of the pipeline

Pressure: $\Pi_1^{n+1} = CP - BQ_N^{n+1}$

Flow:

$$Q_N^{n+1} = -B \cdot C_1 + \sqrt{\left(B \cdot C_1\right)^2 + 2C_1\left(CP - Z_Z\right)}$$

$$C_1 = g \frac{A_C^2}{\xi_Z}$$

Valve at the middle of the pipeline

Pressure:

$$\Pi_{1,N}^{n+1} = CP_1 - B_1 Q_{1,N}^{n+1} \quad ; \quad \Pi_{2,1}^{n+1} = CM_2 - B_2 Q_{2,1}^{n+1}$$

$$CP_1 - B_1 Q^{n+1} - CM_2 - B_2 Q^{n+1} - C_1 Q^{n+1} |Q^{n+1}| = 0$$

If the condition is completed CP1–CM2>0 than follows:

Flow:

$$Q^{n+1} = \frac{-(B_1 + B_2) + \sqrt{(B_1 + B_2)^2 + 4C_1(CP_1 - CM_2)}}{2C_1}$$

If CP1–CM2< 0 than follows:

Flow:

$$Q^{n+1} = \frac{(B_1 + B_2) - \sqrt{(B_1 + B_2)^2 - 4C_1(CP_1 - CM_2)}}{2C_1}$$

6. HYDRAULIC ANALYSIS OF THE BRANCH TYPE WATER SUPPLY NETWORK BY MEANS OF THE HTM – HYDRAULIC TRANSIENT MODEL

Calculation template of zone gravitation water supply system of the branch type water supply network is used for the development of the mathematical model HTM, in which the water from the water source is firstly distributed in the upper elevation zone and the water excess, i.e. the needs for water in the lower zone fill the reservoir for the lower zone. According to the previously stated, it can be concluded that there is no reservoir space for the upper zone, and it can be said that the provided reservoir, in addition to leveling the supply amounts of water including the needs of water for the lower zone, also represents an interruption chamber.

Hydro-mechanical equipment for regular operation of the entire water supply system is provided in the reservoir for the lower zone. Namely, there is a pressure control valve placed before the reservoir which sustains the input pressure in the reservoir (Pressure sustaining valve) to prevent the decrease of the water pressure in the water supply network of the higher zone, i.e. not to cause fall of the hydrodynamic line to the reservoir peak

elevation. After the pressure control, there is a valve by which the level in the reservoir is regulated. The valve in this calculation pattern is practically the initiator for causing non-stationary flow. Namely, in the moment when the reservoir reaches the maximum peak elevation, the valve immediately closes, and vice versa, in the moment when the level in the reservoir drops to a certain limit, the valve opens suddenly.
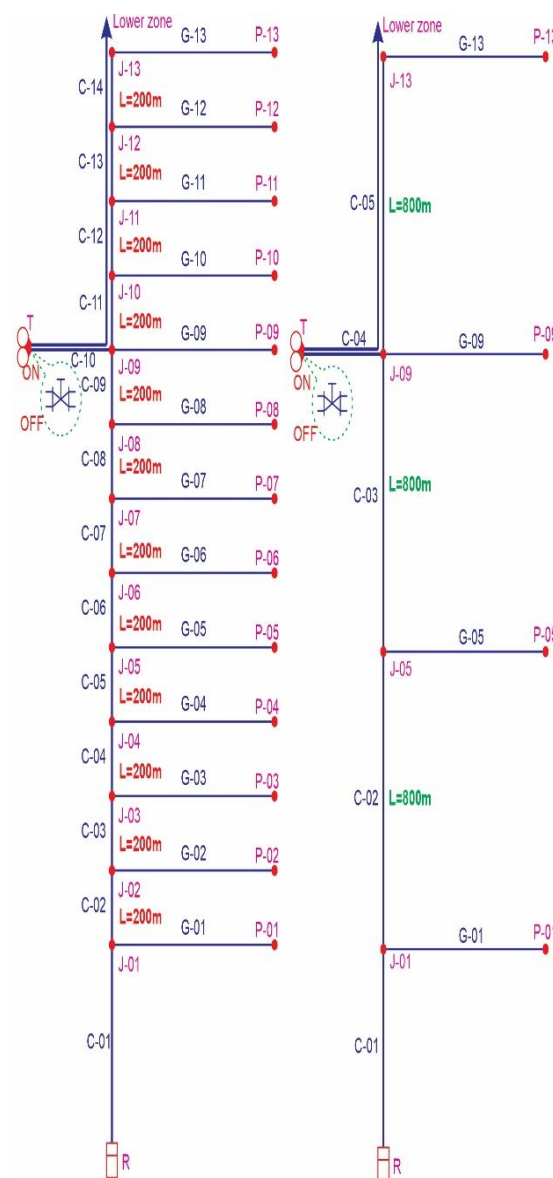

Figure 2. Calculation scheme for the development of the mathematical model HTM

The choice for such calculation pattern (Figure 2) is made in order to analyze the phenomenon of the water hammer in a complex system with gravitation inflow and closing valve at the end of a primary pipeline. This calculation pattern is practically an equivalent to the model of simple system - a

reservoir and a pipeline having a valve at the end. Two scenarios are analyzed:

I. First scenario. Branch connections of the secondary network are at a distance of 200 m, and all the pipes of the water supply network are of the same material - ductile pipes.

II. Second scenario. Branch connections of the secondary network are at a distance of 800 m, and all the pipes of the water supply network are of the same material - ductile pipes.
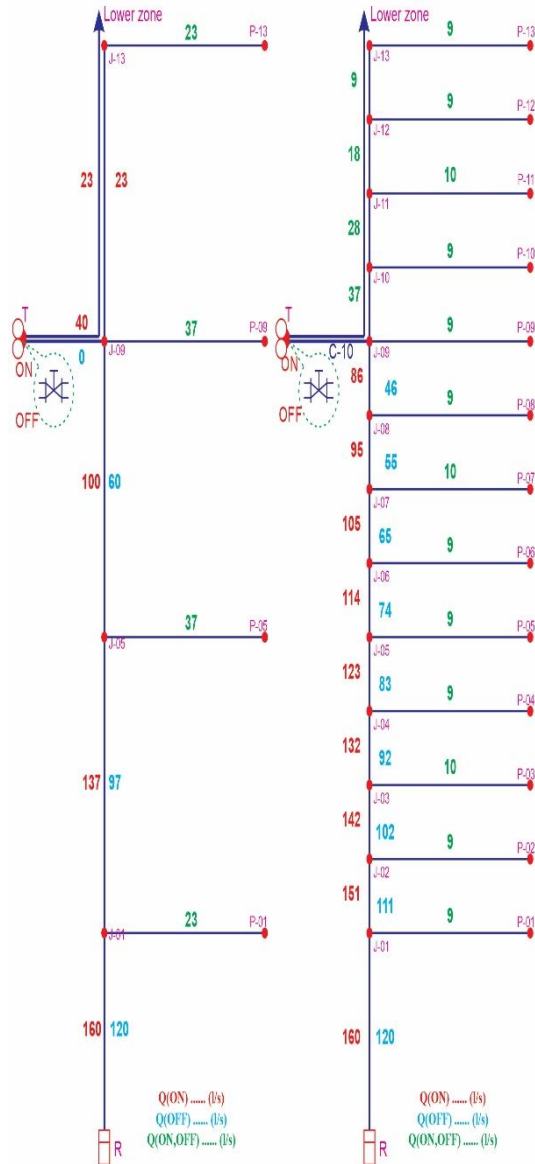
Figure 3. Water flow per pipeline at stationary regime – Scenario I

Table 1 shows the pipeline material characteristics and water as fluid.

Table 1. Material characteristics of pipelines and water as fluid

Characteristics	Value
DUCTIL PIPES	
Young modulus of elasticity	170 GPa
Poisson factor	0.28
FLUID – WATER	
Temperature	20°C
Density	998 kg/m^3
Modulus of elasticity	2.19 GPa
Kinematic viscosity	$1.01×10^{-6}$ m^2/s

The hydraulic analysis in the water supply system at stationary regime of flow in the system is made in the software package WaterGEMS, and Figure 3 shows running quantities of water per line at stationary regime which are input parameters – initial conditions in the mathematical model HTM for the hydraulic impact analysis.

7. RESULTS OF HYDRAULIC ANALYSIS

In addition to the following figures, there is a graphic presentation of the output results of the hydraulic analysis for branch type water supply network of different branch density in hydraulic impact occurrence at sudden valve closure.

Important points subject to analysis are:

- Place of the non-stationarity initiator – valve (junction "T")
- The first junction where the upper zone J-01 users are connected, and
- Final junction of the upper zone J13
-

Figure 4. Pressure distribution at junction T, quick closing valve

Figure 5. Pressure distribution at junction J-01, quick closing valve

Figure 6. Pressure distribution at junction J-13, quick closing valve

8. CONCLUSION

From the results obtained, it can be observed that there is a significant increase in the pressure both at the initiation place of non-stationarity and in the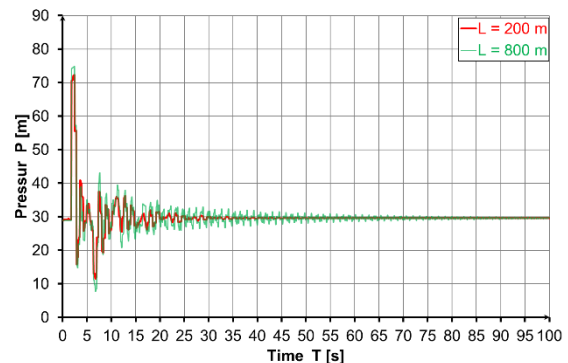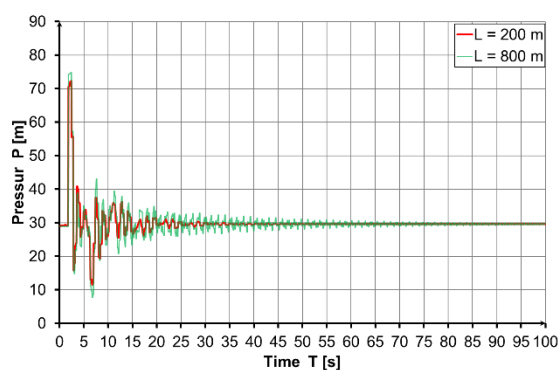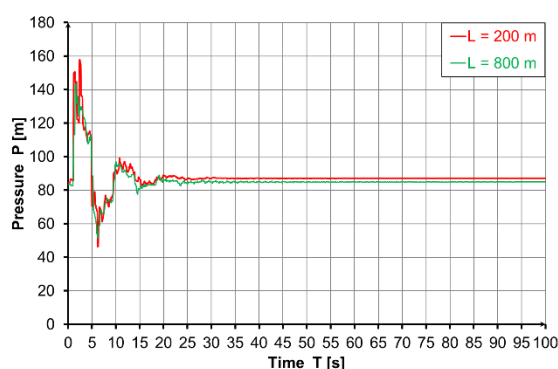 water supply network itself. According to that, a recommendation can be made that for such or similar systems where occurrence of non-stationarity in the water supply system is expected, they need to be analyzed as a system under pressure with non-stationary flow.

From the analyzed non-stationarity, it can be concluded that pressure increase at the non-stationarity initiation place in knot "T" is identical in both analyzed cases. However, the non-stationarity duration in water supply systems of denser branches is much shorter compared to the other systems. Considering the main pipeline – pipeline connecting the water catchment and the reservoir along which the branches "J-01" are connected, in the systems of denser branches the amount of above-pressure is lower compared to the remaining system, and also the non-stationarity duration in denser branches is shorter compared to the other ones. While the

situation is different at the ends of the branches J-13, i.e. the water supply system of denser branches has larger increase of the above-pressure, and the non-stationarity duration is identical, this is due to the fact that the amount of water flowing through the branch in denser branches is much lower.

REFERENCES

[1]. Goce Taseski: „Characteristics of water hammers in water supply networks". Doctorate dissertation, Skopje, Macedonia, 2015

[2]. Goce Taseski, Cvetanka Popovska, Petko Pelivanoski, Water hammer analysis-impact of the pipe material in water supply system, 14th International Symposium on Water Management and Hydraulic Engineering (WMHE2015).

[3]. Goce Taseski, Cvetanka Popovska, Petko Pelivanoski, Defining the time of closing the valve at small hydro power plant on the main pipeline of the water supply system, 14th International Symposium on Water Management and Hydraulic Engineering (WMHE2015).

[4]. Cvetanka Poposka: „Hydraulics". Publisher Civil Engineering Faculty, University Ss. Cyril and Methodius, ISBN 9989-43-100-0, 2000.

[5]. Zhivko Veljanovski „Water supply", Publisher Civil Engineering Faculty, University Ss. Cyril and Methodius, ISBN 978-9989-2922-1-7, 2008.

[6]. Bentley HAMMER V8i Edition User's Guide.

[7]. Streeter, V. L., Wylie, E.B., Hydraulic Transient, McGraw Hill Book Company, New York. 1967.

[8]. A.R.D. Thorley: Fluid Transients in Pipeline Systems, Second Edition (Pipelines and Pressure Vessels), Publisher: The American Society of Mechanical Engineers; 2nd edition, ISBN-13: 978-0791802106, 2004.

[9]. Kaveh Hariri Asli: "Water Hammer Research: Advances in Nonlinear Dynamics Modeling", Publisher: Apple Academic Press, ISBN 9781926895314 - CAT# N10708, 2013.

[10]. A, Betamino de Almeida, E: "Fluid transient in Pipe Networks", Publisher: WIT Press, ISBN-13: 978-1853121678, 1992.

[11]. Josef Zaruba: "Water hammer in pipe-line systems", Publisher: Elsevier Science, ISBN-13: 978-0444987228, 1993.

[12]. John Parmakian: "Water hammer Analysis", Publisher: Prentice Hall, Inc.; 1st edition, ASIN: B0000CJ5U0, 1995.

[13]. Fox, J.A. "Hydraulic analysis of unsteady flow in pipe networks". Publisher: Macmillan Press Ltd, London, UK, ISBN-13: 978-0470270370. 1977.

[14]. Izquierdo, J., Inglesias, L.P., "Mathematical modelling of hydraulic transients in complex systems". Mathematical and Computer Modelling, 39,529-540, 2004.

[15]. Simulation of Water Hammer Flows with Unsteady Friction Factor, ARPN Journal of Engineering and Applied Sciences, 2006.

[16]. Thomas Repp, Fluid Dynamic Water Hammer Simulations with Consideration of Fluid-Structure Interaction, https://www.hzdr.de/FWS/publikat/JB98/jb08.pdf, 2011.

[17]. A.R. Lohrasbi, R. Attarnejad"Water Hammer Analysis by Characteristic Method" American J. of Engineering and Applied Sciences 1 (4): 287-294, 2008.

[18]. Roman Wichowski, Hyd Archives of Hydro-Engineering and Environmental Mechanics Vol. 53 (2006), No. 3, pp. 267–291 Hydraulic Transients Analysis in Pipe Networks by the Method of Characteristics (MOC).

G. Taseski

AUTHORS

Zlatko ZAFIROVSKI

PhD, Assistant Professor

University "Ss. Cyril and Methodius"

Faculty of Civil Engineering – Skopje

zafirovski@gf.ukim.edu.mk

Darko MOSLAVAC

PhD, Full Professor

University "Ss. Cyril and Methodius"

Faculty of Civil Engineering – Skopje

moslavac@gf.ukim.edu.mk

Aleksandar GLAVINOV

PhD, Professor

University Goce Delcev Stip

Military Academy

aleksandar.glavinov@ugd.edu.mk

Zoran KRAKUTOVSKI

PhD, Full Professor

University "Ss. Cyril and Methodius"

Faculty of Civil Engineering – Skopje

krakutovski@gf.ukim.edu.mk

Vasko GACEVSKI

BSc, Teaching Associate

Ss. Cyril and Methodius University

Faculty of Civil Engineering – Skopje

vaskogacevski@yahoo.com

GUIDELINES FOR RISK ANALYSIS AND MANAGEMENT IN TUNNELLING

The concept of risk analysis and management has a big impact and application in various branches of society. Today in civil engineering, especially in infrastructure projects this concept represents a serious matter that should not be avoided or delayed. There are different approaches and definitions for a risk, but it is important every problem to be reviewed separately. In tunneling the uncertainties and risks are always present, so appropriate measures and management should be considered and implemented.

Keywords: Tunnels, uncertainties, risk, risk analysis, risk management

1. INTRODUCTION

Tunnels represent unique underground structures which are used for different purposes. Nowadays their application is bigger and more widespread throughout the world. Tunnel design and construction is a special area i.e. science discipline of the underground structures where the experience and knowledge from other areas are applied such as: geology, soil mechanics, rock mechanics, theory of structures, reinforced concrete, geodesy, organization and mechanization, etc. According to their purpose, the tunnels can be divided into several categories:

- Transportation tunnels (railway, roadway, pedestrian, metro);
- Hydrotechnical tunnels (water, sewage, diversion (outlet), meliorative);
- Communal tunnels (for placing electrical and telephone lines, gas, heating, etc.);
- Underground structures for special purposes (aircraft hangars, submarine shelters, bombing shelters, underground warehouses and garages, underground industrial plants, etc.).

In the modern era, the construction conditions for the tunnels are getting more difficult, because they are placed under densely populated cities, under rivers, lakes, seas and tall mountains on large depths below the surface. In addition, the tunnel lengths in the world are increasing. All of this generates bigger risks, so more severe criteria are placed during the design, construction and exploitation phase.

2. RISK IN CIVIL ENGINEERING

The concept of risk and its management has application in various branches of society. One of the basic definitions for risk is probability of something negative happening, caused by an event or activity. Many engineers desire to define risk as the combination of failure and the probability of failure. The basic concept of risk managing is to accept risks that are reasonably small. In doing so, the risk of human injury and loss of life should be distinguished from the risk of economic loss.

An example of a classification of consequences is given in table 1.

There are different approaches and definitions for risk in civil engineering, but it is important every problem to be reviewed separately. In some cases, different consequences with different probabilities may occur for a same problem. The overall risk in such case would be the sum of the risks associated with each possible consequence.

Table 1. Example of Example of classification of consequences, Eskesen et al (2004) (left – consequences due to injury to third parties, right – consequences due to economic loss)

CLASS	DESCRIPTION	EXAMPLE FROM SERIOUS INJURY	CLASS	DESCRIPTION	ECONOMIC LOSS (MILION €)
1	Insignificant	No	1	Insignificant	< 0.003
2	Considerable	No, in general	2	Considerable	0.003 to 0.03
3	Serious	1	3	Serious	0.03 to 0.3
4	Severe	1 to 10	4	Severe	0.3 to 3
5	Disastrous	> 10	5	Disastrous	> 3

Risk assessment is an important part for the calculation of the project costs, so it should be implemented in every design phase, along with the general objectives of the project. The potential hazards and their consequences should be identified, and then the influence of the risk on the deadlines and costs should be evaluated. After this, the acceptable risk level should be determinated. This risk level will vary with the circumstances. The acceptable level of risk of total collapse of a structure may be different from acceptable risk level of malfunction.
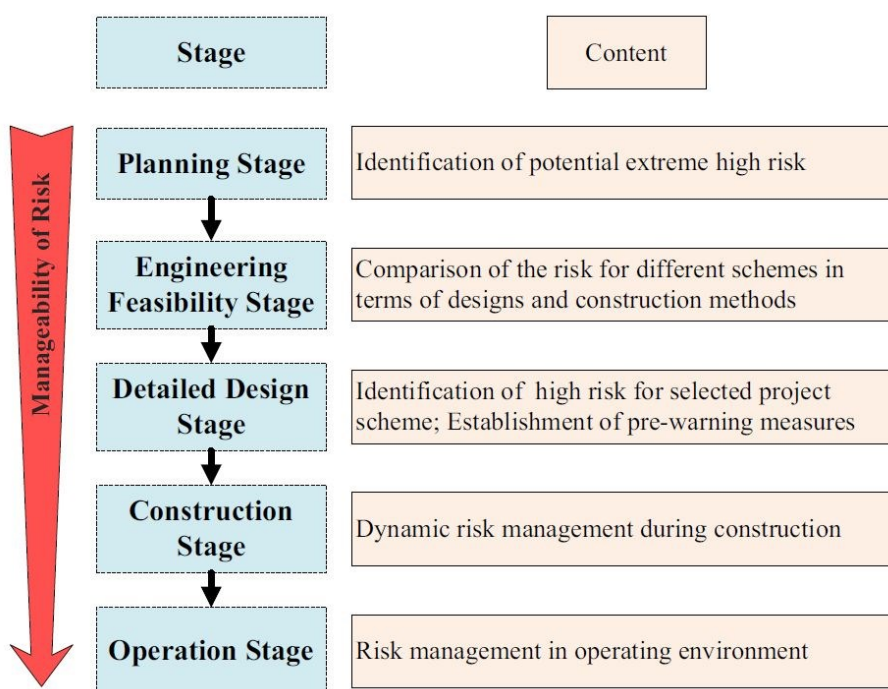

Figure 1. General scheme for long-term risk assessment

Z. Zafirovski, D. Moslavac, A. Glavinov, Z. Krakutovski, V. Gacevski

The results from the risk assessment should be reviewed in consideration with the possibilities for avoiding, transferring or accepting each individual risk. The risk management can contribute to deviation of the main objectives of the project. In construction phase, the analysis of the uncertainties and risks is also essential information for decision making, especially in the infrastructure projects. In general, the analysis and management of risks in civil engineering represent a serious matter, and should be approached with caution in every stage. For economic losses of ordinary projects, the ALARP concept can be used. This implies that all risks should be reduced to level as low as reasonable practicable. General scheme of the risk assessment and management is shown in Figure 1.

3. GEOTEHNICAL UNCERTANTIES AND CONSEQUENCES

According to Muir Wood (1994), the prime source of uncertainty in geotechnical engineering is geology. Unidentified features of the ground may lead to unexpected behaviour and identified features may not be expressible in quantified terms or its behaviour is not fully known. The complexity of the geology may cause communication problems between the parties (human factors). This statement has been confirmed by many case histories of tunnel collapses and claim situations published in literature. The uncertainties can be divided based on their origin as the following:
- Geological scenario uncertainties for underground projects are related to limitations in ability to predict the scenarios in advance, future geological events, changes in engineered components with time and changes in the natural environment due to climate change;
- Model uncertainties may be related to the behavior of the rock mass at tunnel scale, the rock-structure interaction or description of the fracture system and faulting;
- Data uncertainties may be geometry related issues or connected to limitation in the scope of the tests as number of fault and fracture orientations, transmissivity of water-bearing structures and rock mass distribution and quality.

The nature of many underground projects implies that the level of confidence in the estimated ground conditions can be low based on the pre-investigation, especially in complex geological formations.

Usually the most unstable situation is directly after the excavation, and before the installation of the temporary (or permanent) support. In cases with weak rock, the geology and its properties are investigated, mapped and evaluated during tunnel excavation so the conditions of the next round can be predicted. In table 2 few geological factors related with risks during excavation are shown.

The geotechnical consequences can be divided in three groups:
- Consequences due to design mistakes;
- Consequences due to rock engineering mistakes;
- Consequences due to rock excavation mistakes.

Some of the consequences classes are given in the next tables.

Table 2. Example of geological factors related to risks connected to rock excavation

TYPE OF ISSUE	TECHNICAL RELEVANCE	GEOLOGICAL FACTOR
Damage of structures on ground	Damage of third part	Rock cover Rock quality
Environmental or social impact	Ground water lowering Pre and post grouting	Ground water pressure Rock mass permeability
	Vibration disturbance	Attenuation by the rock mass
Workers safety	Front stability	Rock mass quality Initial rock stresses Geometry of geological structures
	Time until initial support has to be installed	
Long term stability	Time before permanent support can be installed	Squeezing ground Swelling ground Raveling ground

Table 3. Consequences classes due to design mistakes

CLASS	RELATIVE ECONOMIC LOSS TO PROJECT COST	CONSEQUNCE CLASS EN 1990:2002	EXAMPLE OR LOSSES
1	< 0.1 %	Small or negligible	Negligible
2	0.1 to 1 %		Minor costs due to construction mistakes
3	1 to 10 %	Considerable	Reparations costs for inadequate design
4	10 to 100 %	Very great	Cost for reparation of local tunnel collapse
5	> 100 %		Rebuilding of the project due to malfunction

Table 4. Example of relative losses (productivity disturbance) due to rock engineering mistakes

CLASS	CLASSIFICATION	RELATIVE ECONOMIC LOSS TO PRODUCTION COSTS	EXAMPLE OF DISTURBANCE OF PRODUCTIVITY
1	Negligible	< 0.1 %	Negligible
2	Minor	0.1 to 1 %	Minor disturbance of the productivity
3	Moderate	1 to 10 %	Medium disturbance
4	Major	10 to 100 %	High disturbance
5	Extensive	> 100 %	Excavation method is not applicable

4. RISK ANALYSIS IN TUNNELLING

With proceeding urbanization and increasing demands on life-quality, the importance of underground infrastructure, including tunnels, is likely to increase in the future. Tunnels minimize the impact of the infrastructure (e.g. road or railway) on the environment, they allow placing the infrastructure in the cities underground and thus improve the life quality of the inhabitants. Tunnels also help to fulfil the increasing demands on the technical parameters of the infrastructure, the modern roads and railways, to comply with the requirements on high design speed, sweeping curves and gentle elevation. In a complicated terrain, this can often be gained only through designing tunnels.

The objectives of a tunnel construction (measurable performance parameters) are as follows:

- Completion of the construction on time;
- Completion of the construction within the budget;
- Fulfilment of the technical requirements;
- Ensuring safety during the construction;
- Minimization of impact on operation of adjacent structures;

- Minimization of damage to third party property;
- Avoidance of negative reaction of media and public.

4.1 QUALITATIVE RISK ANALYSIS

The qualitative risk analysis (QIRA) aims at identifying the hazards threatening the project, to evaluate the consequent risks and to determine the strategy for risk treatment. The QIRA serves as a basis for preparation of contracts, for management of the project and for allocation of responsibilities amongst the stakeholders or their employees and representatives.

The hazards are identified and collected in the so-called risk registers. The risk registers should cover all thinkable events and situations, which can threaten the project. Therefore, experts from many different areas and with varying experiences should participate on the hazard identification. To evaluate the risks, varying classification and rating systems describing the probability of occurrence of a hazard and expected consequences in verbal form are used.

Based on evaluation of the risks, the strategies for their treatment and the responsibilities are determined. All information (causes and

Z. Zafirovski, D. Moslavac, A. Glavinov, Z. Krakutovski, V. Gacevski

consequences of the hazards, risk classification, responsibilities, treatment strategies) is collected in the risk register, which should be actively used and updated in all phases of the project.

4.2 QUANTITATIVE RISK ANALYSIS

The quantitative risk analysis (QnRA) aims to numerically evaluate the risk. Compared to the QlRA, the QnRA requires a clearer structuration of the problem, detailed analysis of causes and consequences and description of the dependences amongst considered events or phenomena. The QnRA provides valuable information for decisions-making under uncertainty such as for the selection of appropriate design or construction technology and it allows efficiently communicating the uncertainties with stakeholders.

Some of the methods and models for quantitative risk analysis during tunnel construction are: Fault tree analysis, Event tree analysis, Bernoulli process, Binomial distribution, Poisson process, Markov process, Bayesian networks and dynamic Bayesian networks.
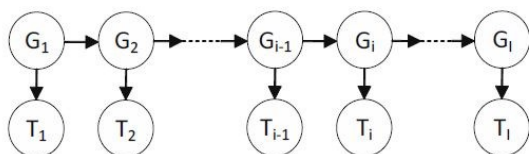

Figure 2. Example of dynamic Bayesian network

5. RISK MANAGEMENT AND QUALITY ASSURANCE

The treatment of unacceptable risks can be done in different ways. Risks can be avoided, mitigated and transferred. Risk mitigation can be seen as part of the quality assurance work.

Optimal methods for mitigating the risks are directed toward the epistemic nature of the uncertainties, which implies that the risk can be reduced by obtaining further information about the geotechnical conditions. This may be achieved by further geological investigations in the preconstruction stages or during excavation. In some cases, adoption of an observational approach will be required. The level of investigation, control and monitoring has to be adapted to the chosen design process and risk level.

5.1 GROUND INVESTIGATION AND GROUND MODEL

The degree of uncertainty depends on the site conditions such as depth of excavation, ease of access to perform investigations, the nature and extent of the investigations, degree of weathering of rocks, and complexity of the geology. The geological conditions of a site may vary within wide limits. Therefore, there is no „standard investigation procedure", which covers all cases. The objective is to perform „appropriate investigations", which means right pre-investigations performed at right time.

The starting point, in order to achieve appropriate investigations, is to use a geological model to guide site characterization and hazard identification.

5.2 GEOTECHNICAL BASELINE REPORT

The Geotechnical Baseline Report, GBR, as proposed by Essex et al (1997), is an excellent tool to set the baseline for the geotechnical conditions anticipated to be encountered during construction.

Ground characterisation has therefore to be divided into construction considerations and design considerations. If a general characterisation of the ground is presented, it must be applicable on both issues. The preparation of GBR is a qualified task and must be carried out by experienced, knowledgeable people.

5.3 SITE ORGANISATION FOR MONITORING AND REVIEW

Having a geotechnical team on site is necessary in order to follow up the encountered geological conditions but also for investigating and detecting conditions that have not been predicted and foreseen. A close cooperation is also required both with the designer in charge and the contractor in order to adequately implement the findings in the design work and the rock engineering planning.

The use of a board of experts or independent reviewers addresses on the geotechnical risks, which are connected to doing the right thing.

5.4 OBSERVATIONAL APPROACH

For many underground projects it is not practical and sometimes even impossible to adequately investigate all ground conditions in advance. Further information is needed in

order to be able to perform the final design. In such cases observational approach can be implemented.

5.5 TIME AND COST ESTIMATION

The definition of risk as the effect of the uncertainties on the objectives is adequate for the purpose of a correct estimation of time and cost for budget or tendering. Therefore, the estimation should be based on a probabilistic approach, which clearly can evaluate the effect of the geological uncertainties. The budget of clients has to cover costs connected to geotechnical risks. It has been found that it is a good strategy to use some of the risk allowances to pay for precaution arrangements. This will increase the risk awareness in the project and can be seen as risk mitigation measures.

5.6 QUALITY ASSURANCE

For achieving a certain quality level, first it must be clear what the investor (client) wants, i.e. see to it that the right thing is done or built. It is also important to ensure that the thing is done or built right. If this is not considered and carefully done there is a probability of handing over substandard product that can increase the maintenance costs which the client didn't

predict, or handing over a more expensive product or breaking the deadline.

The overall quality is governed by both these factors:

- "Doing or building the right thing";
- "Doing or building these things right".

6. CONCLUSION

The uncertainties and risks are always present in underground construction. In every phase of a project from design, planning to execution, the uncertainties, especially the geotechnical will affect the decisions. The effect of the uncertainties on the objective is called the risk. These risks can affect function, construction productivity and environment. The competence with a comprehensive view of the risk situation is mandatory for a successful handling of the risks.

The focus of the risk management process should be to mitigate the risks. Depending on the problem, different approaches can be implemented. The risk management process according to the International Organization for Standardization is shown in Figure 3.
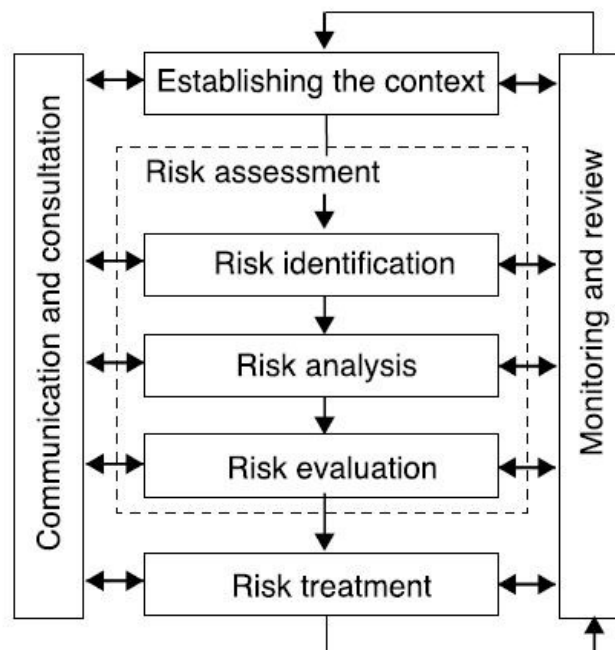

Figure 3. Risk management process according to ISO 31000: 2009

Z. Zafirovski, D. Moslavac, A. Glavinov, Z. Krakutovski, V. Gacevski

REFERENCES

[1] Eskesen D. S., Tengborg P., Kampmann J., Veicherts H. T. (2004), „Guidelines for tunnelling risk management: International Tunnelling Association", Working Group No. 2.

[2] Hakan Stille E. (2017), „Geological Uncertainties in Tunnelling – Risk Assessment and Quality Assurance", Sir Muir Wood Lecture.

[3] Huang H., Zhang D. (2015), „Quantitative Geotechnical Risk Management for Tunnelling Projects in China", Geotechnical Safety and Risk V.

[4] Shpackova O. (2012) „Risk management of tunnel construction projects" Doctoral Thesis, Faculty of Civil Engineering, Czech Technical University in Prague.

[5] Zafirovski Z. (2016) „Тунели (Tunnels)", authorized lectures, Faculty of Civil Engineering – Skopje.

[6] Moslavac D. (2006) „Тунели (Tunnels)", authorized lectures, Faculty of Civil Engineering – Skopje.

[7] Hudec M., Kolic D., Hudec S. (2009) „TUNNELS – Excavation and primary support", HUBITG.

[8] Tomanovic Z. (2015) „Tuneli i podzemne konstrukcije (Tunnels and underground constructions)", authorized lectures, Faculty of Civil Engineering – Podgorica.
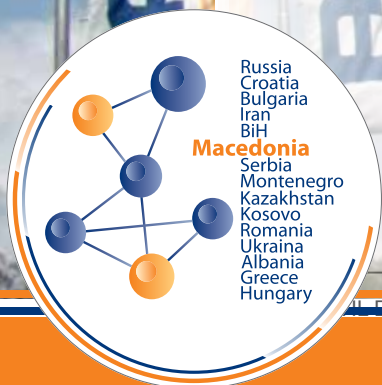
AUTHORS

Zlatko ZAFIROVSKI

PhD, Assistant Professor

University "Ss. Cyril and Methodius"

Faculty of Civil Engineering – Skopje

zafirovski@gf.ukim.edu.mk

Zoran KRAKUTOVSKI

PhD, Full Professor

University "Ss. Cyril and Methodius"

Faculty of Civil Engineering – Skopje

krakutovski@gf.ukim.edu.mk

Aleksandar GLAVINOV

PhD, Professor

University Goce Delcev Stip

Military Academy

aleksandar.glavinov@ugd.edu.mk

Darko MOSLAVAC

PhD, Full Professor

University "Ss. Cyril and Methodius"

Faculty of Civil Engineering – Skopje

moslavac@gf.ukim.edu.mk

Vasko GACEVSKI

BSc, Teaching Associate

Ss. Cyril and Methodius University

Faculty of Civil Engineering – Skopje

vaskogacevski@yahoo.com

TRANSPORTATION AND MOBILITY ANALYSIS OF A TARGET GROUP

Transportation planning is a complex task and a major challenge that plays primary role in the exchange of people and goods. Transport is often analyzed from a socioeconomic and spatial aspect through theoretical approaches for supply and demand of transport. The offer of transport can be expressed through the offered capability of vehicles or through the capacities of the transport network. The transport demand is analyzed by the number of passengers or loads transported at a time of a given distance. An initial representation of the theoretical approach in the analysis of the transport of people or urban mobility through description of a specific case is shown in this paper.

Keywords: Urban transport, mobility, transport analysis, transport planning, offer, demand

1. INTRODUCTION

In order to enable the operation of transport, large financial funds are needed which should be invested for its functioning, that is for the construction of the infrastructure, for the production and procurement of vehicles and for the organization and exploitation of the transport.

These investments are based on the analysis of the functioning of the transport service markets, by studying the characteristics of the demand, the characteristics of the offer and the transport service market.

1.1 TARGET GROUP

The target group whose mobility was studied was a group of students studying at several faculties in the city of Skopje. Common for all the students is the place of residence, i.e. the settlement Dame Gruev located in the municipality of Gjorce Petrov. From this group all the relevant information about their mobility was obtained through a survey process.

1.2 ENVIROMENTAL AND TRANSPORT CONNECTION CHARACTERISTICS

The settlement Dame Gruev is located in the west part of the city of Skopje approximately 7 km from the central area. It extends at 2,5 square kilometers with a modern urban plan and has around 15000 inhabitants. Nearby there is a military barrack and part of the railway that goes towards the cities of Kicevo and Prishtina.

Currently the only way to travel to other city areas is via the road network (city streets), because the existing railway is not used for urban transport and there are no other transportation alternatives. However the approach ("entrance" and "exit") of the settlement Dame Gruev is limited to one street that is through an overpass at the very beginning. The other way that does not represent a suitable approach to the settlement is through the city ring road.

Figure 1. Air distance between the settlement Dame Gruev and the city centre

2. OBJECT OF ANALYSES

This article contains analyses and descriptions of the transportation supply and demand, which affect the target group and the city in general.

2.1 ANALYSIS OF THE TRANSPORTATION SYSTEMS

Considering the transport supply, the alternative to the individual transport (cars) is the public city transport that is represented by the buses of the public enterprise (JSP) in Skopje. 3 different lines of the public city transport pass on the territory of the settlement, the buses 22, 22A and 64A. Two of them (22 and 22A) represent city lines, and the other one is a suburban line.

The line 22 has a length of 14,5 km with 30 stations from which 3 of them are in the settlement Dame Gruev. This line passes

throughout the most vital city areas. The travel time in one direction from the beginning to the end of the line is 1 hour, i.e. the duration of one rotation is 2 hours. The frequency of departure of two consecutive buses varies from 7 (in the morning) to 20 (in the evening) minutes. The line 22 is one of the most busy and most frequent lines in the city of Skopje with in average of 110 rotations per day. The other two lines (22A and 64A) have similar characteristics (length, stations, travel time) as the line 22, but different ending points and drastically less rotations per day.

Generally, on the lines throughout the city, the transporting is done by two-deck buses Fig. 3. These buses have length of 11,8 m, height of 3,9 m and capacity of 80 passengers (60 seating and 20 standing). In addition, there are also single-deck buses with a capacity of 50 passengers with various seating and standing combinations. In average, the commercial speed of the buses on the city lines is around 14 km/h. It should be taken in consideration

Z. Zafirovski, Z. Krakutovski, A. Glavinov, D. Moslavac, V. Gacevski

that the legal speed limit in the cities in Macedonia is 50 km/h. The accuracy of the timetable of the busses is 5 to 10 minutes, and it depends on several factors. Also it should be

emphasized that the frequency of the buses varies throughout the week, i.e. there is difference in the timetable on weekdays and weekends and holidays.
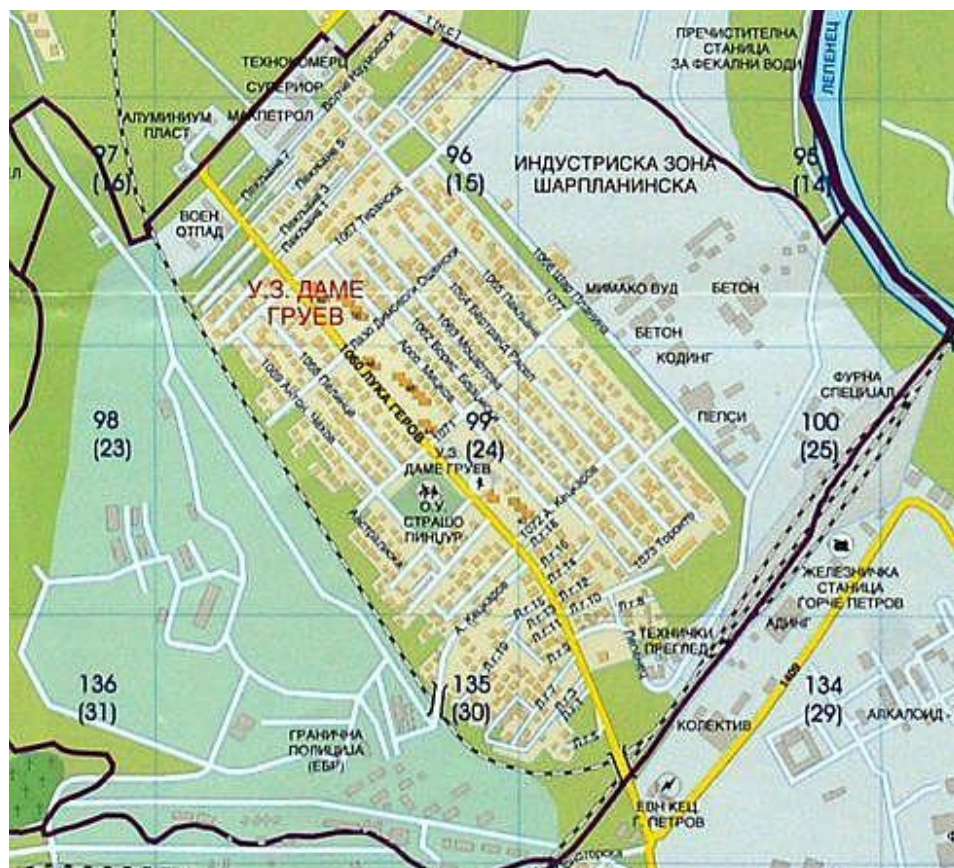

Figure 2. Map of the settlement Dame Gruev

2.1 ANALYSIS OF MOBILITY OF TARGET GROUP

Through the analysis of the target group, valuable information about their mobility has been obtained. Such mobility analysis variables are:

- Generation of trips;
- Destination of trips;
- Main and secondary motives for traveling;
- Distribution of trips by the means of transport;
- Time distribution of trips throughout the year, week and day.

These variables are used for determination of the transportation demand. From spatial aspect the people who travel to destinations near the route of the line 22, have no problem with the public city transport. For the other users of public transport who travel to different city areas, where there is no direct line from the settlement or the rotation intensity is very low (line 22A and 64A), problems occur which lead to loss of time and money.

In terms of transport capacity, there are major problems in the public city transport. The line 22 is one of the busiest and most saturated line in the city of Skopje, because it passes through the most frequent areas and settlements where it is the main transport supply. Due to this and the fact that the other lines (22A and 64A) have low frequency, the buses very often reach their maximum capacity. This mostly occurs in the morning hours (from 7 to 8 o'clock) and the afternoon hours (from 15 to 17 o'clock) when most residents have the need to travel.

Besides the capacity and frequency of the transport vehicles there are problems with the capacity of the streets. Because the infrastructure in the settlement Dame Gruev is reduced to one main street with two traffic lanes, the maximum traffic density is often reached. This condition affects all users of the road and leads to breakdowns in traffic flows, traffic accidents and overall low level of service.

Figure 3. Two-deck city bus

3. RESULTS

The current state based on the data from the analysis of the supply and demand indicates major transport problems in the settlement Dame Gruev and the city of Skopje in general. At the moment besides the individual and the public bus transport there is no alternative solution. Besides the improvement of the current transport offer, possible alternatives for the transport problems in the settlement Dame Gruev and the city of Skopje are:

- Construction of new infrastructure i.e. streets that will improve the access to the settlement and reduce the traffic volume on the existing streets. Positive sides to this solution are: traffic distribution, improvement of the level of service, increased traffic safety, faster time of travel and more. Negative when building a new infrastructure in city areas are the major costs and the problems that arise when constructing in densely populated places.

- Implementation of a tram in the public city transport in densely populated zones would generate great benefits for the users of the public and individual transport. With a tram solution there would be faster, more accurate and cheaper transportation for the users. This solution should be considered at the level of the whole city, and requires detailed analysis, planning and large investments for the infrastructure, vehicles and operation.

- Utilization of the existing railway in the public city transport can be done with an adequate reconstruction and integrating new lines. The existing railway lines pass through a few settlements in the city and most of them have little frequency of trains, which makes them suitable for this kind of transformation.

4. CONCLUSIONS

The analysis of supply and demand of transport represents compulsory process when there is a requirement for solutions to a certain transportation problem. This could be oriented to improvement of the existing state of the transport, as well as finding and implementing a new transport system.

The analysis itself is a complex and long term process that involves several areas of expertise. For the particular case stated above the results of the analysis indicate a major transport problem from several aspects. The solutions for this problem are proposed through three alternatives. The future research based on this analysis should be pointed towards the design of a model, which will serve for the prediction and planning of the mobility in the future.

With detailed analysis, careful planning and proper design, the urban transport can function properly. Skipping or leaving out some of the phases usually lead to problems which are manifested as a loss of time and money.

Z. Zafirovski, Z. Krakutovski, A. Glavinov, D. Moslavac, V. Gacevski

REFERENCES

[1]   Ponnuswamy S., Victor D. J. (2012), „Urban Transportation: Planning, Operation and Management".

[2]   Meyer M. D. (2017), „Transportation Planning Handbook, 4th Edition".

[3]   Hanson S., Giuliano G. (2004), „The Geography of Urban Transportation".

[4]   Chadwick G. F. (1978), „A Systems View of Planning: Towards a Theory of the Urban and Regional Planning Process, Second Edition".

[5]   Litman T. (2017), „Introduction to Multi-Modal Transportation Planning, Principles and Practices".

[6]   Owens S., Cowell R. (2011), „Land and Limits: Interpreting Sustainability in the Planning Process, Second Edition".

[7]   Amekudzi A., Mayer M., Ross C. (2011), „Transportation Planning and Sustainability Guidebook".

[8]   Stainer F., Butler K. (2006), „Planning and Urban Design Standards".

[9]   Golob T. F., Kitamura R., Long L. (1997), „Panels for Transportation Planning: Methods and Applications".

[10] Cascetta E., Carteni A. (2011) „A Quality-Based Approach to Public Transportation Planning: Theory and a Case Study".

[11] Krakutovski Z. (2015)„Assessment of transport infrastructure projects", authorized lectures, Faculty of Civil Engineering – Skopje.

ВО СЛУЧАЈ НА ПОЖАР

BREAK G...

PRESS HER...

БЕЗ ПАНИКА!
ИЗГРАДЕНО Е СО КНАУФ

FIRE WIN

Имајте доверба во Кнауф.
Чувствувајте се заштитен.

Кога ќе избие пожар, секоја секунда е драгоцена. Затоа препуштете ја Вашата доверба во новата програма противпожарни производи од европскиот водечки бренд за производство на градежни материјали: Knauf FireWin. Зголемете ја безбедноста на луѓето и објектот.

- Противпожарни плочи
- Противпожарен малтер за внатрешна употреба
- Противпожарен малтер за надворешна употреба
- Противпожарна боја
- Противпожарни манжетни

KNAUF

Knauf Macedonia   Knauf Macedonia   Knauf_MK   www.knauf.mk
www.knauf-firewin.com

FROM POINT CLOUD TO 3D BUILDING MODEL

AUTHORS

Vancho GJORGJIEV

Ph.D. Full Professor

Ss. Cyril and Methodius University

Faculty of Civil Engineering – Skopje

gorgiev@gf.ukim.edu.mk

Gjorgji GJORGJIEV

PhD, Assistant Professor

Ss. Cyril and Methodius University

Faculty of Civil Engineering – Skopje

gorgi.gorgiev@gmail.com

Natasa MALIJANSKA

MSc, Teaching Associate

Ss. Cyril and Methodius University

Faculty of Civil Engineering – Skopje

3D City Models are virtual representations of urban environments integrating geospatial data like buildings, terrain, landmarks, infrastructure landscapes and vegetation. 3D City Models positively influence urban planning, offer environmental analyses, can help manage risk and leads to better decision-making. Due to the rapid change in urban environments, there is a growing need for more efficient methods for spatial data acquisition as well as processing methods, which will meet the needs of 3D City Models in terms of accuracy, details, but also in terms of time and cost.

In this paper methods for spatial data acquisition and data processing are presented, theoretically and practically, in order to obtain 3D Building Models as the most important component of the 3D City Models. The main goal of the paper is to explore the possibilities of modelling 3D buildings by processing point cloud data generated from photos produced by Unmanned Aerial Vehicle (UAV), as one of the most convenient, fast and cheap ways for spatial data acquisition. The practical example presented in this paper, point out the power of this kind of data as an input for obtaining 3D building models.

Key words: 3D City Model, 3D Building Model, Point Cloud.

1. INTRODUCTION

Ever since the modelling of spatial object has started there is an ongoing tendency for increasing the level of details and the level of quality (spatial or nonspatial). It is an ongoing battle and most probably will continue in the future. Typical representation of the buildings and the objects in the traditional way ware presented/projected on the horizontal plane, where presentation of the characteristics of the buildings is done with symbols. Even though for some applications this way of presenting the spatial phenomenon is still sufficient, there is a strong market request for more detailed and more comprehensive modelling of real world. On the other hand, increasing the level of details creates a need for faster and low-cost data acquisition, data processing and data modelling.

The geospatial industry has developed significantly in this area and today we have many solutions, products, systems, applications where models are far from simple 2D representations of the objects. One of the big movements in the urban area modelling are 3D city models. Introduction of the third spatial component is not new and it was done in the past also, but with surfaces modelling which today is known as 2.5D representation. In this 2.5D models on one known location (Y,X) the model represents only one value (Z), which is not sufficient to present complex urban situations. These needs have driven the science to develop more detailed full 3D model of urban areas, which has resulted with 3D City Models.

3D City Model is a representation of urban environment with 3D geometry of common urban objects and structures, with buildings as most prominent feature (Biljecki, Filip, et al, 2015). These models have constant

development process and in general two phases can be distinguished. The first phase where models ware developed and had purpose of visualization urban areas without serious possibilities for spatial analysis and in the second phase, applications of 3D models has been seriously developed. Today we have wide range of implementation of 3D models in a different area of research, planning, protection, prediction, decision making and many other processes.

The application of these models highly depends of the details of the model and the quality of the model in general. The amount of detail that is captured in a 3D model, both in terms of geometry and attributes, is collectively referred to as the level of detail (LOD), indicating how thoroughly a spatial extent has been modelled. As a result, the LOD is an essential concept in geographical information science (GIS) and 3D city modelling (Biljecki, Filip, 2017).

Figure 1. 3D City model level of details

Based on CityGML classifications, there are five level of details, starting from LOD0 to LOD4. The standard for LOD represents the necessary features of the buildings that need to be presented/modelled. Developed models with different LOD gives a different possibilities in exploitation phase of the model but also more detailed 3D city models require more labour and entail a reduced degree of automation (Jokela J, 2016).

Spatial data acquisition for development of 3D City Model is a hard and long process.

2. MOST COMMONLY USED TECHNOLOGY FOR 3D CITY MODELLING

Technology for spatial data acquisition is in a constant development, striving toward more precise, detailed and faster data acquisition.

Other very important tendency is related with cost of data production.

3D city models are based on a large data quantity gathered in order building models to be as close as possible to the actual appearance, texture and geometrical shape. The process of data collection is not only focusing on spatial but also nonspatial data. Data acquisition technologies can be divided by many criteria, in this paper three are discussed.

The first classification is based on data acquisition technologies. In general, there are three major technologies which provide a satisfactory result in 3D city modelling and those are as follows:

- Classic approach (total stations)
- Photogrammetry
- Laser scanning

Classic approach of modelling buildings has long tradition of implementation and still it is usable method. It is a method of collection of spatial data without high degree of automation but a great level of control. This method is very much time consuming and not very reach with details of the modelled object. It is in general manual data acquisition, that means the number of surveyed points is not very high and has significant influence of the process of creation of the model where intensive labour needs to be invested.

Photogrammetry methods are very much exploited in the last decade. Development of new camera caring platforms like drones, cars or long telescopic poles, together with new software and techniques like Structure from Motion (SfM) has made photogrammetry one of the top technologies for modelling complex objects. The models are produced based on a large number of photography's taken from different positions with overlapping of about 80% which are further processed and point cloud is extracted. Development on the building models are created from the generated point cloud. This method is characterised with high degree of details, depending of the distance between camera and objects, fast data acquisition, low cost of production, and possibility of high accuracy. Many positive sides that photogrammetry has in context of 3D City Modelling has made photogrammetry as one of the technologies most commonly used in 3D City Modelling (Kobayashi Y., 2006). The photogrammetry has gained even more popular when regular digital cameras started to be used in order to obtain images for building spatial products through photogrammetry methods. In the past it was expensive to use airborne images for small scale projects, today with introduction of drone as a camera carrier it is one of the most convenient and cheap ways for spatial data acquisition.

Third technology widely used for data acquisition is laser scanning. It is a powerful technology which has characteristics that are in favour of building precise models accompanied with a lot of details. Laser scanners can be terrestrial or can be scanning from the air. Terrestrial scanners can be static or mounted on a moving vehicle and airborne lidar can be done with sensor mounted on an airplane, helicopter or drone. In the last several years mounting lidar scanner on drones has become very popular for small scale projects. By evaluating the explicit height information contained in laser scanning data together with cues such as surface roughness or laser intensity, objects such as buildings and trees can be extracted automatically (Rottensteiner, F, Trinder J, Clode S, 2005). Lidar data has high accuracy and it has fast data collection period.

There are many academics discussions about better and more suitable method for data acquisition and many researches have been conducted to resolve the dilemma. Bottom line answer is: depends, laser scanning technology requires more preparation and it is more time consuming while image-based point cloud production it takes faster time to acquire images and equipment is rather cheaper. In comparing laser scanning to image-based method, for small and medium size objects and distance image-based method have an advantage in terms of methodology and speed, but on large scale objects laser scanning is better in terms of quality and processing time.

Creating sufficient data quantity for 3D modelling of objects can lead to combination of all previous technologies in providing data that is going to be used in establishing or updating the model. Each of these technologies, due to complexity of objects, could be insufficient source of data, so additional data can be provided with other available technologies for data acquisition or most probably combination of terrestrial and observation from the sky.

Concerning modelling processes, we could categorize modelling methods in three categories: automatic, semi-automatic and manual. The automatic approach is basically modelling of existing buildings, structures, based on point cloud data by using technologies for pattern recognition. The semi-automatic approach is to model a building based on the point cloud data and algorithms for detecting characteristic features of the building, like walls, roofs with some interventions of the operator. The manual building modelling is conducted in classic CAD software by creating each building element manually form the collected data. These three modelling methods are very dependant of the available data type, way of data is collected, accuracy of the data and objects and surroundings that are being modelled. Also, each method is error-prone, so this component it needs to be taken in consideration as well.

3. EXPERIMENTAL RESULTS

The research has been conducted on a test area, which has been selected in order to be an adequate test polygon for the purpose of this research. A flight campaign was conducted in June 2018 using a drone DJI Phantom 4. The flight had an altitude of 50m above ground level. The test area covered approximately 4 ha where ground control points were marked and surveyed. The observed settlement is with densely built houses, with various types of roof constructions, but not so dense built areas are also present in order to see the impact of neighbouring characteristics on the buildings during building extraction process. Vegetation is also present with different heights within observation area.

Figure 2. Orthophoto of the study area

The dense point cloud generated for the study area was made of more than 15 million points. The model is georeferenced by 7 ground control points and the position error after georeferencing the model is 4.4 cm. The point cloud as a result is shown in the next figure.

Figure 3. Point cloud data of the study area

V. Gjorgjiev, G. Gjorgjiev, N. Malijanska

4. PROCESS DESCRIPTION

In this research an automatic and semi-automatic method for feature extraction was used. The focus are roofs of the buildings, and the buildings as a whole, having in mind that buildings are the most important part of the 3D City Models. The buildings are created of planar surfaces as a best approximation of the created point cloud and the composition of the building is consisted of walls and roofs.

Data processing of created point cloud starts with importing the point cloud in the software, manual removing of unwanted points accompanied with automatic point filtering based on a given parameters. Vegetation detection is the next step and it should be made in order to differentiate vegetation points from the points that represent the rest of the objects. The software for classification of point cloud data offers the possibility of defining different parameters for detecting points from vegetation and points form building for more effective automatic classification. After the detection of points which represent vegetation, the next step is the detection of points from buildings roofs. A choice of parameters for automatic detection of the points that represent roofs of the objects can be made. These parameters refer to the minimum height of the roof construction, the maximum slope of the roof construction, the minimum and the maximum number of points per roof construction, etc.

As mentioned earlier, two methods were used, automatic and semiautomatic building modelling. In both methods creation of the model is based on definition of planar surfaces as a best fit to the point cloud. In the manual modelling process, borders of the roofs are delaminated and best fit plains are created, also similar process is used for a wall modelling.

A basic processing workflow for automatic creation of 3D building form point cloud is shown below:
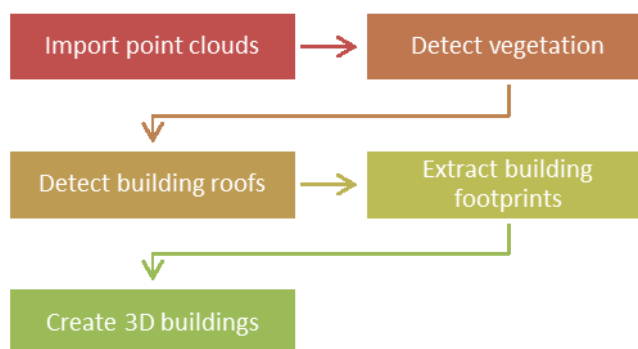
If automatic modelling of buildings is conducted, the next step is extraction of building footprints and creation of 3D models of buildings from classified point cloud data. 3D buildings can be modelled at a different level of detail as mentioned earlier in the paper. In this research an automatic modelling method was applied and two 3D building models were created with different level of details, LOD1 and LOD2. Results are presented at Figure 4, a) LOD1 and b) LOD2. The LOD1 presents buildings as objects with flat roof, while LOD2 presents the buildings with geometry which is close to the actual geometry of the roof but without details about some additional elements of the roof like chimneys.

Automatic extraction of 3D buildings will be successful if a good classification of the point cloud data has been previously made. Under conditions where buildings are rare and the vegetation around the buildings is not dense, the automatic classification and extraction of 3D buildings yields good results. But in conditions of dense construction and the presence of dense vegetation it is necessary to make corrections to the automatic classification and extraction of building elements semi-automatically in order to obtain good results. Automatic 3D modelling is sufficient to get a 3D City Model at a lower level of detail. In order to get a 3D model at a LOD3 or LOD4, more efforts and application of semi-automatic or manual processing of point cloud data should be done. For this purpose, we use mathematical algorithms in order to extract planes from a point cloud data. In this process, it can be chosen different planes as well as contours of those planes from which a model of 3D objects can be created. The following figure represents model of different types of roof constructions by extracting plains a) without and b) with defined boundary.
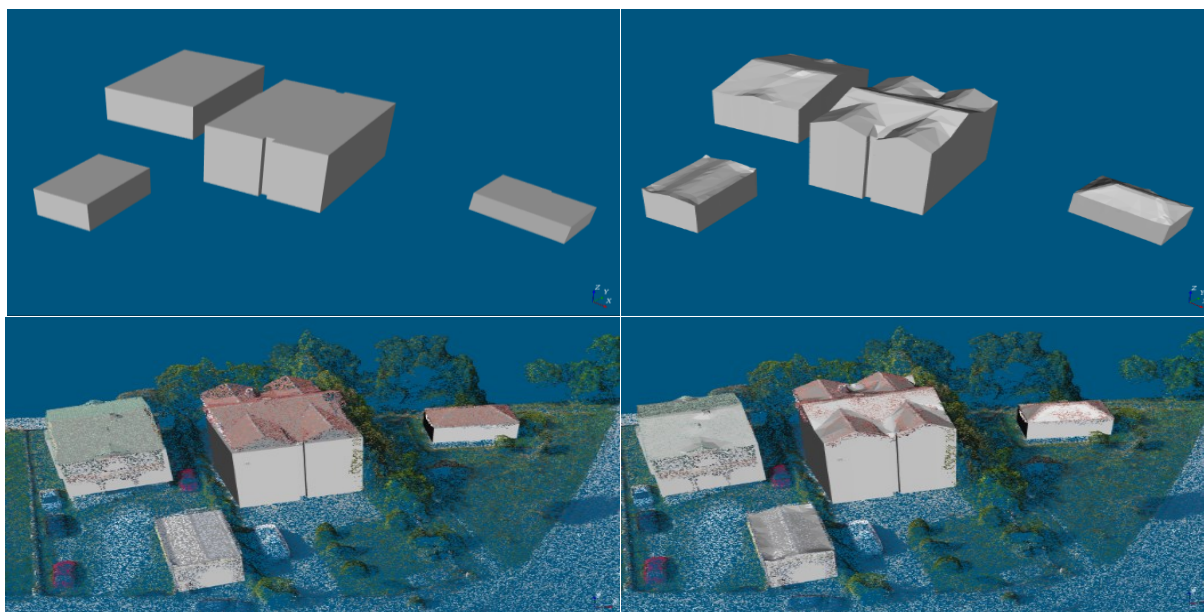
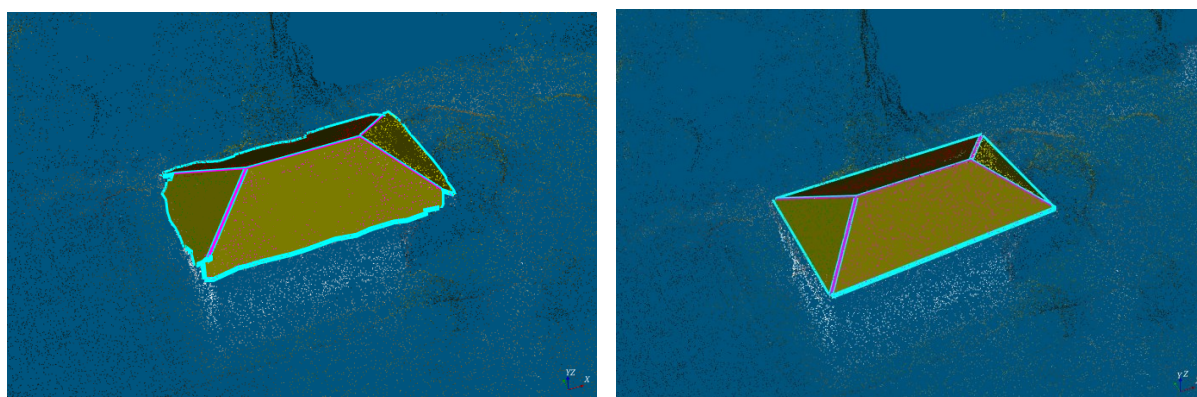Figure 4. a) Buildings at LOD1; b) Buildings at LOD2

Figure 5. a) Extraction of plain without defined boundary; b) Extraction of plain with defined boundary

This procedure can be used to model other elements of 3D objects and not only the roofs. The Figure 6 shows model of the object at a LOD3 created with semi-automatic extraction by extracting planes which represent roofs and walls of the building.
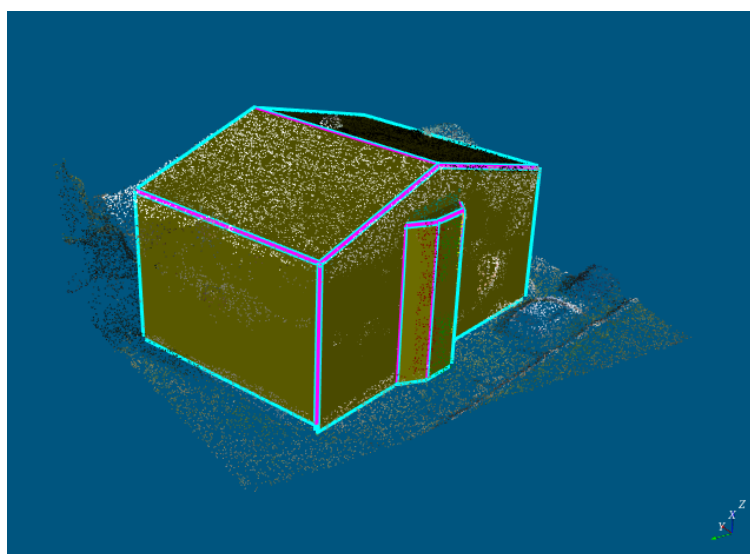

Figure 6. 3D building modelled by extraction of plains

V. Gjorgjiev, G. Gjorgjiev, N. Malijanska

5. CONCLUSION

The industry together with researchers are in a constant struggle for development of a new technologies for data acquisition and data processing where 3D City Models are going to be produced in faster and more efficient manner. For small and middle size projects, UAV together with image processing algorithms have made a small revolution in 3D modelling. Point clouds have become standard data source for feature extraction at mass data collection projects and models produced in this way are becoming more and more competitive with other technologies such as laser scanning. However, Image based point cloud data has its limitations, particularly in the areas where dense vegetation is present and algorithms for automatic data extraction shows their downsides. Aerial photos are producing good results for roof modelling but walls of the buildings especially in a densely build areas are not modelled very well, in this case and oblique image need to be taken. Very often a manual intervention is necessary in order a better-quality model to be created. If higher level of details is requested, bigger manual interventions are going to be needed in order to produce a higher quality result.

REFERENCES

[1]   Biljecki, Filip, Stoter, J., Ledoux, H., Zlatanova, S., and Arzu Çöltekin (2015). Applications of 3D City Models: State of the Art Review. ISPRS International Journal of Geo-Information, Vol. 4, no. 4, 18 Dec. 2015.

[2]   Biljecki, Filip (2017) Level of details in 3D city model, Phd dissertation, TU Delf, ISBN 978-94-6186-800-8

[3]   Jokela J (2016): CityGML building model production from airborne laser scanning. Master's thesis, Aalto University, Aalto, Finland.

[4]   Kobayashi Y., (2006), Photogrammetry and 3-D City modelling, Digital Arch, School of Architecture and landscape Architecture, Arizona State University, USA.

[5]   Rottensteiner, F, Trinder J, Clode S, (2005) Data acquisition for 3D city models from LIDAR extracting buildings and roads, Geoscience and Remote Sensing Symposium, 2005. IGARSS '05. Proceedings. 2005 IEEE International, Volume: 1.